

DTIC FILE COPY

2



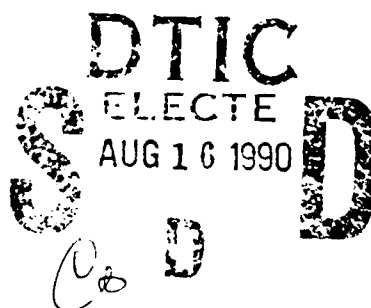
AD-A225 248

WRDC-TR-90-2027

RYDBERG STATE STARK SPECTROSCOPY AND  
APPLICATIONS TO PLASMA DIAGNOSTICS

Capt. James R. Shoemaker  
Power Components Branch  
Aerospace Power Division

March 1990



Final Report for Period October 1985 - September 1989

Approved for public release; distribution unlimited.


AERO PROPULSION AND POWER LABORATORY  
WRIGHT RESEARCH AND DEVELOPMENT CENTER  
AIR FORCE SYSTEMS COMMAND  
WRIGHT-PATTERSON AIR FORCE BASE, OHIO 45433-6563

## NOTICE


When Government drawings, specifications, or other data are used for any purpose other than in connection with a definitely Government-related procurement, the United States Government incurs no responsibility or any obligation whatsoever. The fact that the government may have formulated or in any way supplied the said drawings, specifications, or other data, is not to be regarded by implication, or otherwise in any manner construed, as licensing the holder, or any other person or corporation; or as conveying any rights or permission to manufacture, use, or sell any patented invention that may in any way be related thereto.


This report is releasable to the National Technical Information Service (NTIS). At NTIS, it will be available to the general public, including foreign nations.

This technical report has been reviewed and is approved for publication.

  
JAMES R. SHOEMAKER, Capt, USAF  
Power Components Branch  
Aerospace Power Division  
Aero Propulsion and Power Laboratory

FOR THE COMMANDER

  
LOWELL D. MASSIE  
Chief, Power Components Branch  
Aerospace Power Division  
Aero Propulsion and Power Laboratory

  
MICHAEL D. BRAYDICH  
Chief, Aerospace Power Division  
Aero Propulsion and Power Laboratory

If your address has changed, if you wish to be removed from our mailing list, or if the addressee is no longer employed by your organization please notify WRDC/POOC, WPAFB, OH 45433-6563 to help us maintain a current mailing list.

Copies of this report should not be returned unless return is required by security considerations, contractual obligations, or notice on a specific document.

REPORT DOCUMENTATION PAGE				Form Approved OMB No. 0704-0188		
1a. REPORT SECURITY CLASSIFICATION UNCLASSIFIED			1b. RESTRICTIVE MARKINGS			
2a. SECURITY CLASSIFICATION AUTHORITY			3. DISTRIBUTION/AVAILABILITY OF REPORT Approved for public release; distribution is unlimited			
2b. DECLASSIFICATION/DOWNGRADING SCHEDULE						
4. PERFORMING ORGANIZATION REPORT NUMBER(S)  WRDC-TR-90-2027			5. MONITORING ORGANIZATION REPORT NUMBER(S)			
6a. NAME OF PERFORMING ORGANIZATION Aero Propulsion and Power Laboratory, WRDC, AFSC		6b. OFFICE SYMBOL (If applicable) WRDC/POOC-3	7a. NAME OF MONITORING ORGANIZATION			
6c. ADDRESS (City, State, and ZIP Code)  Wright-Patterson AFB, OH 45433-6563			7b. ADDRESS (City, State, and ZIP Code)			
8a. NAME OF FUNDING/SPONSORING ORGANIZATION Same as 6a		8b. OFFICE SYMBOL (If applicable)	9. PROCUREMENT INSTRUMENT IDENTIFICATION NUMBER			
8c. ADDRESS (City, State, and ZIP Code)			10. SOURCE OF FUNDING NUMBERS			
			PROGRAM ELEMENT NO. 61102-F	PROJECT NO. 2301	TASK NO. S1	WORK UNIT ACCESSION NO. 15
11. TITLE (Include Security Classification)  Rydberg State Spectroscopy and Applications to Plasma Diagnostics						
12. PERSONAL AUTHOR(S) Capt. James R. Shoemaker						
13a. TYPE OF REPORT Final		13b. TIME COVERED FROM Oct 85 TO Sep 89		14. DATE OF REPORT (Year, Month, Day) March 1990		
15. PAGE COUNT 110						
16. SUPPLEMENTARY NOTATION						
17. COSATI CODES			18. SUBJECT TERMS (Continue on reverse if necessary and identify by block number)			
FIELD	GROUP	SUB-GROUP	Rydberg atoms, Stark effect, <i>Stark effect, Rydberg atoms</i>			
20	09					
09	03					
19. ABSTRACT (Continue on reverse if necessary and identify by block number)  Rydberg state Stark spectroscopy of triplet and singlet helium has been applied to measure the electric field profile in DC glow discharges. Stark splittings of triplet helium were used to map the field profile in the cathode sheath of a parallel plate discharge. Simulations of the observed spectra enabled the direct determination of the field gradient, hence the space charge density, in the sheath. The polarization dependence of the Stark effect was exploited to determine the field direction as well as magnitude (electronic field vector). Measurements of low electric fields (50 v/cm) were attempted by observing the linewidth of high Rydberg states (n 25) and applying standard line broadening approaches used in plasma diagnostics. However, it is shown that these approaches use approximations which are inappropriate for helium spectra and for the plasma conditions found in the glow discharges investigated in this study. <i>K. A. ...</i>						
20. DISTRIBUTION/AVAILABILITY OF ABSTRACT <input type="checkbox"/> UNCLASSIFIED/UNLIMITED <input checked="" type="checkbox"/> SAME AS RPT <input type="checkbox"/> DTIC USERS				21. ABSTRACT SECURITY CLASSIFICATION UNCLASSIFIED		
22a. NAME OF RESPONSIBLE INDIVIDUAL Major Thomas E. Gist				22b. TELEPHONE (Include Area Code) (513) 255-2923		
				22c. OFFICE SYMBOL WRDC/POOC-3		

## TABLE OF CONTENTS

I	INTRODUCTION.....	1
II	STARK EFFECT: HISTORICAL REVIEW.....	5
III	DC GLOW DISCHARGE ELECTRIC FIELD PROFILE.....	21
IV	RELATED EXPERIMENTS.....	25
V	EXPERIMENTAL .....	33
VI	EXPERIMENTAL RESULTS.....	40
VII	ANALYSIS AND SIMULATION OF SPECTRA.....	63
VIII	CONCLUSION.....	94
IX	REFERENCES .....	98

TITLE AUTHOR DATE PROJECT	<div style="font-size: 2em; text-align: center;">J</div> CLASSIFICATION SECURITY CODES DISTRIBUTION STATEMENT
<div style="position: absolute; left: 10px; bottom: 10px; font-size: 1.5em;">A-1</div>	



## LIST OF FIGURES

Figure	Page
1. Triplet helium Stark manifolds, $n=17$ s polarization . . . . .	18
2. Triplet helium Stark manifolds, $n=17$ $\pi$ polarization . . . . .	19
3. DC glow discharge spatial variations of electric field and other operating parameters . . . . .	22
4. Experimental setup. . . . .	34
5. DC discharge tube configurations . . . . .	37
6. Triplet helium cathode sheath Stark spectrum, $\Delta m = 0$ polarization. . .	42
7. Triplet helium Stark spectra recorded at varying distances from the cathode. . . . .	44
8. Cathode sheath electric field profile from $\Delta m = 0$ polarization spectra .	46
9. Triplet helium cathode sheath Stark spectrum, $\Delta m = \pm 1$ polarization. .	48
10. Triplet helium Stark spectra recorded at varying distances from the cathode. . . . .	49
11. Cathode sheath electric field profile from $\Delta m = \pm 1$ polarization spectra .	50
12. Singlet helium Rydberg series spectrum, $\Delta m = \pm 1$ polarization . . . . .	54
13. Triplet helium Rydberg series spectrum, $\Delta m = \pm 1$ polarization . . . . .	56
14. Triplet helium Rydberg series spectrum, $\Delta m = 0$ polarization . . . . .	57
15. Singlet helium Rydberg series spectra recorded at various radial locations in the positive column of a DC glow discharge . . . . .	59
16. Vector electric field measurement. . . . .	61
17. Calculated Stark splitting of triplet helium, $n = 19$ . . . . .	66
18. Calculated triplet helium spectra, $n = 19$ , $\Delta m = \pm 1$ polarization for various electric field gradients. . . . .	68
19. Measured triplet helium spectra for electric fields of 740, 575, and 340 V/cm. . . . .	69
20. Calculated triplet helium spectra for electric fields of 740, 575, and 340 V/cm . . . . .	70

Figure		Page
20.	Calculated triplet helium spectra for electric fields of 740, 575, and 340 V/cm . . . . .	70
21	Theoretical hydrogen $n=30$ polarization dependent intensity distributions . . . . .	73
22	Calculated hydrogen $n=30$ polarization dependent Stark line profiles . .	75
23.	Calculated hydrogen $n=30$ , $\Delta m = \pm 1$ polarization Stark line profiles using a Voigt profile fit . . . . .	77
24.	Comparison of several approaches for describing hydrogen line broadening. . . . .	79
25	Triplet and singlet helium $n = 30$ , $\Delta m = \pm 1$ polarization Stark line profiles. . . . .	81
26.	Comparison of hydrogen, singlet helium, and triplet helium line broadening . . . . .	82
27.	Calculated singlet helium Rydberg series at electric fields of 4.86, 13.26, and 23.91 V/cm . . . . .	88
28.	Experimental resolution limit on electric field sensitivity . . . . .	90
29.	Comparison of the $n$ -dependent intensity of calculated and experimental singlet helium Rydberg series at various electric fields . .	95

## LIST OF TABLES

Table		Page
1	Triplet helium energy and eigenvector ( oscillator strength) matrices . .	13
2.	Comparison of various methods for analyzing helium spectra. . . . .	92

## I. INTRODUCTION

The application of an electric field on an atom modifies the potential in which the electrons orbit, which in turn modifies the energies of bound states and transition probabilities between states. The internal electric field in an atom is very large,  $5.142 \times 10^9$  V/cm for ground state hydrogen, so an external electric field must be of a similar magnitude to cause an observable perturbation on the atom's spectrum. Reducing the internal electric field by increasing the nuclear-electron separation, i.e., exciting the electron to a higher principal quantum number, reduces the external electric field required to produce a measurable effect on the atom to fields which can easily be achieved in the laboratory. Experimental evidence of this effect on the Balmer series of hydrogen was first reported independently in 1913 by Stark<sup>1</sup> and LoSurdo<sup>2</sup>, and is commonly known as the Stark effect. To produce their spectra, both Stark and LoSurdo used glow discharges in nonstandard configurations. Stark used the discharge to produce canal rays (fast ions and neutrals) which were passed through a perforated cathode into an observation region where an electric field was maintained between two electrodes independent of the discharge. The effect of electric fields from 10 to 100 kV can be observed on the modestly excited states, principal quantum number  $\approx 7$ , contained in the neutral component of the canal rays and excited by the canal rays. Stark's experiment allowed the electric field in the observation region to be varied independently of the discharge; however, the number of excited atoms was low and the photon signals were very weak. LoSurdo used a glow discharge with a constriction in front of the cathode to observe the electric field effect on hydrogen spectra. A glow discharge in this configuration can produce the combination of



the high electric fields and excited atomic states (through electron impact, recombination, and other processes) required to produce a measurable effect, and has the advantage of producing a much higher signal level than Stark's method. However, it is difficult to produce a stable discharge which can produce electric fields high enough to affect these low lying n-states.<sup>3</sup> In addition, the electric field in a discharge cannot be varied independently and cannot be accurately measured because the high electric fields (in the cathode sheath) are accompanied by very high field gradients which make probe measurements unreliable. Thus an absolute comparison of the spectra to the theoretical predictions cannot be made.

The invention and development of tunable dye lasers has enabled excitation to high principal quantum number (Rydberg) states, extending the range of electric field sensitivity<sup>4</sup> down to  $\mu\text{V/cm}$ . Improved detection techniques coupled with laser excitation has made Stark's technique a very powerful tool for investigating the atomic physics of the interaction of very well characterized electric fields with well defined excited states of atoms and molecules. Laser excitation of selected Rydberg states meant that greatly reduced electric fields are required to produce a measurable effect, and the electric fields produced in conventional glow discharge configurations became accessible to measurement.

In this report we discuss the application of Rydberg state Stark spectroscopy of helium to the measurement of electric fields in various regions of a DC glow discharge: the cathode sheath, negative glow, and positive column. Spectroscopic electric field measurements on glow discharges are preferred because, unlike Langmuir probe measurements, spectroscopic measurements are non-

intrusive. Helium was selected for these investigations for several reasons. First, the theoretical description of the Stark effect on helium is well founded and can be readily computed for a wide range of principal quantum numbers. Second, it has long been assumed that the behavior of Rydberg states of helium would be indistinguishable from that of hydrogen, an assumption which is shown to be invalid on the basis of the data collected in these experiments. Recent high precision Stark cell measurements of helium published after the inception of our measurements demonstrate this fact conclusively.<sup>5</sup> Lastly, because helium has the highest ionization energy of any atom or molecule, it would not greatly affect the operation of glow discharges in other species when introduced as a minority species, and thus has the potential to be an electric field tracer in other gases for which the Stark effect cannot be easily interpreted.

In this report, a review of the development of the theory and of measurements of the Stark effect on hydrogen and helium is presented, as well as a description of how the Stark effect manifests itself on spectra, Sec II. In Sec. III, a brief description of the electric field profile anticipated in a normal DC glow discharge is presented, as well as a matching of the various spectral manifestations of the Stark effect to the different regions of the discharge. Recent pertinent experiments on Rydberg state Stark spectroscopy and non-intrusive electric field measurements in glow discharges are described in Sec. IV. The experimental setup is described in Sec. V. The experimental results are described in Sec VI, and a new analysis of low electric field spectra, recorded in the negative glow and positive column, are discussed in Sec VII. This analysis shows that the standard implementations of spectral line broadening and series ter-

mination on high Rydberg states are inadequate and require modification for application to the low electric field regime,  $< 50$  V/cm. The differences between the Stark spectra of singlet and triplet helium Rydberg states are highlighted, as well as the difference between helium and hydrogen spectra. The impact of these differences on electric field measurements in plasmas is discussed.

## II. STARK EFFECT: REVIEW

After the discovery of the effect of an external magnetic field on spectral lines by Zeeman in 1896, it was natural to expect that a similar effect would be caused by an external electric field. Voigt considered the electric field perturbation of atoms as early as 1899, and also attempted (unsuccessfully) to observe an effect on the D lines of sodium.<sup>6</sup> Bohr's theory of quantized electron orbits in atoms was published in 1913,<sup>7</sup> the same year as Stark and LoSurdo's measurements, and it was an important success for this theory when Epstein<sup>8</sup> and Schwarzschild<sup>9</sup> used it to calculate the hydrogen line displacements and obtained good agreement with the experimental results. Kramers applied Bohr's correspondence principle in an attempt to calculate the hydrogen line intensities, however, the disagreement of his results with experiment helped demonstrate the incompleteness of Bohr's theory.<sup>10</sup> The Stark effect on hydrogen was not properly treated until after the introduction of wave mechanics by Schrodinger in 1926, where this problem was used as the first application of the perturbation method.<sup>11, 12</sup> Since the Bohr theory had been successful in predicting the line shifts it was reassuring that the first order terms (linear Stark effect) obtained from both approaches were identical; however, the two differed significantly in higher order field terms. The major improvement of the wave mechanics approach was that it provided much better agreement with the line intensities measured by Stark, though some discrepancies still remained. Foster revisited this experiment and made more precise measurements of the line intensities, which removed any discrepancies between experiment and theory.<sup>13</sup>

The initial calculation of the high field Zeeman effect (Paschen-Back) was performed by Lorenz from a classical approach <sup>14</sup> , however, the Stark effect can only be accounted for using quantum theory. The calculation of the Stark effect on hydrogen is a special case because of hydrogen's unique symmetry, however the overall method of solution is similar for other species. The unperturbed wave equation for hydrogen is

$$H_0 \Psi = E\Psi \qquad H_0 = \frac{p^2}{2} - \frac{1}{r} \qquad (1)$$

This equation is separable in polar coordinates, and its solution results in the hydrogen energy levels given by :

$$E_n = - \frac{1}{2n^2} \quad (\text{Atomic Units}) \qquad (2)$$

where  $n$  is the principal quantum number. An interesting feature of this result is that the energies do not depend on the electron's angular momentum  $l$ . The wavefunctions for the various  $l$ -states are different but the central potential remains the same for all  $l$ -states so the value of  $l$  does not change the energy for a given  $n$ . This is customarily stated as all the  $l$ -states in hydrogen have quantum defects of zero, and are degenerate, neglecting relativistic effects.

The application of an external, one-dimensional, DC electric field modifies the Hamiltonian to the form

$$H = H_0 - e \overline{F} z \quad (3)$$

where  $F$  is taken to be along the  $z$  axis. The addition of the field removes the separability of the problem in polar coordinates. The general method of solution is to construct a perturbation matrix using the eigenfunctions in polar coordinates and to find the energies from the eigenvalues of the matrix. However, for hydrogen only, the perturbed equation remains separable when transformed into parabolic coordinates. Following Schrodinger, the perturbation method is applied and results in the following solution ( to second order)

$$E = -\frac{1}{2n^2} + F \frac{3}{2}n(n_1 - n_2) - F^2 n^4(17n^2 - 3(n_1 - n_2)^2 - n - 9m^2 + 19) \quad (4)$$

where  $m$  is the magnetic quantum number and  $n_1, n_2$  are the parabolic quantum numbers.<sup>15</sup> In the parabolic basis set,  $n_1$  ranges from 0 to  $n - |m| - 1$ ,  $n_2$  from  $n - |m| - 1$  to 0, and  $n_2$  ranges from  $n - m - 1$  to 0. Thus, the  $l=0$  (s) state corresponds to  $n_1 = 0$ ,  $n_2 = n - |m| - 1$ , the  $l = 1$  (p) state corresponds to the  $n_1 = 1$ ,  $n_2 = n - |m| - 2$ , etc. For all  $n_1, n_2$  states in an  $n$ -manifold, the relation  $n_1 + n_2 + |m| + 1 = n$  holds. Higher order terms in the series of equation 4 have been calculated<sup>16</sup>, and good agreement between the third order expansion and hydrogen spectra recorded in electric fields up to  $10^6$  V/cm has been obtained.<sup>17</sup> The second order term is small compared to the linear term for electric field

values found in most glow discharges, and higher order terms can be safely neglected in most situations. The relative intensities for the different  $n_1, n_2$  states are given by<sup>15</sup>

$$I = (n_1 - n_2)^2 \quad \Delta m = 0 \text{ Transitions} \quad (5a)$$

$$I = (n_1 + 1)(n_2 + 1) \quad \Delta m = \pm 1 \text{ Transitions} \quad (5b)$$

This formula is only valid when the effect on the lower state is small compared to the effect on the upper state of the transition.

The calculation of the Stark effect on helium is more complicated because the Hamiltonian contains terms for the interaction of each electron with the nucleus plus the interaction between the two electrons. For excited states of helium, one can treat the inner electron and the nucleus as a single entity, the core, with an effective charge of 1, and set up the problem as an approximate hydrogen atom. The Hamiltonian then takes the form

$$H = H_0 + H'(l) \quad (6)$$

The term  $H'(l)$  appears because the interactions between each  $l$ -state and the core are no longer identical. For  $l < 4$ , the wavefunction of the outer electron is such that it sees the nucleus and the inner electron as separate entities, so the energies must reflect this additional interaction. For  $l \geq 4$ , the outer electron essentially sees a hydrogen nucleus, so the higher  $l$ -states energies match those for hydrogen

and are described as quasi-hydrogenic.  $H'(l)$  is difficult to calculate, however, it can be easily obtained from spectroscopic data. The energy difference is described in terms of a quantum defect, with the energy given by the modified hydrogen formula:

$$E_{n,l} = -\frac{1}{2(n-\delta_l)^2} \quad (7)$$

The Hamiltonian for helium with an external electric field is then:

$$H = H_0 + H'(l) - eFz \quad (8)$$

The wave equation describing the helium Stark effect is not separable in either polar or parabolic coordinates so it cannot be solved using a perturbation expansion. However, wave mechanics was not applied to this problem mainly because the "rival camp", i.e., Heisenberg's matrix mechanics group, first tackled this problem. J. Stuart Foster, a Canadian, and Jane Dewey, an American, were working with Heisenberg in 1926.<sup>18</sup> Both were interested in the Stark effect on helium from previous experimental work. At the time Dewey was new to the problem, while Foster already had a long affiliation with it. In their calculations of the Stark effect on helium, they both benefitted from Heisenberg's treatment of the neutral helium atom described above, which simplifies helium energies to modified hydrogen energies.<sup>19</sup> In order to proceed with practical calculations, Foster made use of the perturbation theory for degenerate systems



developed by Born, Heisenberg, and Jordan.<sup>20</sup> For a given principal quantum number  $n$ , he set up an energy matrix of dimension  $(n-m) \times (n-m)$ . The diagonal elements of the matrix are the helium energies arising from  $H_0$ . Because the internal electric field of helium is centrally symmetric,  $H'(1)$  is also diagonal. The interaction with the external asymmetric electric field gives rise to off-diagonal elements of the matrix. To calculate these terms, Foster copied Pauli's treatment of the Stark effect on hydrogen. Since helium wavefunctions can be well approximated by hydrogen wave functions, elements in the matrix corresponding to transitions of  $\Delta l > 1$  are neglected. This results in a tridiagonal matrix, which greatly simplifies calculations. Only first order terms in the electric field which are proportional to the dipole matrix elements connecting optically allowed states need be included.<sup>21</sup> The singlet and triplet (ortho and para) states of helium are well separated in energy so their interaction is negligible, and in Stark effect calculations they can be treated individually. Foster considered only the range of electric fields and  $n$ 's such that fine structure splittings are overshadowed by Stark splittings so fine structure effects could be ignored. Since helium fine structure effects are small this condition does not impose a tight restriction on the parameter space of  $n \cdot F$ . The electric field shifted energies are obtained from the eigenvalues of the perturbation matrix. The energies of transitions are obtained by connecting perturbed upper and lower states according to the selection rule on  $\Delta m$ .

The intensities of the  $l$ -state transitions can be found from the eigenvector matrix which is generated from the diagonalization. In the treatment of the hydrogen Stark effect, one can define a coordinate transformation in which the

perturbed energies are diagonal. Diagonalizing a matrix is equivalent to performing a coordinate transformation. Since the Stark coordinate system is defined in terms of the polar basis set, it is easy to visualize how the intensity from a single dipole allowed transition becomes distributed among the manifold. Table 1a shows the energy matrix for triplet helium,  $n=5$ ,  $m=0$ , with an applied electric field of 25 kV/cm. (All values are in atomic units) The eigenvector matrix for this manifold in the polar basis set, shown in Table 1b, is the identity matrix, which is simply another representation of the normal polar basis set. Table 1c shows the energy matrix after diagonalization; Table 1d shows the eigenvector (transform) matrix which contains information describing the new coordinate system in terms of the polar coordinate system. The axes of the diagonal coordinate system are composed of projections of each of the axes of the unperturbed polar coordinate system, namely the normal angular momentum states. Stated equivalently, the angular momentum wavefunctions of an electron under the influence of an external electric field are linear combinations of the field-free wavefunctions. The intensity transfer is now readily apparent from these projections.

For our experiments, we used the helium 2S metastables as the lower states, thus the normally allowed transition would be to the 5P-state. In the absence of an electric field, only one state in the  $n=5$  manifold is described by the 5P wavefunction. As soon as an electric field is applied, 5 transitions are possible since each of the 5 angular momentum states is now partially described by the 5P wavefunction. The relative intensities of each transition is proportional to the square of the coefficient of the 5P wavefunction it contains, which are the elements in the P row of the  $n=5$  manifold. Strictly speaking, the electric field will affect the

2S,m=0 state. However, for helium the effect on the  $n=2$  manifold is negligible except for very high fields,  $F > 1$  MV/cm. In general, the Stark effect on both upper and lower states must be accounted for.

Helium Stark spectra are markedly different from hydrogen spectra, even though helium has small quantum defects.<sup>20, 21</sup> While the electric field modified energy levels of helium l-states with zero quantum defects calculated by either diagonalization or the hydrogen Stark formula are approximately equal (the two methods differ significantly for the energies of states with non-zero quantum defects), the l-state intensities highlight the differences between helium and hydrogen. While the hydrogen intensities are independent of field and can be given in an analytic form, the relative helium intensities are strongly field dependent and cannot be even approximated in a closed form. In addition, the l-state intensity distribution within a helium n-manifold is a strong function of the exact quantum defect values used. As a result, the helium singlet and triplet lineshapes display drastically different responses to the same electric field. This has important consequences for electric field measurements based on helium Stark broadening, namely that the linewidth, full width at half intensity maxima, of triplet helium is not a linear function of the applied electric field (this is discussed in detail in Sec 7). Foster's technique neglects interactions between adjacent n-manifolds, and therefore it is only valid for field values lower than the n mixing field  $F=1/3n^5$ , at which value the outermost l-states of two adjacent n's

**Table 1 Triplet helium energy and eigenvector (oscillator strength) matrices.**

(a.)  $n = 5$  energy matrix,  $\pi$ -polarization, under an applied electric field of 25 kV/cm. Energies are given in wavenumbers; the zero field energies (diagonal elements) are given as the magnitude of the energy below the ionization limit.

4968.139	2.828	0	0	0
2.828	4498.500	2.366	0	0
0	2.366	4409.211	2.028	0
0	0	2.028	4388.956	1.512
0	0	0	1.512	4369.312

(b.) Eigenvector matrix before diagonalization.

	s'	p'	d'	f'	g'
s	1	0	0	0	0
s	0	1	0	0	0
d	0	0	1	0	0
f	0	0	0	1	0
g	0	0	0	0	1

(c.) Energy matrix after diagonalization.

4967.061	0	0	0	0
0	4496.155	0	0	0
0	0	4392.408	0	0
0	0	0	4389.597	0
0	0	0	0	4398.895

(d.) Eigenvector matrix after diagonalization. The relative intensities are given by the squares of the matrix elements in the p-row which is the projection of the wavefunction of the zero electric field allowed transition from the  $2s^3S$  lower state onto the field perturbed wavefunctions.

	s'	p'	d'	f'	g'
s	0.998	-0.047	0.00488	-0.00411	0.00316
p	0.0477	0.982	-0.120	0.105	-0.0837
d	0.00156	0.179	0.549	-0.0594	0.559
f	$10^{-5}$	0.0268	0.711	0.00403	-0.702
g	$10^{-6}$	0.002	0.421	0.797	0.432

become equal equal in energy.<sup>21</sup>

Using a similar approach one should be able to calculate the Stark effect on other species with "hydrogen-like" electronic configurations. Recently Zimmerman<sup>22</sup> devised such a procedure for alkali atoms, however, his procedure has several important differences because the approximations Foster made for helium are not valid for the alkalis. First, fine structure effects are significant in the alkalis, so the energy matrix must contain the energies of both spin states for each  $l$ -state, giving a dimension of  $2 \times (n - |\Delta m|)$  for each  $n$ -manifold. Second, several of the alkalis have quantum defects greater than one, so an energy matrix must contain several  $n$ -manifolds to include these interactions. Third, alkali wavefunctions cannot be approximated by those of hydrogen, so Zimmerman's procedure includes a numerical integration of the radial wavefunctions to calculate the off-diagonal terms in the energy matrix. The resulting energy matrix is sparse but not merely tridiagonal. The Stark energies and intensities are again obtained from diagonalization of the energy matrix and the corresponding eigenvector matrix. Zimmerman's procedure reduces to Foster's in the simple case of helium or hydrogen, and both procedures produce exactly the same results. The program which Zimmerman wrote to calculate the Stark (and Zeeman) effect has been distributed to many groups (including this group) throughout the world and is commonly used for calculations of alkali atoms, and has also been used in conjunction with high resolution helium Rydberg measurements.

A limitation of the energy matrix diagonalization methods for calculating the Stark effect is that only bound-bound transitions are considered. The applica-

tion of an electric field imparts a finite tunnelling probability to the excited electron, so an exact calculation must include interactions with a continuum of states. This is impossible for matrix techniques, because one would need an infinite basis set to include interaction with the continuum, i. e., an energy matrix of infinite dimension. An alternative approach, multichannel quantum defect theory (MQDT) has been developed which can deal with continuum interactions and other available channels. A good description of the situations where MQDT must be used is found in Ref 5 (and references therein). In our measurements, for bound-bound transitions the matrix diagonalization of Foster was found to be adequate within our experimental resolution.

Selection rules for optical transitions in the presence of an electric field are modified from the  $\Delta l = \pm 1$  to  $\Delta m = 0$  ( $\pi$  polarization) and  $|\Delta m| = 1$  ( $\sigma$  polarization), where polarization is defined with respect to the vector direction of the applied electric field. Removal of the l-state degeneracy transforms a single transition into a family of l-state transitions, collectively described as an n-manifold. When the separation between adjacent l-states is larger than the experimental resolution the result is termed Stark splitting; when the separation is below experimental resolution, the result is customarily referred to as line broadening. This effect is not the line broadening caused by the electric field induced tunneling probability<sup>23</sup> which appears when the electric field approaches  $n^{-4}$ . Most analyses of Stark line broadening have considered the n-manifold as a single line whose FWHM is equal to the separation between the extreme l-states in the manifold. This is an approximation because the intensities of the extrema will not equal one-half of the maximum intensity in the manifold. The validity of this approximation

will be discussed later. In the  $\pi$  polarization the  $\Delta m=0$  selection rule is satisfied by  $2s^1,^3S - ns^1,^3S$  transitions, thus this field free forbidden transition appears in Stark spectra. The s-states have the largest quantum defects and so appear as distinct lines well separated from the rest of the manifold. Because the field broadens the lines, proportional to  $n^2$ , manifolds of different  $n$  will begin to overlap.

Examples of triplet helium Rydberg state Stark spectra,  $n=17$ , s polarization, recorded at various locations in the cathode fall of a glow discharge (which is described in Sec V) are presented in Fig 1 to show the spectral modifications caused by an electric field. The rest of this report will describe how these spectral features can be used to measure the electric field in plasmas, however, it is informative to use these examples to outline the general features of Stark modified spectra. The spectra in Fig 1 were recorded at electric fields of 340, 575, and 740 V/cm respectively. As the electric field decreases from the bottom spectrum to the top, the splittings (separations between adjacent l-state transitions) decrease and the overall shape of the manifold (l-state intensity distribution) changes. Both features are unique functions of the electric field present. An additional feature visible in these spectra, an apparent change in the l-state linewidth across the manifold, is a consequence of the electric field gradient present in the cathode fall. Fig 2 shows Stark spectra for triplet helium,  $n=17$  in the  $\pi$  polarization, also recorded in the cathode fall of a glow discharge at electric fields of 300, 500, and 620 V/cm respectively. As in the s polarization, the splittings decrease with decreasing field and the manifold shape changes. Unlike the s polarization, the distinct peaks visible on the low energy side of these spectra are the  $2s^3S$  to  $17s^3S$  transitions, which are Stark allowed in the  $\pi$  polarization.



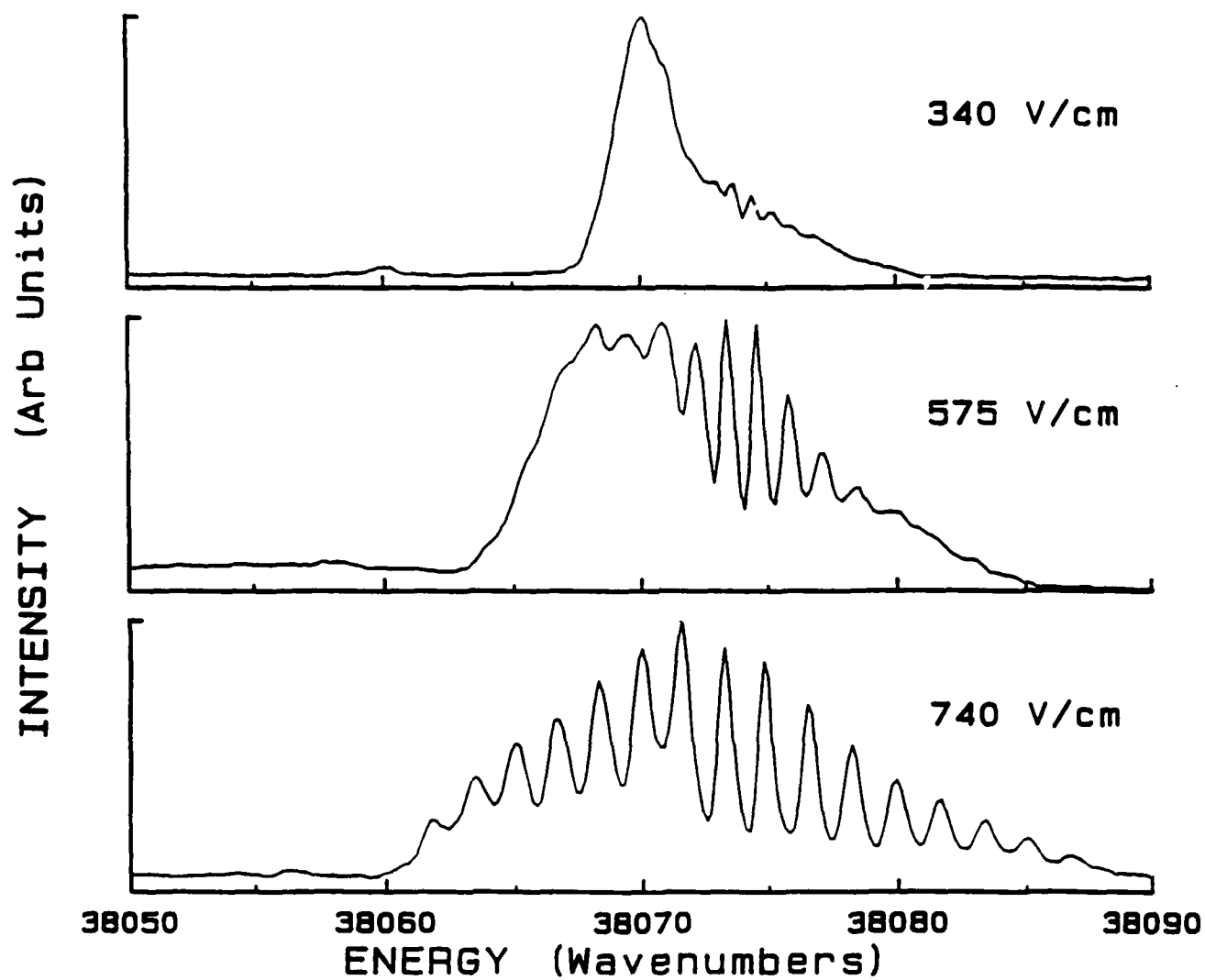


**Figure 1** Triplet helium Stark manifolds,  $n=17$ , s polarization, as a function of electric field.

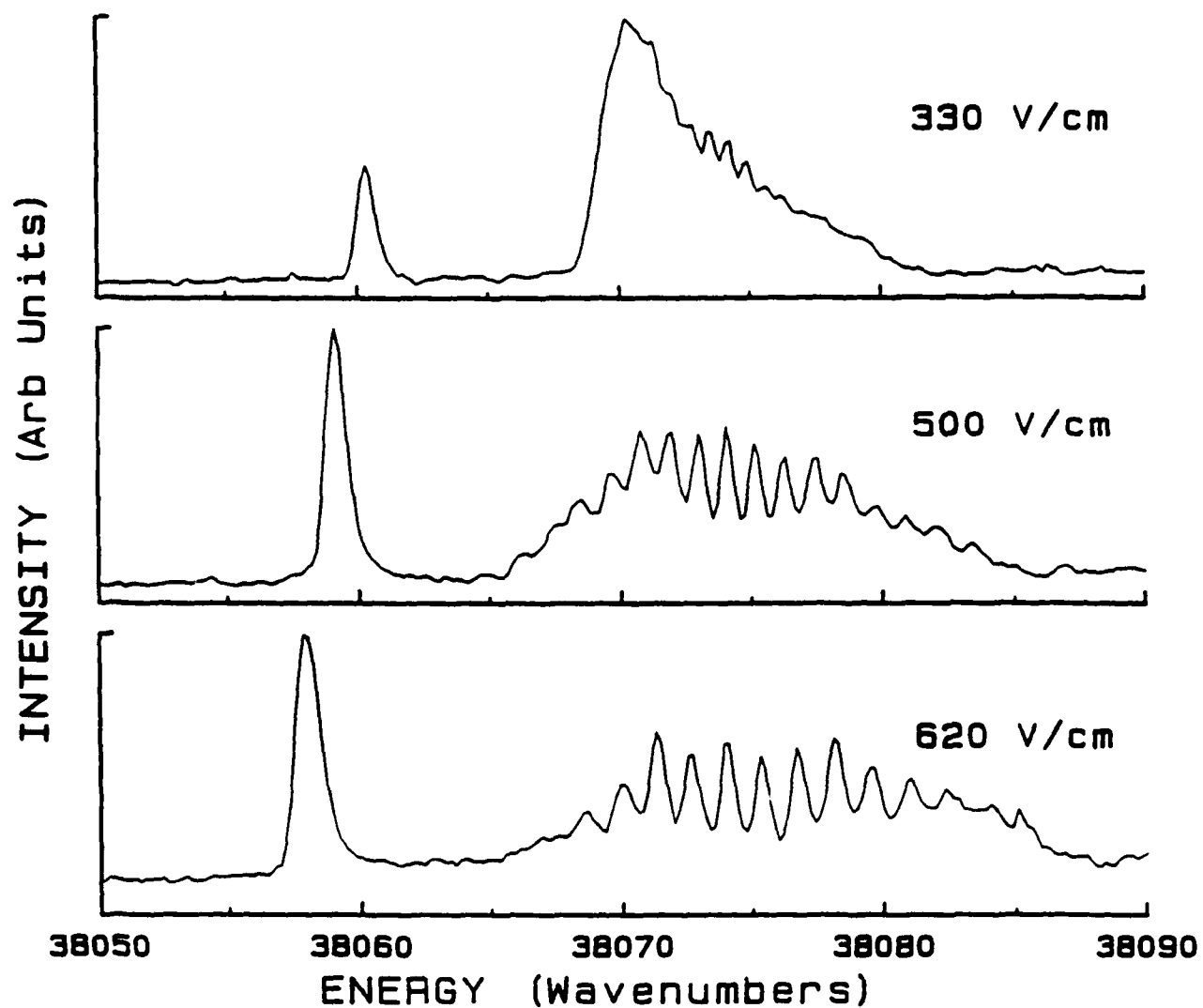


**Figure 2** Triplet helium Stark manifolds,  $n=17$ ,  $\pi$  polarization, as a function of electric field.

The advantage of the large separation of the s-peaks from the rest of the manifold from a diagnostic viewpoint is discussed in Sec V.

### III DC GLOW DISCHARGE ELECTRIC FIELD PROFILE

The energy gained by an electron from the electric field in a plasma determines its influence on ionization, dissociation, excitation, and recombination. Near a cathode the energy gained by ions determines secondary emission and material modification properties as in ion assisted etching. One can measure the local electric field in plasmas using Langmuir probes provided that the plasma is uniform, that there is no net space charge, and that there are no species present which would react with the probe material and influence the measurement. These constraints make probe measurements unsuitable for electric discharges which are characterized by a highly non-uniform field distribution. Fig 3a shows the electric field profile of a normal DC glow discharge. The space charge distribution which gives rise to this field profile is shown in Fig. 3b. The electric field has its highest value at the cathode and decreases linearly over a few mm to a value near zero. This region, which has a positive net space charge, is called the cathode fall or sheath. The sheath occupies a small portion of the discharge yet often accounts for typically 90% of the total voltage drop across the discharge. The field has a small, fairly uniform value past the sheath in a region known as the negative glow, where ionization balancing losses are satisfied by the high-energy beam component of the electron energy distribution function (EEDF) emitted from the sheath. The beam component's energy will be relaxed by inelastic collisions. Elastic collisions randomize the electron velocities. In a transition region known as the Faraday dark space, ionization and excitation by the beam component are complete and there are sufficient electrons diffusing

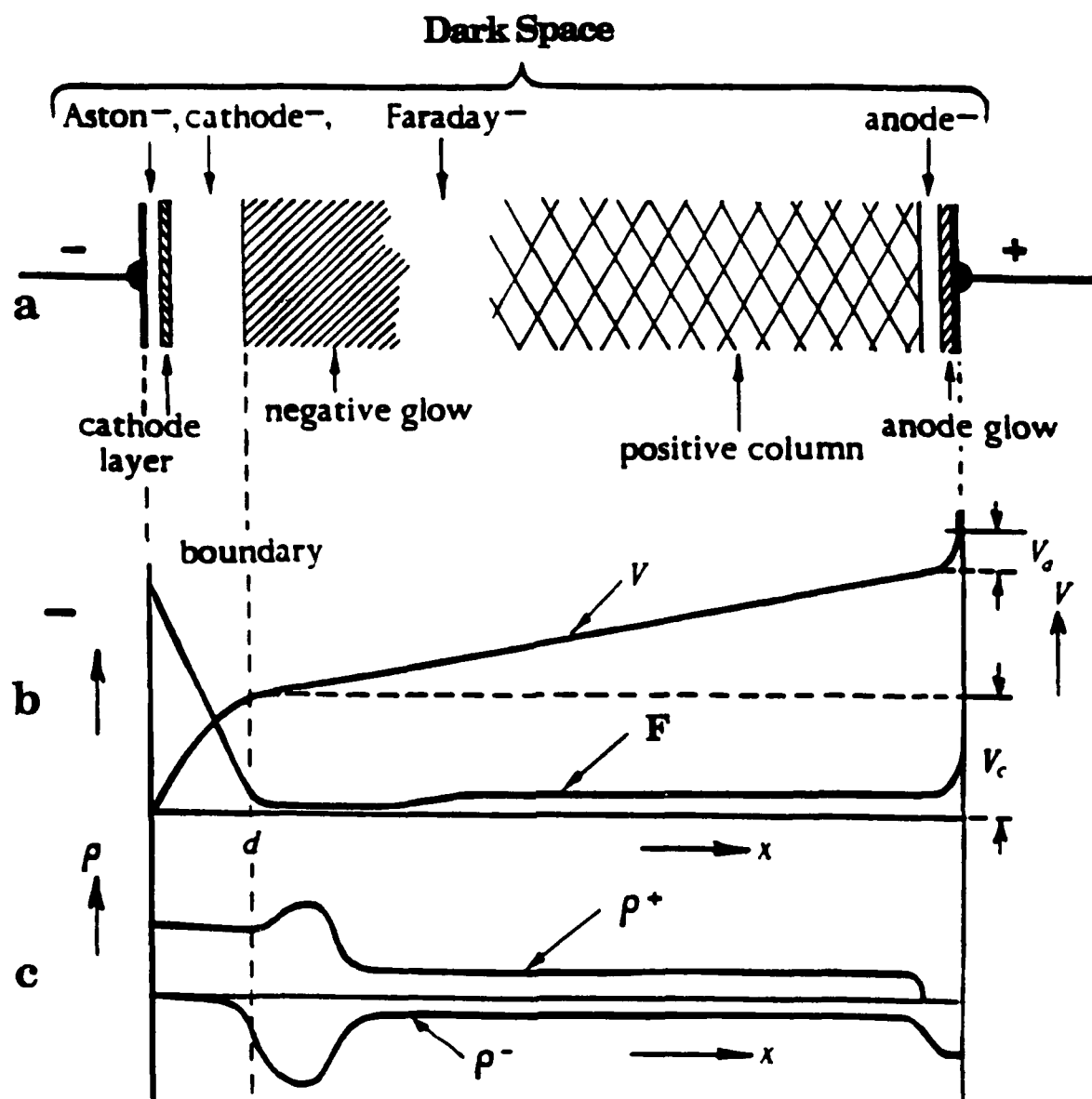


**Figure 3** DC glow discharge spatial profiles

(a.) Spatial distribution of dark and luminous zones in a DC glow discharge. (b.) Electric field ( $F$ ) and voltage ( $V$ ) profiles. (c.) Space charge density profiles ( $\rho^+$  and  $\rho^-$ ).

from the negative glow to satisfy current continuity. As the density decays, the electric field increases and eventually ionizations of an approximately isotropic EEDF are sufficient to satisfy ionization balance; this marks the beginning of the positive column. The axial electric field in the positive column is reasonably small and uniform in the absence of instabilities, but ambipolar diffusion sets up strong radial fields and gradients. The positive column is terminated by the anode, which attracts or repels electrons depending on its area, setting up negative or positive space charge. This space charge sets up an anode sheath, whose voltage drop is usually less than the ionization energy of the species present. The axial dimension of the anode sheath is very small, typically on the order of 100 microns.

The space charge distribution which is required for a stable, self-sustained discharge has been investigated in detail by many researchers.<sup>24</sup> This brief description is presented to introduce the range of electric field values, field direction, and other complications which can affect field measurements. Because the electric fields vary over a wide range,  $\sim 1000$  V/cm, to near zero, one cannot use the same spectral feature to measure the fields in all regions of the discharge. One can make a rough estimate of which feature is most appropriate for different conditions by comparing the linear splitting,  $3nF$ , to the instrumental resolution  $R$ . If  $3nF > R$  Stark splitting should be easily observable. If  $3nF \sim R$ , the energy shift of the  $s$ -peaks is easily measured if  $\Delta m = 0$  spectra are available. If  $3nF < R$ , one must fit the manifold profile for helium. For the  $|\Delta m| = 1$  polarization of helium and for the singlet series only the hydrogen line broadening formula can be applied with confidence. For the triplet series, helium line broadening is much

different than that of hydrogen. If  $3nF \ll R$ , manifold overlap of high Rydberg states,  $n > 35$ , is the only technique which can be applied. In this last case, the differences between helium singlet and triplet lineshapes do not significantly affect the results.

#### IV RELATED EXPERIMENTS

Rydberg state Stark spectroscopy has been a topic of considerable interest in the past 15 years, both for validation of theory as well as for plasma diagnostics. The earliest experiments on the Stark Effect were, perforce, emission measurements and thus limited to the low principal quantum number states ( $n \leq 7$ ) produced in glow discharges. Unusual discharge configurations were employed to produce the requisite electric fields (10's to 100's of kV/cm); a good description of one such discharge configuration known as a LoSurdo source is given by Ryde.<sup>3</sup> Although Foster was interested in the atomic physics of the Stark Effect, his plates provide a complete measurement of the cathode sheath electric field profile. The plates show the interesting result that the maximum of the electric field appears to occur some distance away from the cathode for both hydrogen and helium.<sup>14, 20, 25</sup> The helium data in Ref 26 shows the presence of molecular impurities, and that similar field profiles have recently been observed in this laboratory in a hydrogen discharge in geometries where there are guard insulators adjacent to the electrodes, and are likely to be configuration dependent.<sup>26</sup>

The development of tunable dye lasers enabled the production of Rydberg atoms independent of discharge sources. This has lead to two classes of Rydberg Stark spectroscopy experiments: atomic physics oriented experiments conducted under well defined field conditions (Stark cells), DC and RF, and plasma diagnostic experiments. The Stark structure of hydrogen Rydberg states would be the obvious first choice because its theoretical description is the simplest, however, excitation of hydrogen is difficult because of its high ionization energy, 13.6 eV. Koch and Mariani<sup>27</sup> developed an excitation scheme based on a fast atomic beam.



A fast proton beam is generated and charge exchanged to create the fast neutral beam. The charge exchange process creates a distribution of excited states in the neutral beam; electric field ionization (EFI) is used to eliminate excited states with  $n > 10$ . A collinear  $^{12}\text{C}^{16}\text{O}_2$  laser is used to excite transitions from  $n=10$  to high Rydberg states,  $n=60$  to  $100$ . Doppler tuning of the neutral beam, and/or a series of EFI plates is used to select specific transitions. The electric field ionization of specific  $l$ -states of the high Rydberg states was then investigated in detail. Pinnaduwa<sup>28</sup> later used this setup with microwave fields to investigate the chaotic aspects of the field ionization of Rydberg states. Nayfeh<sup>29</sup> used laser excitation of the hydrogen ground state to investigate hydrogen Rydberg states. Two photon absorption at  $243\text{ nm}$  connects the  $1s$  and  $n=2$  states of hydrogen; a second tunable laser excites the Rydberg levels from  $n=2$ . The power of the  $243\text{ nm}$  laser must be carefully adjusted because three photon absorption will ionize hydrogen. In Nayfeh's experiments the  $243\text{ nm}$  beam was produced by mixing the Nd:YAG  $1.06\text{ micron}$  fundamental with the doubled output of dye laser pumped by the first harmonic of the Nd:YAG. Delsart et. al. <sup>30</sup> used very narrow linewidth two-step laser excitation from the atomic hydrogen ground state and were able to resolve the manifold splitting of  $n=33$  under an electric field of  $23.6\text{ V/cm}$ . Agreement between the measured  $l$ -state relative intensities and those predicted by Schrodinger was found to be excellent. Recently, nonlinear crystals have been developed which can frequency double at  $486\text{ nm}$  and produce the  $243\text{ nm}$  photons more directly.

Experimental investigation of the Stark Effect on alkali atoms is easier because their low ionization energy makes excitation from atomic ground states

possible. In conjunction with his calculations, Zimmerman<sup>23</sup> measured the spectra of the  $n=15$  and adjacent manifolds in cesium and lithium from 0 to 6000 V/cm. As in subsequent alkali experiments, a thermally generated, collimated atomic beam is crossed with one or more laser beams between electrodes designed to produce a spatially uniform electric field. The background pressure is kept low, around  $10^{-6}$  T, to preclude breakdown. After the excitation, a ramped high-voltage pulse is applied to ionize the Rydberg atoms, and the resulting ions or electrons are collected. Several groups<sup>3, 4</sup> have applied very narrow linewidth (Mhz) lasers and well shielded Stark cells to observe very high Rydberg states. The highest reported state observed in the laboratory is  $n = 520$  in barium<sup>4</sup>. This means that the stray fields present were less than  $45 \mu\text{V/cm}$ .

An interesting feature of Stark spectra which has received considerable experimental and theoretical attention is the so-called avoided crossing which arises from interactions between adjacent principal quantum number manifolds. As can be seen from Eq 4, the energies of  $l$ -states with  $l < 0.5 n$  ( $n_1 < 0.5 n$ ) are shifted lower (more tightly bound) as the electric field increases, while the energies of  $l$ -states with  $l > 0.5 n$  ( $n_1 > 0.5 n$ ) are shifted higher in energy (less tightly bound). If the energies of the  $l$ -states of two adjacent  $n$ -manifolds are plotted as a function of field, the red shifted  $l$ -states of principal quantum number  $n$  would apparently overlap with the blue shifted  $l$ -states of the  $n=n+1$  manifold. However, with the exception of hydrogen which possesses a purely symmetric Coulomb central potential, the  $l$ -states repel each other as they approach, producing the feature known as an avoided crossing<sup>31</sup>. This level repulsion is actually stronger than the Stark effect, because the levels are actually shifted

opposite to the field induced energy shift. Chardonnet<sup>32</sup> has measured this interference in cesium over the range of  $n$ 's from 40 to 50. In his theoretical approach, the  $l$ -states of the cesium manifold with zero quantum defects are treated as an incomplete hydrogen manifold interacting with a few discrete states, the low  $l$ -states with appreciable quantum defects. This approach is conceptually simpler than a diagonalization of the complete multi- $n$  energy matrix, however, diagonalization is still required to accurately calculate the relative line intensities.

The interaction of the states involved in an avoided crossing changes the lifetimes of these states, sometimes by as much as a factor of  $10^3$  across the range of electric fields where the avoided crossings occur. This means that the electric field can be measured with very high accuracy, but only over a very narrow range of electric fields.<sup>33, 34</sup> For example, one might be able to measure the electric field between 3000 V/cm and 3040 V/cm with mV/cm accuracy around one avoided crossing. However, if the electric field value is outside this narrow interval, this technique will not have any sensitivity. There are a number of such discrete avoided crossings distributed over a wide range of electric fields, however, in order to exploit the high sensitivity of any one of them, one must be able to predict the electric field to within approximately 1%. In most (if not all) plasma experiments, this requirement is too restrictive to make this technique useful as an electric field diagnostic.<sup>35</sup>

The Stark structure of helium Rydberg states is of considerable interest because helium is the simplest multi-electron atom. However, helium has the largest ionization energy of any species, 24.7 eV, making excitation difficult. Cooper and Saloman<sup>21</sup> were able to excite helium from the ground state to  $n=7$  to

10 in electric field up to 31.5 kV/cm using synchrotron radiation from the SURF II storage ring. Foster's diagonalization procedure was used to calculate the energy shifts and manifold intensity distributions for  $n=7$  and 8 in both the  $\Delta m=0$  and  $\pm 1$  polarizations. The linewidth of the synchrotron radiation was very large, 27 cm<sup>-1</sup>, larger than the Stark splittings at 31.5 kV/cm so the manifolds were not resolved. Qualitative agreement with Foster's diagonalization was obtained, but the low resolution of the experiment hampered quantitative comparisons. Recently Lahaye and Hogervost<sup>5, 36</sup> have performed high resolution (Mhz) measurements on helium. They used the flowing afterglow of a helium discharge to produce 2S metastables, which lie approximately 20 eV above the ground state. A frequency doubled CW ring dye laser (approx 260 nm) was used to excite the metastables to the Rydberg states around  $n=40$  to investigate avoided crossings. Since Foster's procedure cannot handle  $n$ - $n$  interactions, Zimmerman's procedure was used. Because of the high resolution, up to 5  $n$  values (38,39,40,41,42) were included in the matrix to match the experimental spectra. Because the model does not account for effects such as the enhanced tunneling probability, i.e., interaction with the continuum states, the theory does not discuss the experimental linewidths. Mariani<sup>37</sup> investigated the ionization of helium Rydberg states around  $n=30$  in microwave fields. The Rydberg states were produced using a fast neutral beam and CO<sub>2</sub> excitation, as in the hydrogen experiments described above. The ionization threshold for microwave fields was found to be lower than the static field value, and corresponds to the field value at which the outermost  $l$ -states of adjacent  $n$ -manifolds overlap. Knight and Wang<sup>38</sup> measured the Stark structure of xenon from 0 to 2000 V/cm. They excited the  $n=17$  manifold from the

6s'[1/2] metastable state. Calculation of the xenon Stark structure was not attempted because extensions of present theoretical treatments would have been required to predict the Stark structure of the heavy noble gases.

Emission spectroscopy of Stark broadening of low lying hydrogen transitions has long been used as a diagnostic for high temperature, fully ionized plasmas, however, the electric fields found in a normal glow discharge are too low to produce a measurable effect on these low lying states. Lawler<sup>39</sup> first applied Rydberg state Stark spectroscopy to measure the electric field in the cathode sheath of a DC glow discharge in helium. The experimental procedure used in this work is essentially the same as his, however, Lawler had a more limited dye laser hence a more limited range of n's which he could address. As previously discussed, excitation from the helium ground state is difficult, however, a significant number of helium metastables are produced in a discharge. At the operating conditions used, pressure of a few Torr, current density 0.1 to 0.5 mA/cm<sup>2</sup>, approximately 10<sup>10</sup> /cm<sup>3</sup> 2S metastables will be produced, which is a sufficient density for laser excitation and detection of the Rydberg states. The linearly polarized, frequency doubled output of a nitrogen pumped dye laser was focused with a cylindrical lens to a strip approximately 0.01 cm wide and 1 cm long. The laser excites transitions from the 2S metastable to the n=11 manifold, with the laser polarization parallel to the electric field in the cathode sheath ( $\Delta m = 0$  polarization). Better spatial resolution is possible, but in this experiment a larger excitation volume was required to improve signal to noise. The Rydberg states produced are very rapidly ionized by collisions with the background neutrals at these pressures because the Rydberg states lie within  $kT_{\text{Neutral}}$  of

ionization, and their collision cross sections, which scale as  $n^4$ , are huge. This increase in ionization causes a change in the discharge conductivity, which can be recorded as a change in discharge current, is called the optogalvanic effect. Because the electric field is measured when the atoms absorbed the laser light, before the collisional ionizations, this technique is truly non-perturbative. At this pressure range, the perturbation to the discharge relaxes in a few microseconds, which constrains the repetition rate of the laser to be slower than this timescale to insure non-perturbative measurements. Foster's diagonalization procedure was used to calculate the helium Stark spectra, and the field was measured from the manifold splittings. This experiment revealed a linearly decreasing electric field in the cathode sheath, as predicted by several theories.<sup>40</sup> Levels up to the  $n=11$  manifold were excited and fields below 500 V/cm were not measured because the splittings could not be resolved. The validity of the spectroscopic field measurements was made by comparing the integrated field profile with the measured discharge voltage; these agreed to within 5%. An effect which was noted in this experiment was the varying linewidth of the l-states across the n-manifold. This effect was ascribed to the width of the laser beam in the presence of an electric field gradient. This effect was later exploited by other experimenters to make direct measurements of the space charge density in the sheath.<sup>41</sup> Lawler later used two-step excitation of the neon metastable to improve spatial resolution and measured the cathode sheath electric fields in a neon discharge.<sup>42</sup> Similarly, one would like to take advantage of metastables in a hydrogen to measure electric fields, however, electric field mixing of the 2S and 2P states in hydrogen removes the metastability of the 2S-state.<sup>43</sup>

Just as an electric field mixes oscillator strength from normally allowed to forbidden atomic transitions, a similar effect also occurs in the electronic spectra of molecules. Gottscho<sup>44</sup> exploited this effect in BCl to measure the cathode sheath electric fields in DC and RF  $\text{BCl}_3$  discharges up to 1 MHz. Laser induced fluorescence was used to measure the ratio of the allowed R branch to the forbidden Q branch. Different vibrational transitions must be used to cover a range of fields. Derouard et. al.<sup>45</sup> have applied this technique to NaK dimers, making both time-resolved field measurements and have mapped out the two-dimensional field profile in a discharge exploiting the polarization of the NaK spectra.<sup>46</sup>

## V EXPERIMENTAL

As mentioned above, the experimental setup used in this work closely parallels that used by Lawler, the significant difference being tunability to shorter wavelengths that enabled excitation of a wider range of helium Rydberg states. This improves the field sensitivity and highlights the  $n$ -dependent manifold intensity distribution. The polarization dependence of the spectra is also accessible in our setup, enabling the measurement of the electric field vector. A diagram of the experiment is shown in Fig 4. The second harmonic of a Spectra Physics DCR-2A Nd:YAG (YAG denotes Yttrium Aluminum Garnet) laser pumps a Spectra Physics PDL-2 dye laser using Coumarin 500 dye. The linearly polarized dye laser visible output ( $0.25 \text{ cm}^{-1}$  FWHM) is frequency doubled by a potassium dihydrogen phosphate (KDP) crystal which is continuously angle tuned to produce the UV output between 260 and 265 nm required to excite the atomic helium Rydberg states from the triplet  $2S$  metastable state. The doubled output of the dye laser using DCM dye is used to produce the 310 to 315 nm output required to excite the singlet  $2S$  helium metastable state. The dye laser fundamental and frequency doubled UV are spatially separated with a Pellin-Broca prism. The visible output of the dye laser is calibrated from atomic argon transitions from the optogalvanic effect on an argon hollow cathode lamp. The optogalvanic voltage changes of the helium discharge and the argon lamp are simultaneously recorded with two separate wideband amplifiers and boxcar averagers, PAR Model 160. The spectra are recorded and stored using a Hewlett Packard 9836A computer which also controls the dye laser scanning. Each data point is averaged



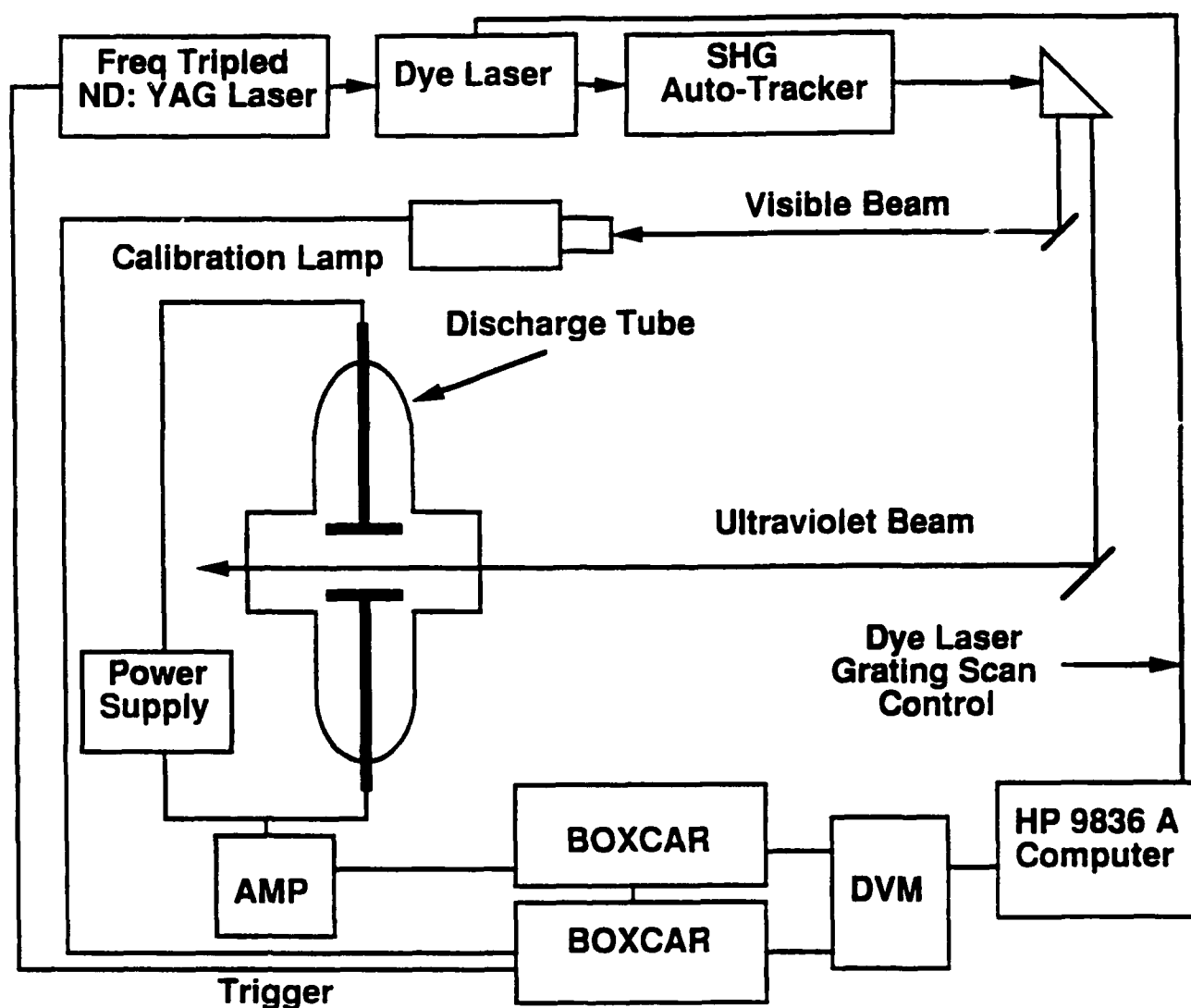


**Figure 4** Experimental setup. A neon hollow cathode discharge lamp was used for calibration of the helium singlet spectra; for the triplet spectra an argon lamp was used.

over at least 10 laser shots with a typical spectrum containing 2000 data points. The Nd:YAG laser operated at 10 hertz with a pulse length of 7 nanoseconds FWHM. The photogalvanic response of the helium discharge has a relaxation time of a few microseconds, so all measurements were made on the unperturbed operation mode of the discharge.

A question which should be considered in the measurement of electric fields by laser excitation of Rydberg states is the effect of the laser electric field on the spectra. In our experiments we typically operate with 200  $\mu\text{J}$ , 7 nsec UV laser pulses with a beam diameter of 200 microns, providing an intensity of approximately  $9 \times 10^7 \text{ W/cm}^2$ . This corresponds to a peak laser electric field of 500 V/cm which is up to 50 times as large as the electric fields spectroscopically measured in the discharges from manifold splittings and Stark induced features. One might expect that the spectra would exhibit the effect of the sum of the laser and discharge fields. The reason that this does not occur is that the laser field is oscillating with a frequency of  $10^{15}$  hertz while the discharge field is a static field. The effect of an AC field is fundamentally different than the effect of a DC field, where DC means that the frequency of the field is very much less than the electron orbital frequency. Bayfield<sup>47</sup> provides an excellent review of the AC Stark effect, in which the primary effect is Rabi splitting. Several authors<sup>48, 49, 50</sup> have considered the effect of laser fields on Rydberg atoms and the related phenomenon of ionization by intense ( $10^{14} \text{ V/cm}^2$ ) laser fields<sup>51</sup> where the primary effect is an enhancement of the ionization rate.

For the laser intensities used in our experiments, such laser induced effects are well below the experimental resolution. A comparison with the high

resolution helium measurements of Ref 37 demonstrates this point. In these experiments, a CW UV laser with an average power of 3 mW was employed. The laser intensity is not reported, however, the authors state that the laser was focussed onto a metastable helium beam approximately 200 microns in diameter. Assuming a laser focus diameter of 50 microns, the laser intensity would be around  $10^6$  W/cm<sup>2</sup>, within an order of magnitude of our experiments. However, the resolution in these experiments is more than a factor of  $10^3$  better than ours (MHz vs GHz) and their spectra do not show any laser induced AC Stark effects.

The negative glow and positive column measurements were made in a sealed 22 cm long hollow (aluminum) cathode discharge tube (Fig 5a) a configuration similar to a HeNe laser. The inner diameter of the pyrex tube is 6 mm, but widens to approximately 8 mm in the observation region because of window mounting stems. The discharge current ranged from 1 to 10 mA with a static gas pressure of 1.2 Torr. For the cathode sheath profile measurements, a sealed parallel plate discharge tube (Fig 5b) with 5 cm diameter aluminum electrodes spaced 18 mm apart was used. All measurements on this tube were taken at a static pressure of 1.5 Torr and a current of 2.5 mA with the discharge always confined to the front sides of the electrodes (normal glow). Two inch diameter Suprasil windows mounted parallel to the discharge axis enable the UV laser beam, collimated to 200 microns diameter to achieve high spatial resolution, to probe the entire discharge volume. The discharge tubes were mounted on motor driven translation stages, Oriel Model 18512 "Stepper Mike", with a spatial resolution of  $\pm 1$  micron. For the cathode sheath profile measurements, the location of the cathode was determined by moving the tube until the UV laser

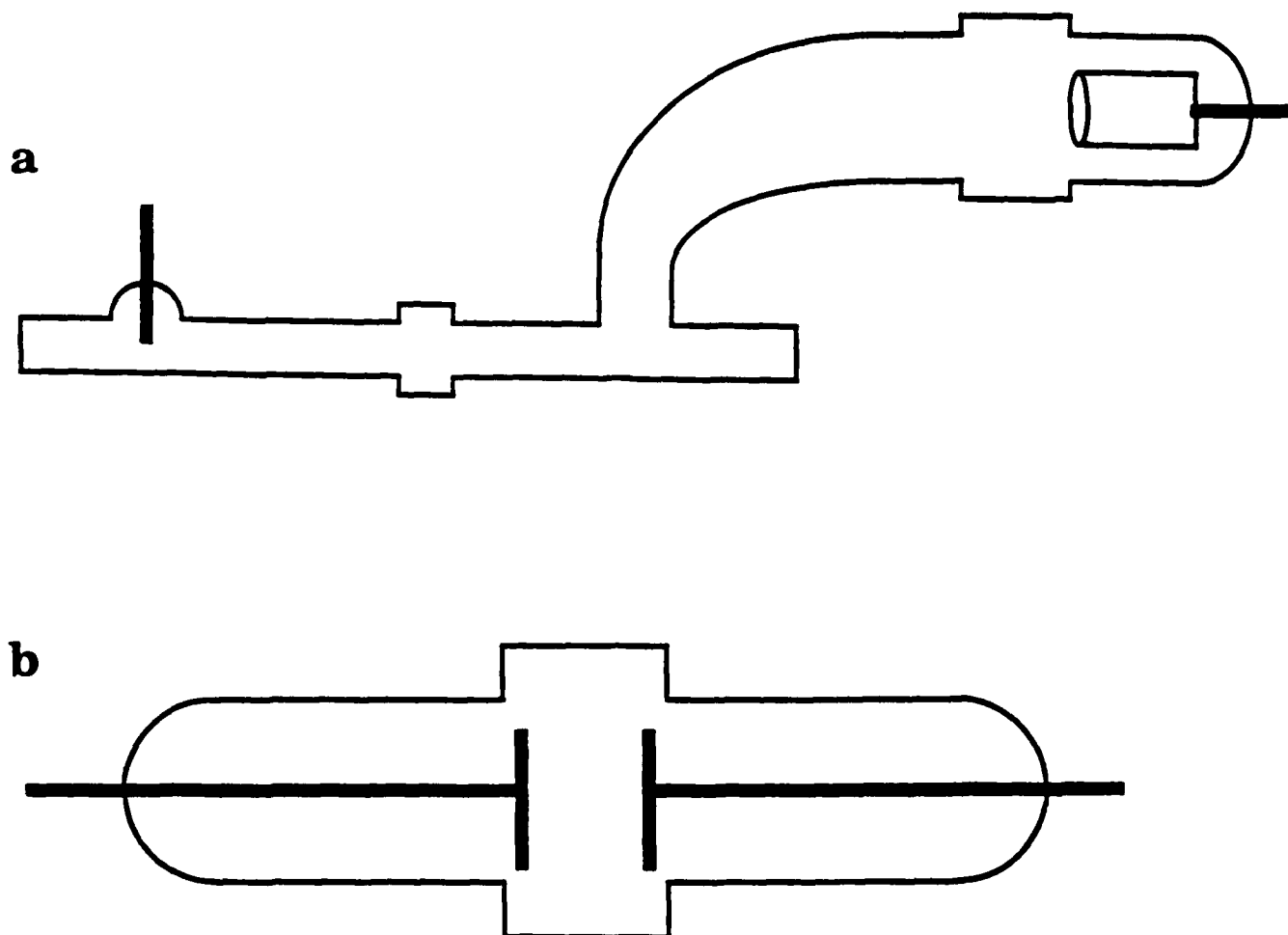


**Figure 5** DC discharge tube configurations

(a.) Hollow cathode discharge tube used for the negative glow and positive column measurements. (b.) Parallel plate discharge tube used for the cathode sheath electric field measurements. Both tubes were constructed out of pyrex with suprasil windows mounted around the regions measured to pass the UV laser beams at normal incidence.

beam struck the front surface of the cathode. This produces photoelectric emission and an easily measured response in the discharge current. The parallel plate tube was mounted either horizontally to record  $\Delta m = 0$  spectra ( laser polarization parallel to discharge electric field vector) or vertically ( laser perpendicular) to record  $\Delta m = \pm 1$  spectra.

The use of optogalvanic detection requires a very quiet discharge tube, especially for the high Rydberg states,  $n=25$  to  $50$ , where the oscillator strengths are very small. Much of the success of our experiments can be attributed to the skill and experience of our glassblower who devised a standard discharge tube processing procedure. After being fabricated, a tube is baked at  $400^{\circ}\text{C}$  for 12 to 24 hours while being pumped, reaching a base pressure  $< 10^{-8}$  Torr at temperature. The tube is then filled with 1 Torr of argon and run up to several hours, switching anode and cathode, to clean the electrodes. The discharge is monitored by observing the voltage drop through a 5-megohm resistor with an oscilloscope. When the white noise of the discharge is less than 5 nA RMS ( out of a current of a few mA) the argon sputtering is stopped. The argon is pumped out and the tube filled with a few Torr of hydrogen. A hydrogen discharge is then run for roughly an hour to clean the inner walls of the tube. The hydrogen is pumped out, the tube filled to the desired pressure of helium, and then sealed. A current-voltage curve for the fresh tube is recorded. Before each day's experiments, the current voltage curve of the tube is recorded. When the current voltage relation for the tube changes by more than 20%, presumably from the diffusion of molecular atmospheric gases whose ionization energies are much less than that of helium, measurements are stopped and the tube reprocessed. Typically a tube will operate

for 2-3 weeks before reprocessing is required.

## VI EXPERIMENTAL RESULTS

### A. Parallel Plate Cathode Sheath Field Measurements

The electric field profile of a glow discharge has long been a topic of interest, both theoretically and experimentally, however measurements in the cathode sheath are hampered by its small spatial dimension and the large field gradients present. Early measurements of the cathode sheath field profile were made using electron beam deflection and showed an electric field which decreased linearly to a small value below instrumental resolution and remained at this low value for some distance into the negative glow.<sup>52, 53</sup> However, this technique is limited to very low pressure discharges, where the electron beam will not be scattered by collisions or cause additional ionization, perturbing the discharge. The spatial resolution of this technique is also limited. Langmuir probe measurements are unsuitable for the cathode sheath because of the high field gradients present, as well as the fact that the presence of a metal probe near the cathode is certain to perturb the discharge. Rydberg state Stark spectroscopy provides a non perturbing, high spatial resolution electric field measurement and can be used over a pressure range used in practical discharges.

Stark induced features of Rydberg state spectra can easily be observed at modest  $n$ 's ( $12 < n < 20$ ) for the range of electric fields found in typical glow discharge sheaths. The helium metastable density is roughly constant across the diameter of the cathode sheath so there is no effect from averaging along the laser beam. The electric field in the cathode sheath is oriented perpendicular to the cathode ( neglecting edge effects ) so the polarization dependence of the Rydberg spectra can be examined in detail. Fig 6 shows a typical  $\Delta m = 0$  polarization

(laser parallel to the discharge field) triplet helium spectrum showing the Rydberg states  $n=14$  to  $20$ . The top scan is the argon calibration spectrum recorded simultaneously with the dye laser fundamental. The polarity of the argon optogalvanic signal is inverted for convenience of display. The absolute wavelength accuracy, using known argon lines, was found to be  $\pm 0.125 \text{ cm}^{-1}$  in the visible, essentially limited by the step size of the tuning of the dye laser grating. This spectrum was taken at an axial distance of  $0.4 \text{ mm}$  from the cathode with a discharge current of  $2.5 \text{ mA}$  and pressure of  $1.5 \text{ Torr}$ . ( All measurements were made under these last two conditions.) This spectrum contains 2000 data points, with the complete spectrum of typically seven manifolds taking about 45 minutes to collect. One can measure the electric field reliably from a single manifold, however, we were interested in comparing the behavior of a range of  $n$ -manifold spectra as well as measuring fields. The narrow, single peaks on the low energy side of the manifolds are the  $2s \text{ } ^3\text{S}$  to  $ns \text{ } ^3\text{S}$  transitions, which are well separated because the S-state quantum defects are an order of magnitude larger than the rest of the l-states.

Several Stark induced features are visible in this spectrum. The manifold splitting is clear and many of the manifolds are completely resolved. At this location the field is large enough that adjacent manifolds for  $n>19$  overlap. Since Foster's procedure does not include  $n$  mixing these manifolds are not used to measure the field. For a constant electric field, the relative intensity distribution of the manifolds changes markedly as a function of  $n$ . The intensity of the s peak grows with  $n$ , while the separation of the s peak from the rest of the



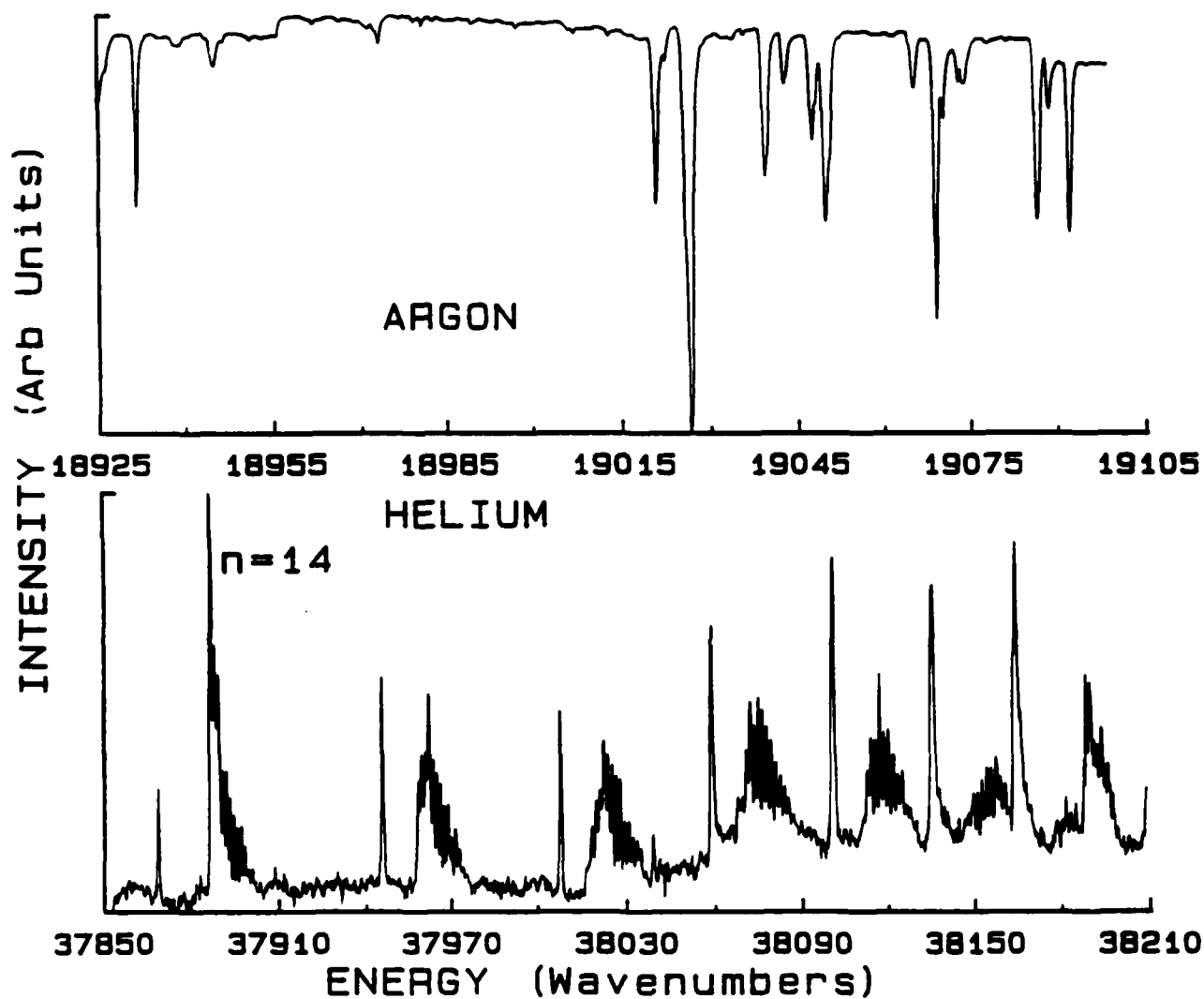


**Figure 6.** Typical triplet helium Stark spectrum,  $\Delta m = 0$  polarization, recorded in the cathode sheath of a parallel plate DC glow discharge. The upper trace is an argon calibration spectrum.

manifold decreases. The background in this spectrum is fairly noisy compared to other cathode sheath spectra because it was taken close enough to the cathode that some of the UV laser beam is scattered onto the cathode causing photoelectric emission. The optogalvanic signal caused by the laser directly striking the cathode is roughly two orders of magnitude larger than the Rydberg signal.

The triplet  $\Delta m = 0$  spectra for  $n=16$  to 18 at three axial distances is shown in Fig 7. Here one can compare field-dependent Stark features for the same  $n$ -manifolds. As the field decreases with increasing distance from the cathode, the location of the  $s$  peaks is seen to shift towards its field free location, and the relative intensity contained in the transition decreases. Because the  $s$  peak can be unambiguously identified, the electric field can be easily measured from the displacement of this peak from its zero field energy. As noted in Ref 21, the hydrogen Stark formula substituting  $n-\partial_s$  for  $n$  fails poorly to predict the field dependent energy shift of the  $nS$  peaks; diagonalization must be employed. The manifold splitting decreases with decreasing field, with only peaks near the center of the manifolds resolvable at 2.5 mm from the cathode. No splittings could be resolved farther than 3.0 mm from the cathode, even though the splittings calculated from the field measured from the  $s$  peak shifts were larger than the laser linewidth. This fact, and the observation that the linewidths of the  $l$ -states near the manifold centers were always narrower than those on the wings of the manifolds, indicated that spatial averaging of the electric field gradient across the laser beam diameter was occurring. We are able to exploit this effect to make direct measurements of the cathode sheath space charge density, which will be discussed later. While the hydrogenic theory will not provide the correct absolute

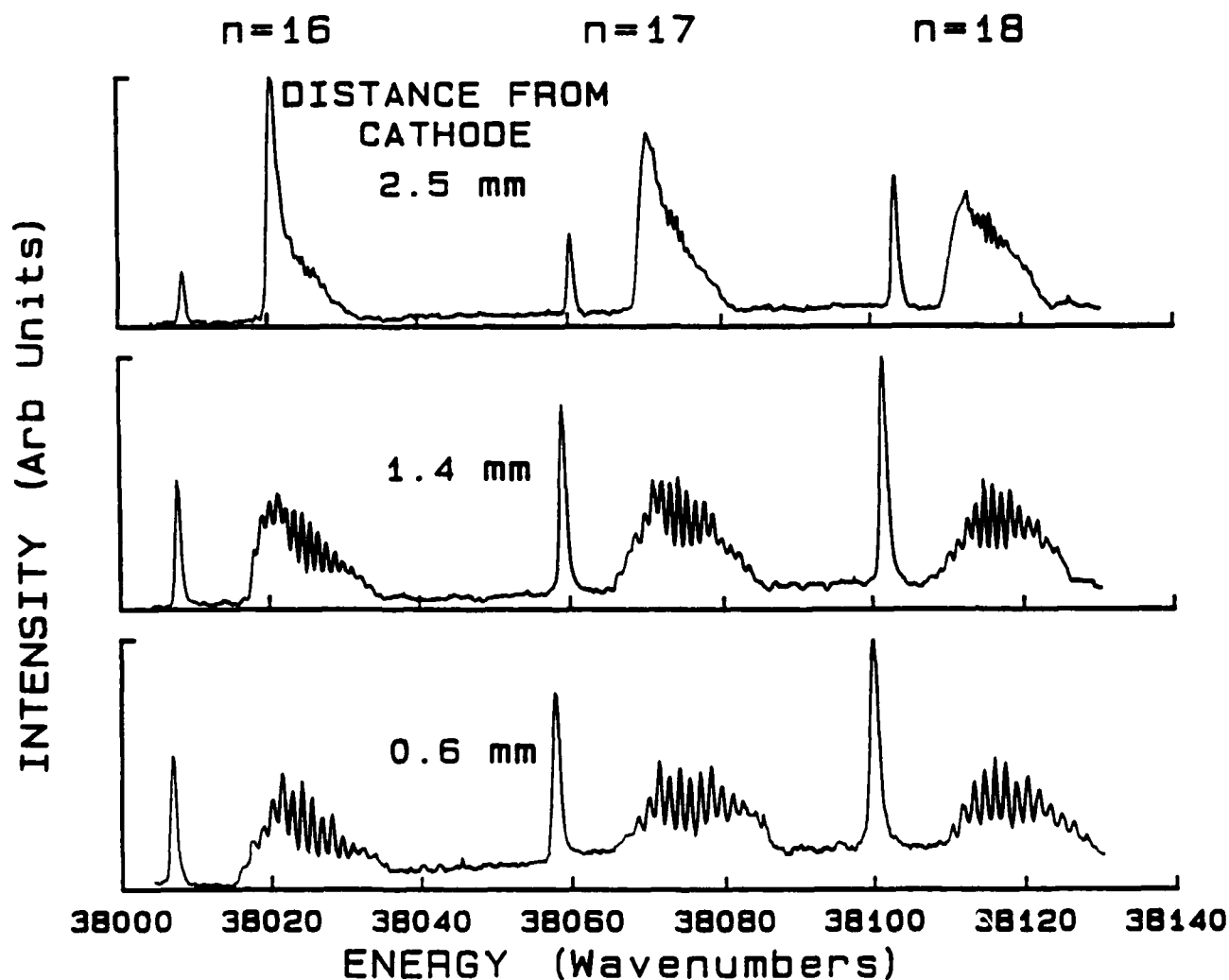


**Figure 7.** Triplet helium Stark spectra recorded at various distances from the cathode. A horizontal slice shows the  $n$  dependence at a constant field value; a vertical slice shows the field dependence at a constant  $n$ .

energies for helium, the calculated separations between adjacent l-states are essentially identical to the diagonalization results for  $l > 4$ , i.e., states with zero quantum defects. However, the correct relative intensities can only be obtained from diagonalization.

The cathode sheath electric field profile obtained from the energy shift of the s peaks as well as the manifold splittings are shown in Fig 8. The values plotted represent the average over several manifolds. The field values obtained by either technique agree well. For these discharge conditions the electric field in the cathode sheath drops off linearly. A check on the accuracy of the spectroscopic field measurements can be made by comparing the integral of the field profile with the measured voltage drop across the tube. The integrated sheath field is 167 volts; the contribution from the negative glow and positive column is estimated from previous measurements to be 15 volts, while the anode sheath drop is estimated to be 25 volts ( the ionization energy of helium). Thus the spectroscopically determined tube voltage is 207 volts, while the measured tube voltage was 212 volts, showing agreement to within 2.5 %.

All measurements were taken on the discharge axis, using the assumption that there is no radial variation of the cathode sheath electric field. This was verified by recording spectra at a fixed axial distance of 2 mm and several locations off axis. The electric field was measured up to 10 mm off axis, where no variation in electric field was found above experimental uncertainty.

In order to investigate  $\Delta m = \pm 1$  polarization spectra, the discharge was rotated 90° so the laser polarization was then perpendicular to the sheath field. In this polarization the 2S to nS transitions are not allowed; the absence of this

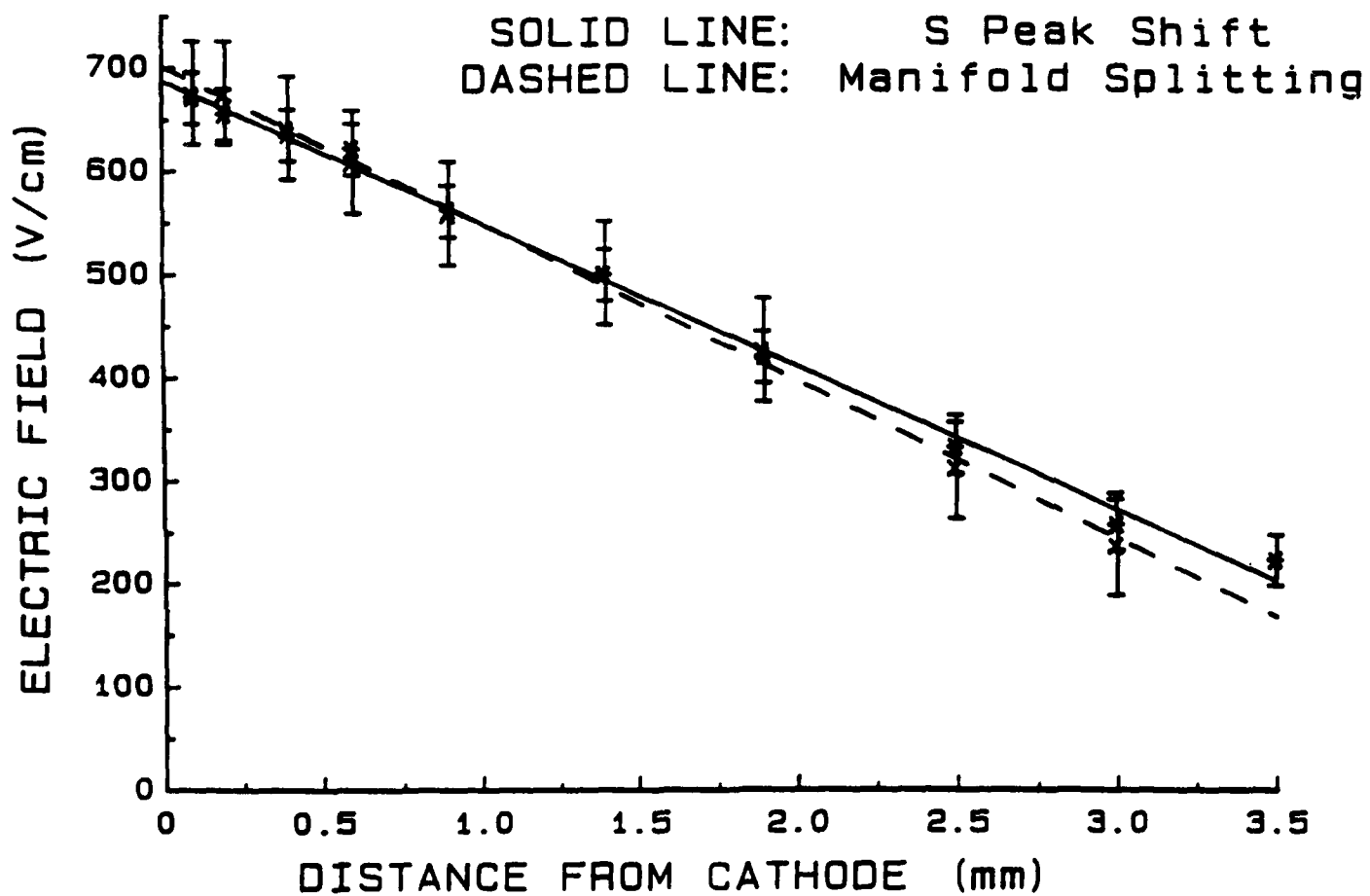


**Figure 8.** The electric field profile in a DC glow discharge cathode sheath measured from the manifold splittings and the shift of the  $nS^3S$  peaks.

transition affects the intensity distribution of the entire manifold. A typical  $\Delta m = \pm 1$  spectrum with  $n=14$  to 21 recorded at a distance of 0.6 mm from the cathode is shown in Fig 9, with the argon calibration spectrum shown above. The small, sharp peaks near the  $n=15$  and 16 manifolds are the 15S and 16S peaks, which appear because the tracking of the frequency doubler used (Inrad Autotracker) was imperfect and rotated the angle of the output UV beam a small amount. This feature was reproduced in all  $\Delta m = \pm 1$  spectra taken in this set of measurements. Because it is a small effect and occurs over only a small portion of the scan range it did not affect the field measurements. However, this highlights the need for laser polarization purity in field measurements.

The triplet helium  $\Delta m = \pm 1$  spectra for  $n=16$  to 18 at several axial distances from the cathode are shown in Fig 10. As in the  $\Delta m = 0$  spectra, the manifold splittings decrease with increasing distance from the cathode. Again the peaks near the manifold centers remain resolved for the lowest field, reflecting field averaging. The variation of linewidths across the manifolds caused by field averaging can also be observed in this data, and the decrease in oscillator strength with  $n$  is apparent. The cathode sheath electric field profile measured from the manifold splittings is shown in Fig 11. Notice that the electric field values are approximately 100 V/cm higher than measured in the  $\Delta m = 0$  polarization spectra. This difference reflects a change in the discharge conditions, not a difference in the field sensitivity between the two polarizations. The  $\Delta m = \pm 1$  measurements were made 5 weeks before the  $\Delta m = 0$  measurements, and the discharge tube was reprocessed during this time. Before reprocessing, the measured tube voltage was 222 volts, and the decrease in tube voltage to 207 volts at

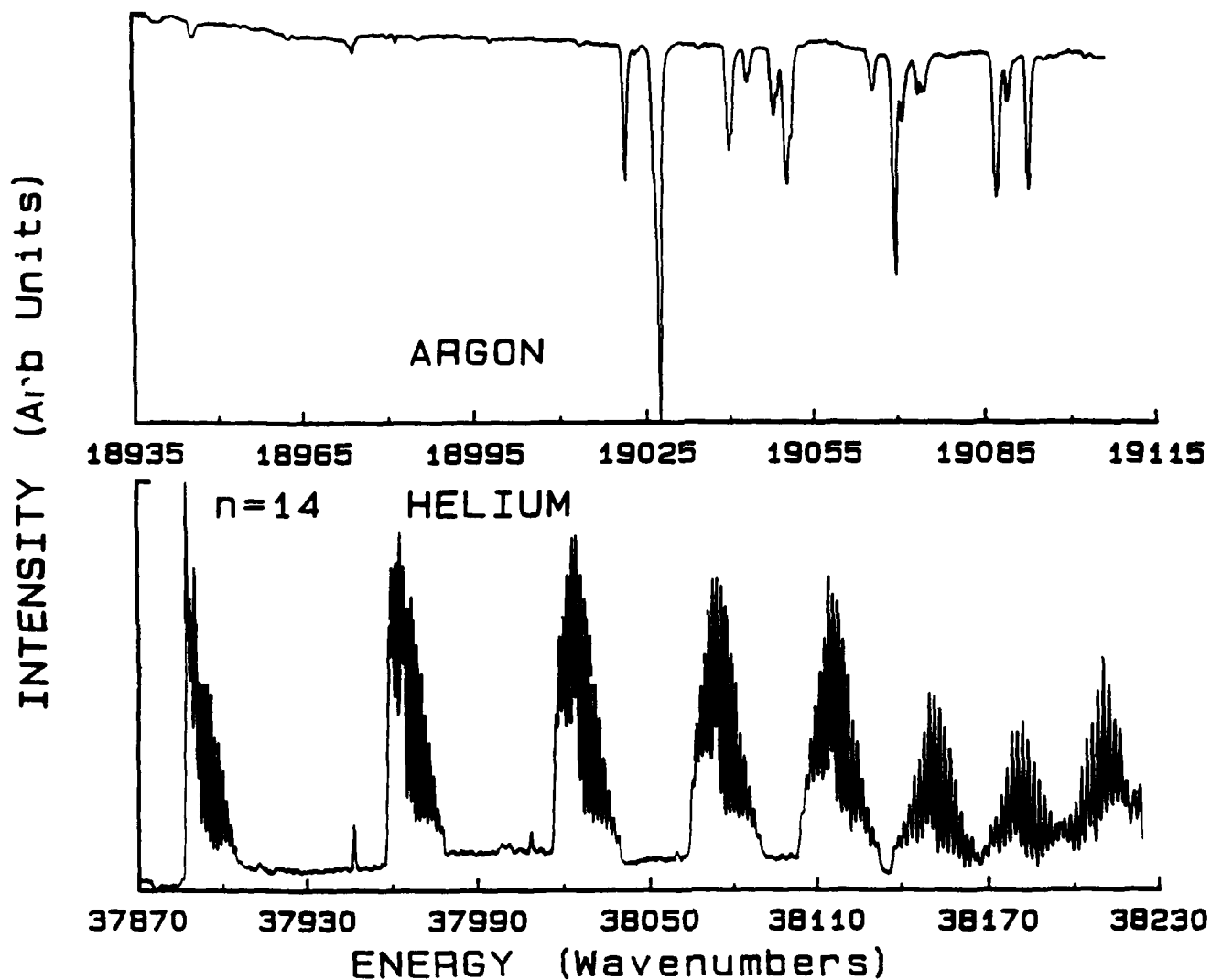


**Figure 9.** Typical triplet helium Stark spectrum,  $\Delta m = 1$  polarization, recorded in the cathode sheath of a parallel plate DC glow discharge. The upper trace is an argon calibration spectrum.

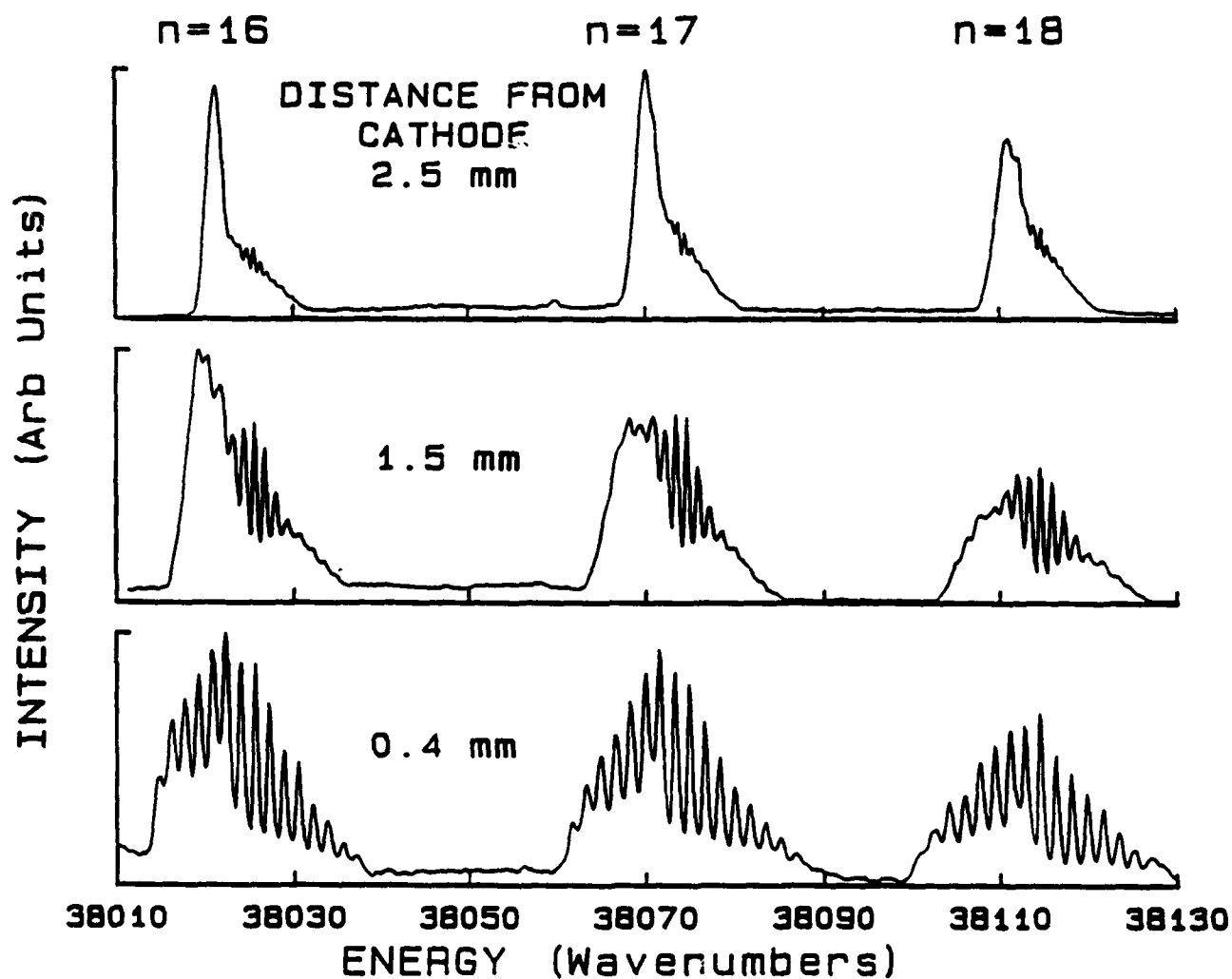


**Figure 10.** Triplet helium Stark spectra recorded at various distances from the cathode. A horizontal slice shows the  $n$  dependence at a constant field value; a vertical slice shows the field dependence at a constant  $n$ .



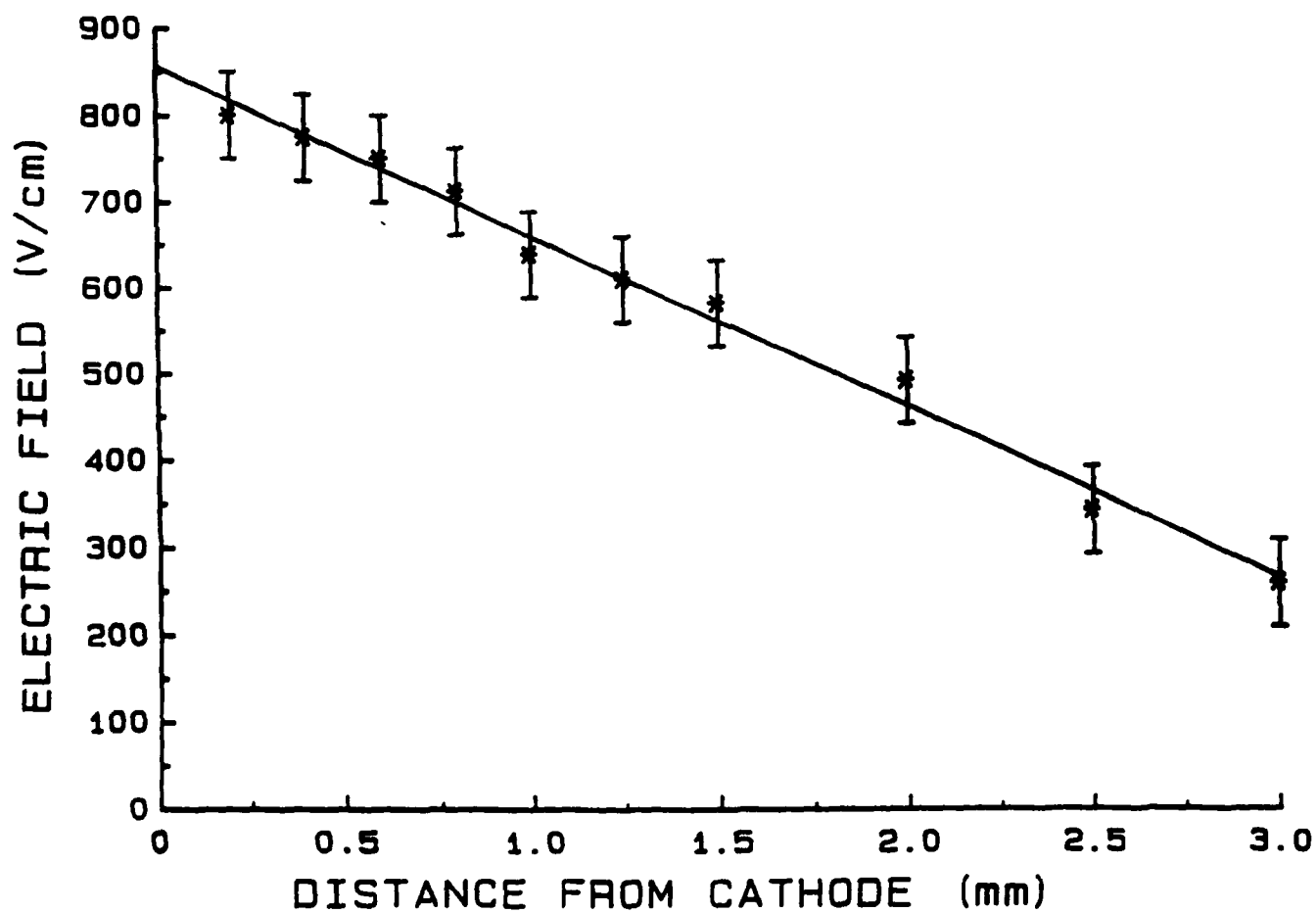


**Figure 11.** The electric field profile in a DC glow discharge cathode sheath measured from the manifold splittings.

the same current, 2.5 mA, was not thought to be significant. However, as the data shows, this assumption proved to be false, highlighting the sensitivity of these measurements to small changes in the discharge. The accuracy of the spectroscopic field measurements was again verified by comparing the integrated field profile, 227 volts, to the measured tube voltage of 222 volts, again agreeing to within 2.5%.

#### B. Negative Glow and Positive Column Measurements

Measurement of the electric fields in a discharge outside the cathode sheath is a much more complicated problem for a number of reasons. The magnitude of the electric fields are low, less than 40 V/cm, so Stark splitting even for high Rydberg states,  $n > 25$ , cannot be resolved with the standard laboratory pulsed dye laser resolution of 0.3 to 1.0  $\text{cm}^{-1}$ . The energy shifts of the  $nS$  peaks are also below resolution, and their-field dependent intensity often makes them difficult to distinguish from the background. One must rely on other Stark induced features, "broadening" and series termination, for field measurements. However, the interpretation of these features is often ambiguous under discharge conditions where one must worry about charged particle collision induced field effects (microfield) as well as axial field effects. In most applications the effect of the microfield has been treated under the quasistatic approximation, however, our data suggests that this approximation may not be valid for high Rydberg states. Because the positive column is diffusion dominated, a radial field, which for narrower tubes can be larger than the axial field, is also present. The direction of the net field will be a vector combination of all these fields which cannot be predicted, however, one can exploit the polarization selection rules to measure the

field vector.

The data to be presented are the results of several previous experiments.<sup>54</sup> Because they were taken over a wide range of operating conditions correlations between the different sets will not always be made. In the previous papers the data was analyzed using standard literature treatments of hydrogen line broadening and series termination. Since high Rydberg states of helium were involved, the consensus at the time was that the behavior of these states would be sufficiently hydrogen-like that using the techniques derived for hydrogen was acceptable. Subsequent analyses have shown that this assumption is invalid, and that the standard treatments of broadening and series termination are only approximations which fail for high Rydberg states. The definition of series termination was also misquoted, and unfortunately the error has been propagated in the literature for the past 50 years. The problems with these techniques will be discussed in detail in the next section of this report, as well as the inherent limits on electric field measurements in glow discharges using Rydberg state Stark spectroscopy.

A representative singlet helium negative glow spectrum is shown in Fig 12. A neon calibration spectrum recorded from the photogalvanic signal of a neon lamp using the visible output of the dye laser (DCM dye) is shown above with the 621.728 nm line present. Because of the low electric field present in the negative glow is low, helium transitions up to  $n=45$  can be observed. The absence of the 2S to nS transitions indicates that this polarization purity ( $\Delta m = 1$ ) of this spectrum is (nearly) 100%. Features which should be noted are the decrease in peak intensity as a function of  $n$ , the increase in linewidth with  $n$ , and the symmetry of

the lineshapes. Because the electric field broadens the peaks, and the separation between adjacent  $n$  peaks is fixed, the electric field will modify the last  $n$  value which can be resolved in the Rydberg series spectrum. Inglis and Teller<sup>24</sup> derived a relation for this lowering of the continuum which is commonly described as "series termination." The electric field measured from this "series termination" of this spectrum is given by

$$F = \frac{1}{3n_m^5} \quad (9)$$

where  $n_m$  is the  $n$ -state peak which has merged into the continuum, customarily, and incorrectly, taken to be several  $n$ -states beyond the last resolved peak.. For  $n_m$  of 45 the electric field is  $9.2 \pm 3$  V/cm. The uncertainty in the field arises from an uncertainty in identifying the series termination by  $\pm 1$ . The electric field measured from the broadening of the  $n = 30$  transition is  $18.8 \pm 5$  V/cm using the formula given by Griem<sup>55</sup>

$$\Delta\omega = \frac{3h}{2emz}(n_i^2 - n_f^2)F \quad (10)$$

where  $\Delta\omega$  is the half width at half maximum. The field values obtained from these two techniques vary by more than a factor of two, and the broadening result is high for the negative glow. Since the field measured is the sum of the axial and microfields, this value may not be unreasonable. However, one can infer that the influence of the microfield is small because the polarization purity of the spectrum indicates that the field present is dominantly anisotropic.

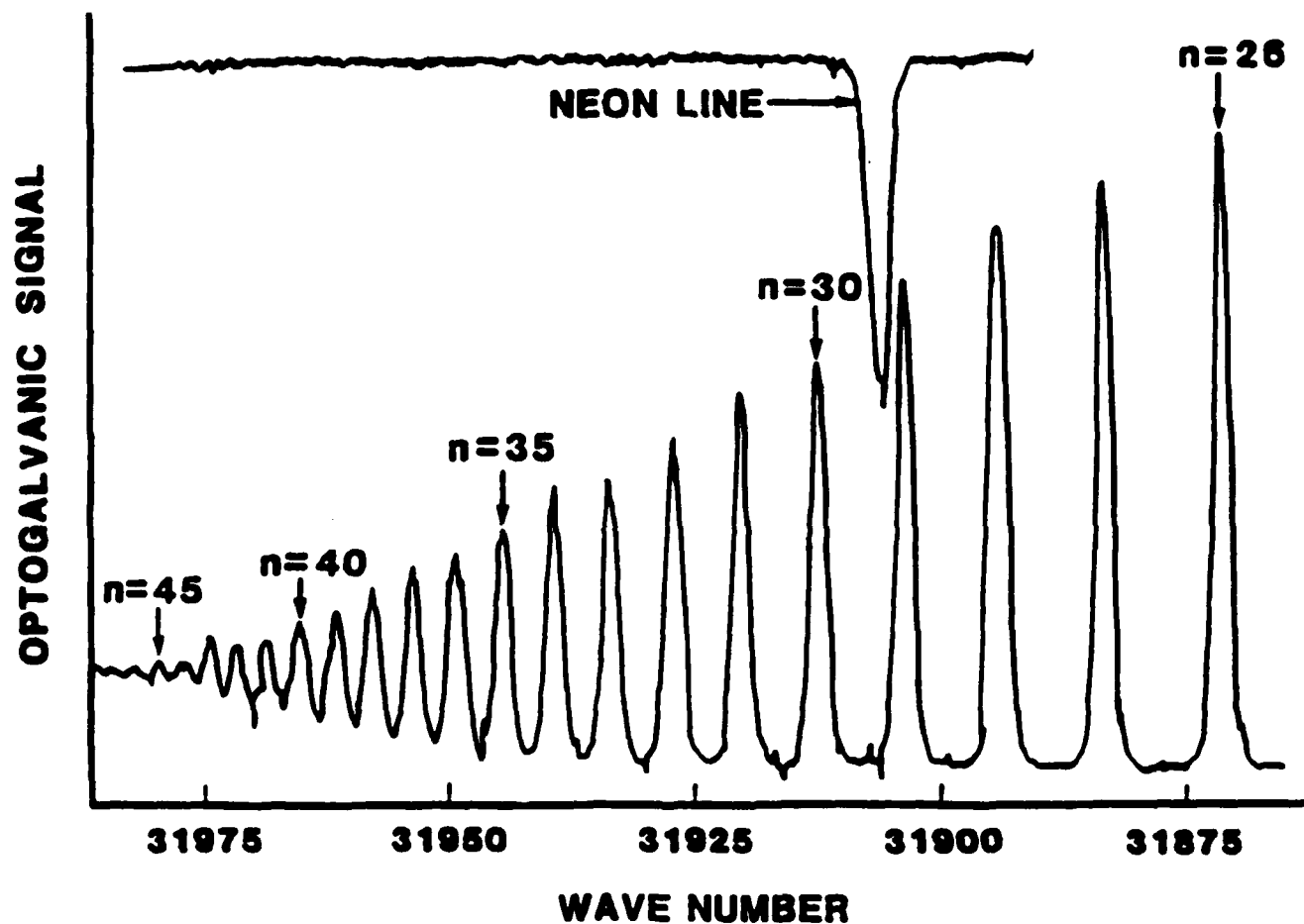


**Figure 12** Singlet helium Rydberg series spectrum,  $\Delta m = \pm$  polarization, recorded in the negative glow of a DC glow discharge. The upper trace is a neon calibration spectrum.

For contrast, a triplet helium negative glow spectrum with an argon calibration spectrum is shown in Fig 13. The conditions under which this spectrum was taken are similar to the singlet spectrum because the last resolved peak is also  $n=45$ , and the absence of the  $2S$  to  $nS$  transitions indicates good polarization ( $\Delta m = 1$ ) purity. However, the triplet peaks are seen to be asymmetric for the lower  $n$ 's, gradually becoming more symmetric near the series limit. This is a clear indication that even for high  $n$ 's, the behavior of Rydberg states of helium still shows the effect of the quantum defects, i.e., helium behavior really never becomes "hydrogenic". We will later show that the symmetry of the singlet peaks occurs because the  $n^1P$  quantum defects are negative. The asymmetry of the triplet peaks raises a question about applying hydrogenic line broadening, however, ignoring this issue for now, a field value of  $26 \pm 5$  V/cm is obtained, again quite high for a negative glow. For comparison, a  $\Delta m = 0$  polarization triplet helium spectrum is shown in Fig 14. Here the  $2S$  to  $nS$  transitions are clearly visible. The relative intensity of the  $S$  peaks grows with  $n$ , but because the spacing between the  $n$ -manifolds is decreasing they become buried in the background. Note that the linewidths of the peaks from the rest of the  $n$ -manifolds do not increase very much, being essentially constant to within experimental uncertainty, though from Griem's formula the linewidth should increase as  $n^2$ .

The oscillator strength of the  $n$ -state transitions falls off as  $n^{-3}$ ; line broadening goes as  $n^2$ . Thus the intensities of the  $n$ -state peaks would be expected to fall off as  $n^{-5}$ . However, it is apparent that the decrease in the  $n$ -state peak intensities in the experimental spectra do not follow the same relation, and as will be shown later, deviate significantly from an  $n^{-5}$  fall off. The laser power was not

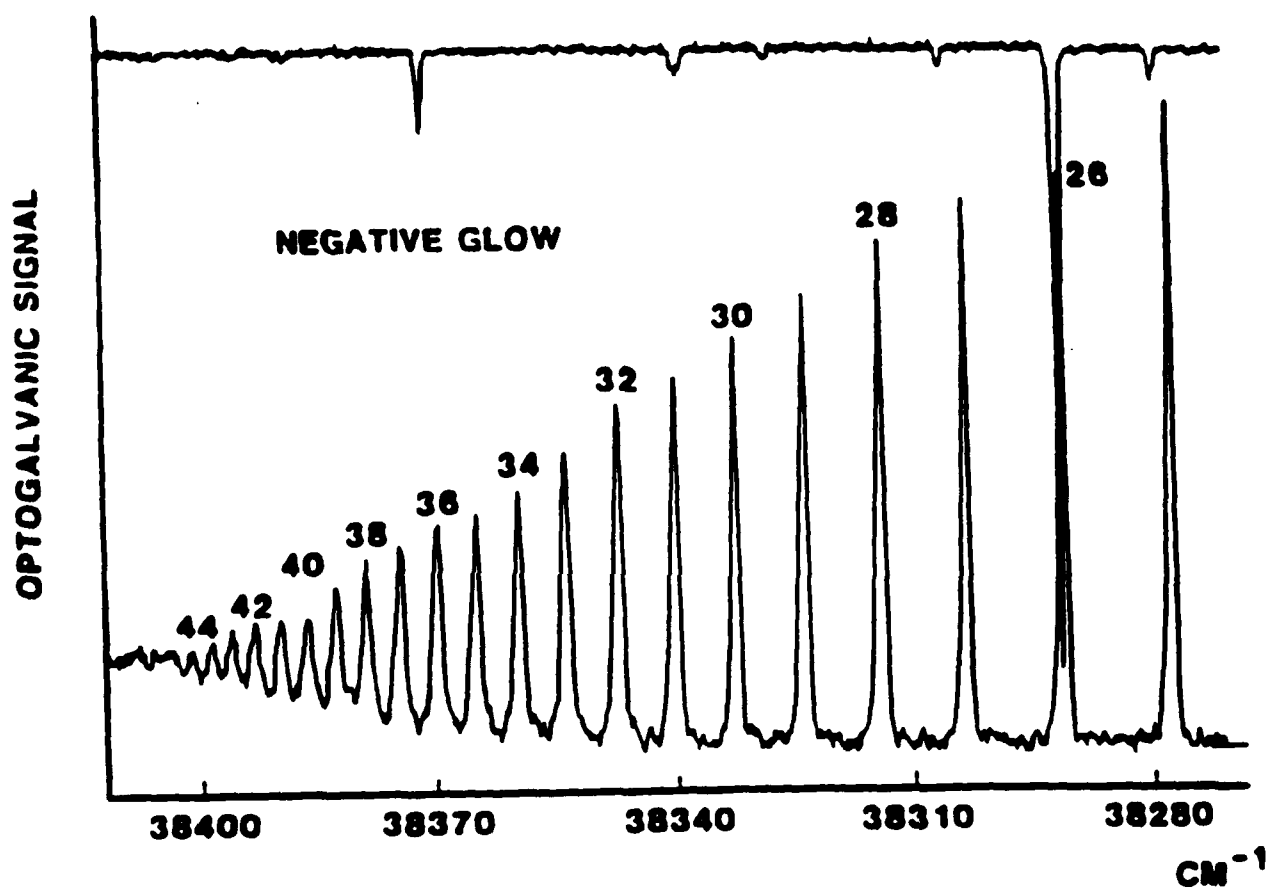


**Figure 13** Triplet helium Rydberg spectrum,  $\Delta m = \pm 1$  polarization, recorded in the negative glow of a DC glow discharge. The upper trace is an argon calibration spectrum.

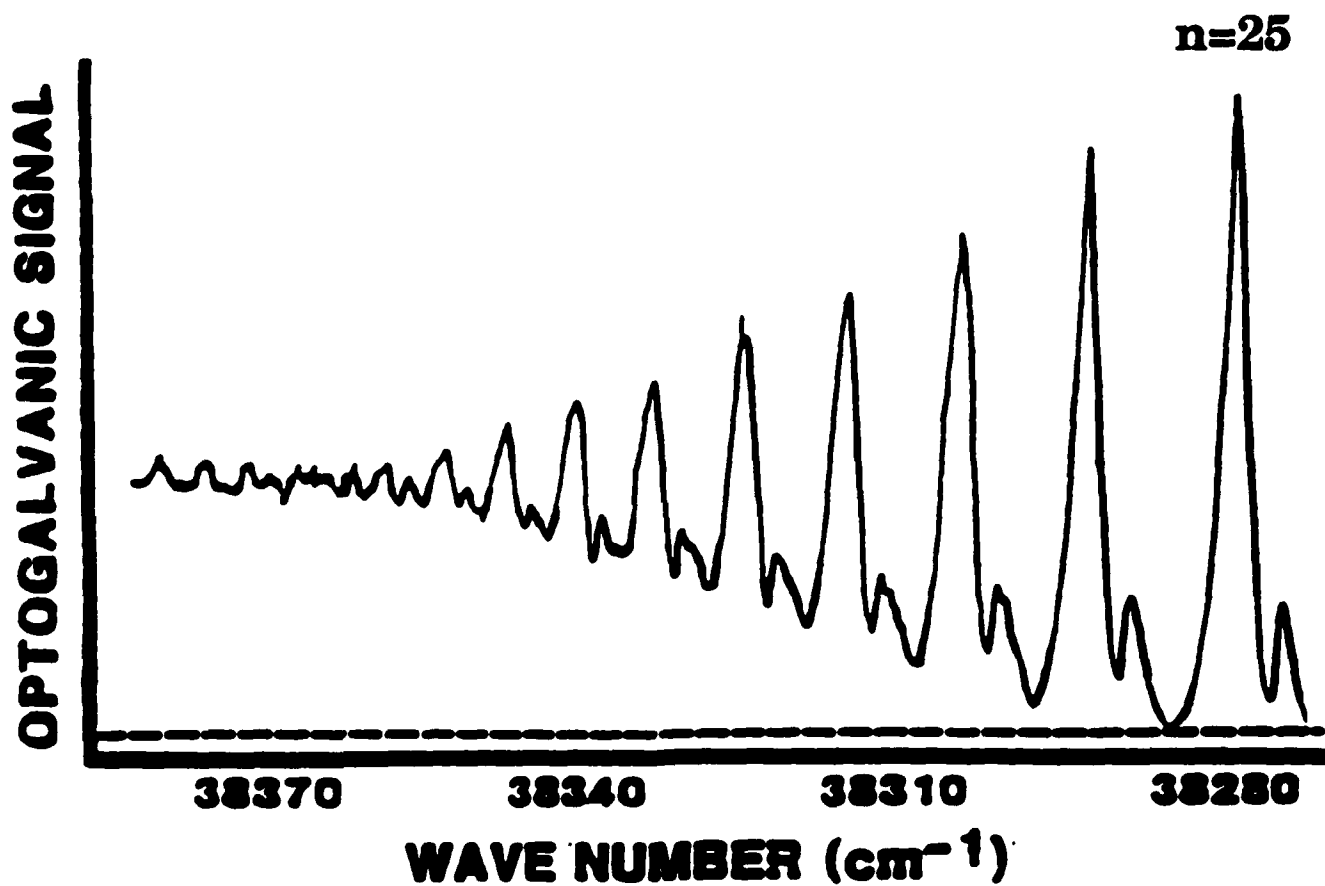


**Figure 14** Triplet helium Rydberg series spectrum,  $\Delta m = 0$  polarization, recorded in the positive column of a DC glow discharge.



recorded while these spectra were taken, however, DCM (singlet helium) and Coumarin 500 (triplet helium) laser dyes produce essentially constant power over the wavelength regions over which these spectra were taken, so the abnormal intensity drop-off cannot be attributed to a variation of laser power. Because these experiments rely on collisional ionization of the Rydberg states to produce the optogalvanic signal, an  $n$ -dependence in these cross sections could account for the abnormal intensity drop-off. However, Rydberg state collision cross sections are in general roughly constant for  $n > 20$ , so the difference in the  $n$ -state cross sections is not enough to account for this feature. The  $n$ -state intensity drop-off is important because it implies that electric field broadening is not the dominant source of broadening in these experiments, under these conditions the Rydberg state-background ground-state helium atom collisions provide the major contribution to the measured linewidth. Thus the standard line broadening approach to measuring electric fields, as well as series termination which relies on line broadening, is not valid for these plasma conditions, and different approaches are required.

The net electric field in the positive column is a sum of an axial field, a radial field arising from diffusion, and the so-called microfield created by the presence of the space charge. Depending on discharge conditions and radial location in the discharge, the relative magnitudes of these three fields will change. Because the Rydberg atom will respond to the net electric field present, the spectrum will show the effect of the vector sum of these three fields, whose individual contributions can be difficult to separate. Fig 15 shows singlet helium spectra taken at various radial positions in a positive column. The center

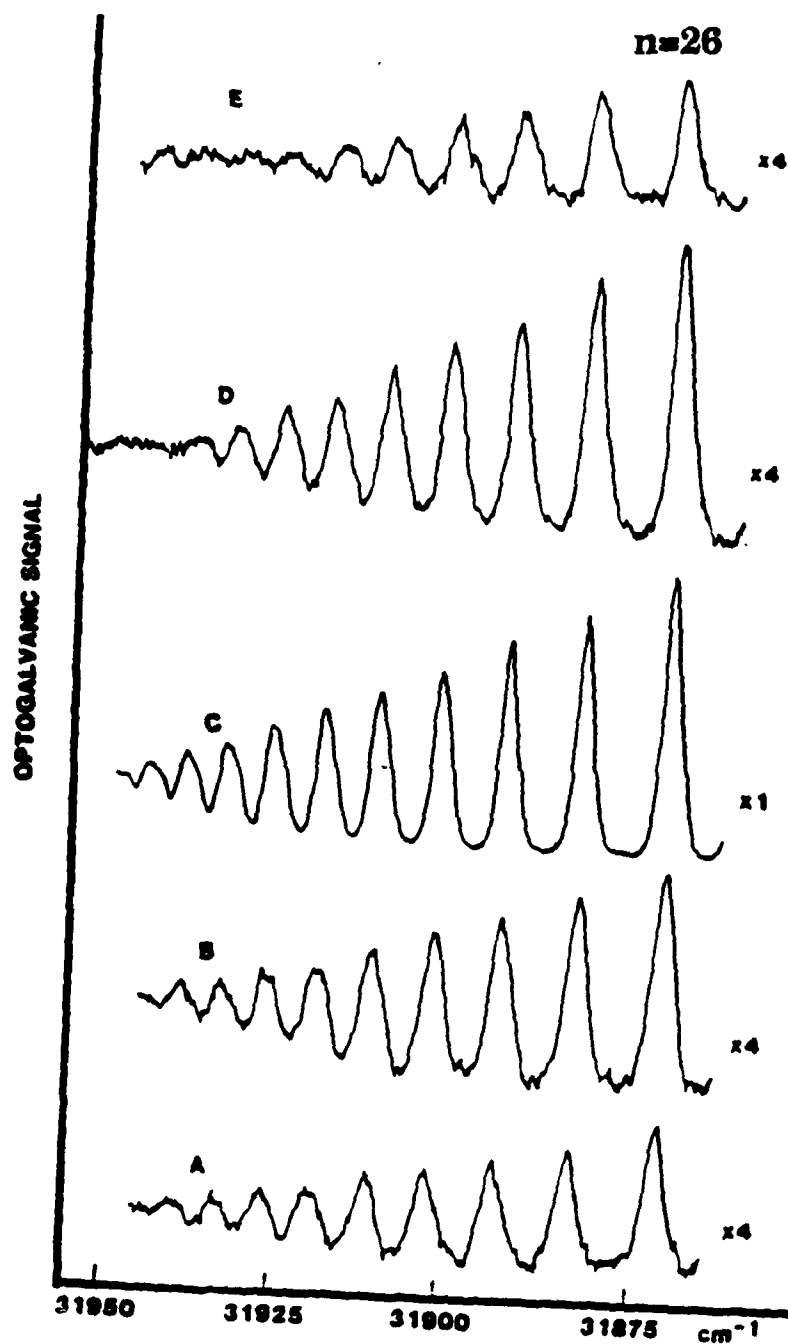


**Figure 15** Singlet helium Rydberg series spectra,  $\Delta m = \pm 1$  polarization,  $n=25$  and above, recorded at varying radial locations in the positive column of a DC glow discharge. Spectrum C was recorded on axis; B and D, A and E were recorded as symmetric radial distances.

spectrum was taken on axis; the others were taken symmetrically off axis. The off axis spectra show increasing linewidth with increasing distance from the axis, and the last resolvable transition shifts to lower  $n$ . The off axis spectra are multiplied by a factor of 4 reflecting the metastable population profile in the positive column. The electric fields present, using Griem's line broadening formula on the linewidth of the  $n=30$  transition, are  $29 \pm 4$  V/cm on axis,  $33 \pm 4$  V/cm at locations B and D, and  $37 \pm 4$  V/cm at locations A and E. While these values are high, the spectra do show good radial symmetry as one would expect in the positive column. Using series termination, defined as the onset of line overlap, one obtains field values of  $74 \pm 10$  V/cm,  $98 \pm 15$  V/cm, and  $113 \pm 20$  V/cm at the same locations, which are about one order of magnitude higher than seems reasonable! These results are obviously wrong because the integrated electric field across the tube would greatly exceed the tube voltage. Clearly there is something wrong with the implementation of these techniques.

The measurement of the electric field vector is demonstrated by the spectra in Fig 16. For this measurement, the discharge tube was tilted at an angle of  $50^\circ$  with respect to the laser polarization. Thus the center spectrum, taken on axis, contains a mixture of both  $\Delta m = 0$  and  $\Delta m = \pm 1$  polarizations, shown by the presence of the s peaks. In the top spectrum, taken 2 mm above the discharge axis, the relative intensities of the s peaks is larger, indicating that the laser polarization is more parallel to the field direction. In the bottom spectrum, taken 2 mm below the discharge axis, the s peaks have essentially vanished, indicating that the laser polarization is nearly perpendicular to the field direction, as one would expect from the symmetry of the positive column. The electric field

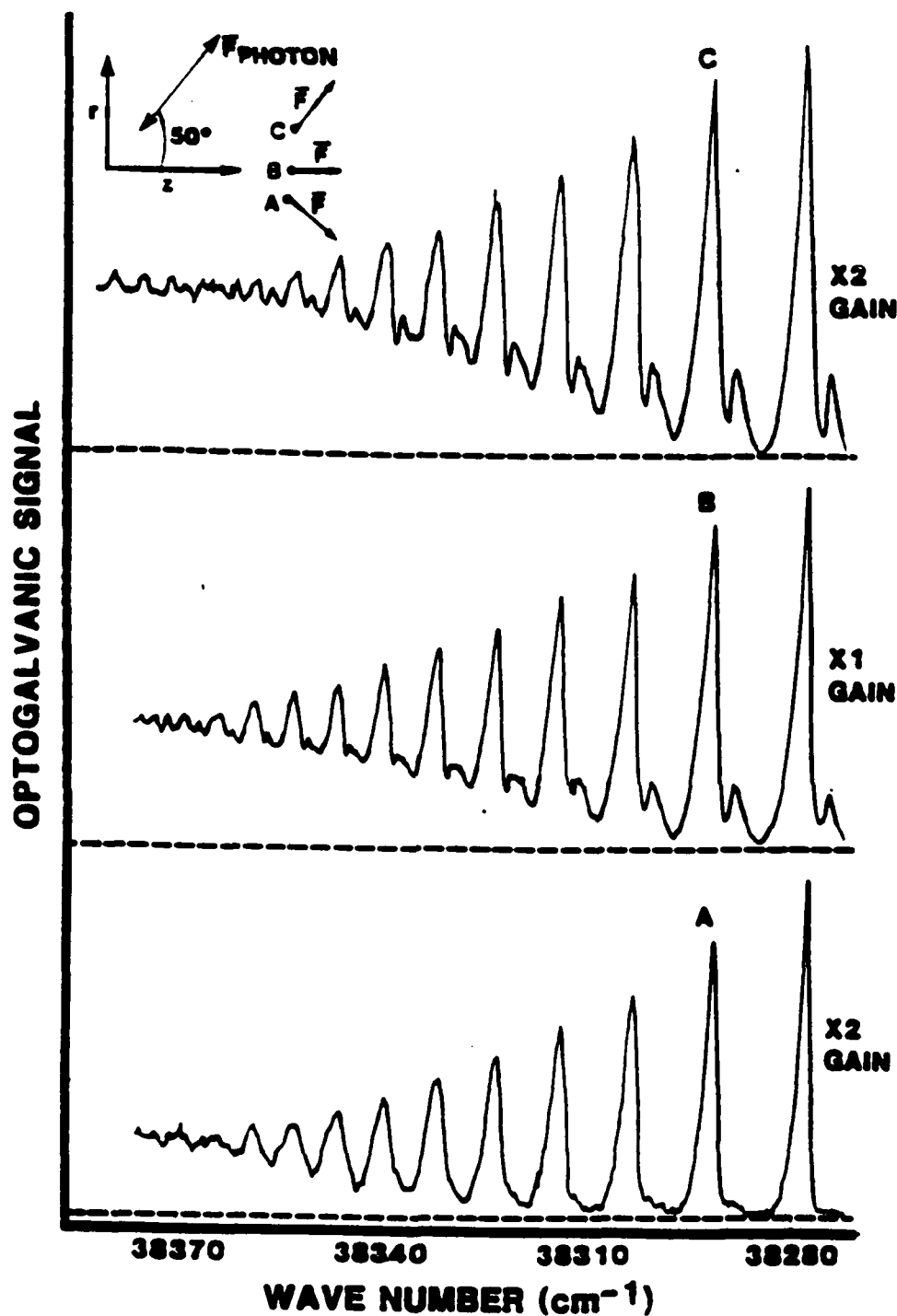


**Figure 16** Triplet helium Rydberg spectra from  $n=25$  and above recorded for three different radial locations in the positive column as shown in the insert. The spectrum labeled B is on the radial axis. The spectra labeled A and C are 2 mm away from the axis. The spectrum labeled B is at two-times reduced gain as compared to spectra A and C.

values previously reported for these spectra were based on the broadening of the triplet helium Rydberg state lines. The next section of this report shows that line broadening is an inappropriate diagnostic for triplet helium spectra, so the electric field values reported are probably in error. These measurements were taken at a current of 0.8 mA to minimize the microfield.

## VII ANALYSIS AND SIMULATION OF SPECTRA

As discussed previously, a number of techniques were employed to measure the electric fields present in various regions of the discharge: l-state energy level shifts and level splittings for fully and partially resolved spectra, line broadening and series termination for unresolved spectra. However, outside the cathode sheath, this analysis led to results inconsistent with other measured experimental parameters, namely, the voltage drop across the tube. Because the line broadening and series termination formulae used had been derived for hydrogen and merely assumed to hold for Rydberg states of helium, the validity of this assumption seemed to be the most likely reason for the discrepancies. Up to this point in our studies, full advantage of Foster's diagonalization had not been taken; while the calculated energy level shifts were used to measure the field, the relative l-state oscillator strength information had been ignored.

To better understand the helium Rydberg state spectra and characterize the glow discharge, the following procedure was employed to simulate helium Rydberg state spectra. For a selected electric field value, polarization, and principal quantum number, Foster's technique is used to calculate the l-state energy levels and their relative intensities. Each l-state is treated as a separate line, whose characteristics are varied to mimic one of a number of possible mechanisms present in the discharge or the instrumental response thought to constrain spectral resolution. For example, initially the laser linewidth was thought to be the major constraint on resolution, so a Gaussian line profile with a FWHM of  $0.4 \text{ cm}^{-1}$  was used to describe each l-state line. The individual l-state

lines are then convolved to obtain the overall  $n$ -state manifold lineshape. The initial simulations showed good qualitative agreement with the experimental data, however, there were distinctive features present in the data which were not reproduced by this simple modelling.

The power of the spectral simulations is that they enabled the investigation of the influence of various aspects of the plasma environment on the helium Rydberg state spectra. For example, changing the linewidth mimics changing the electric field gradient. By changing the line profile, Gaussian to Voigt, the relative importance of neutral collision broadening can be determined. These spectral simulations also provide a clean calibration set against which the results of the hydrogenic line broadening and series termination formulae can be benchmarked. The simulations also enabled a comparison of the triplet and singlet Rydberg series of helium, whose spectra had been assumed to exhibit the same response to electric fields.

#### A. Electric Field Gradient Measurements

The cathode sheath Rydberg spectra display a variation of the linewidths of the different  $l$ -state peaks across the  $n$ -manifolds, with  $l$ -states near the manifold centers having a minimum width which increases monotonically towards both wings. These characteristics of the measured helium spectra are the consequence of the presence of a finite electric field gradient across the excitation laser diameter and the dominance of the linear Stark effect for the range of  $n$ 's and fields investigated. The measured spectrum thus represents a summation of Rydberg states created within a range of electric fields,  $F + \Delta F$ , where  $F$  is the

average electric field at the location of the probe laser. This effect is illustrated in Fig 17 for the  $n=19$  triplet helium manifold,  $\Delta m = \pm 1$  polarization, at an average field of  $F$  of 740 V/cm with a  $\Delta F$  of 60 V/cm. The linear Stark energy shift is (approximately for helium)

$$\Delta E = \frac{3}{2} n F (n_1 - n_2) \quad (11)$$

where  $n_1, n_2$  are the parabolic quantum numbers. For states near the manifold center,  $n_1 \approx n_2$ , so these states exhibit very small energy shifts as a function of field. Thus measurement of these states over a range of fields does not affect the measured linewidth. For states at the manifold wings,  $|n_1 - n_2|$  is maximized, so their field dependent energy shifts are large. Measurements of these states produces a large apparent linewidth. The dimension of the boxes along the x-axis represents the width of the laser beam, which is the same across the manifold. The dimension of the boxes along the y-axis represents the measured linewidth, which minimizes at the manifold center and increase on either wing. The resolution of the manifold is determined by the  $\Delta F/F$  ratio, and the linewidth of each  $n_1, n_2$  state is proportional to  $\Delta F$  ( $\Delta F/F$  can be greater than 0.2 for a few hundred micron diameter laser beam in the cathode sheath).

The following procedure was used to model the field gradient. A sequence of manifold profiles was generated for a range of electric field values. These individual profiles were weighted by a factor proportional to the laser intensity profile across the probe laser beam diameter and then summed to produce a calculated profile which best fit the experimental data. A representative set of



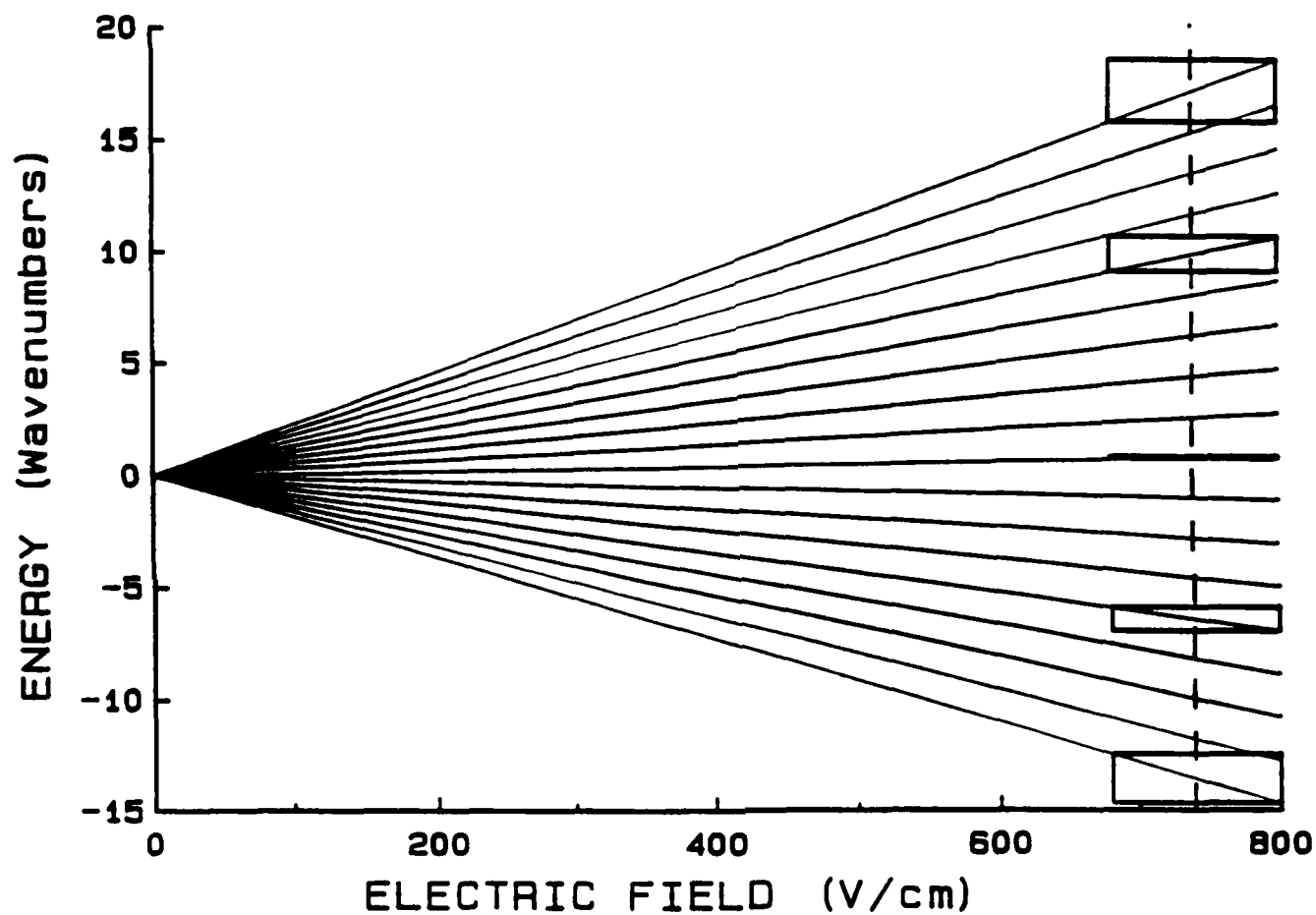


**Figure 17** Calculated Stark splitting of the  $n=19$  manifold of triplet helium vs electric field. The effect of a linearly varying electric field on the linewidth of different substates is illustrated by the projections on the y ordinate.

calculated Stark spectra for  $n=19$ ,  $\Delta m = \pm 1$  polarization, is shown in Fig 18. The average electric field  $F$  is 340 V/cm, with  $\Delta F$  ranging from 0 to 60 V/cm. The Stark spectrum corresponding to the zero field gradient shows a fully resolved manifold, and with increasing gradient, only states near the manifold center remain distinct. The dashed line in Fig 18 represents the zero field energy of the  $2^3S$  to  $19^3P$  transition.

Stark spectra for  $n=19$ ,  $\Delta m = \pm 1$  polarization, measured at 0.4, 1.25, and 2.5 mm from the cathode are shown in Fig 19. The average electric fields at these locations, measured from the manifold splittings, are 740, 575, and 340 V/cm respectively. Note that fully resolved manifolds are not observable below 600 V/cm, confirming the presence of a strong field gradient in the sheath. The calculated intensity profiles for these average electric field values are shown in Fig 20. A constant value of  $\Delta F = 60$  V/cm and a flat top intensity profile<sup>56</sup> of the probe beam was used to obtain the best fit to the data set shown in Fig 19. For the measurements conditions used the  $\Delta F$  of 60 V/cm equates to a field gradient of 2000 V/cm<sup>2</sup>. The use of a single valued field gradient fit to the spectra for a distance of 0.4 mm out to 2.5 mm from the cathode positively shows a linear dependence of electric field with distance from the cathode. This electric field gradient also agrees well with the slope of a linear fit to the sheath electric field profile shown in Fig 11. It should be emphasized that gradient measurements from spectra fitting can also be applied to situations where nonlinear gradients are present. Invoking Poisson's equation, the direct measurement of  $dF/dZ$  indicates a net space charge density of  $10^9$  cm<sup>-3</sup>. The changes in the manifold lineshape caused by a  $\Delta F$  of only 10 V/cm ( $dF/dZ \approx 300$

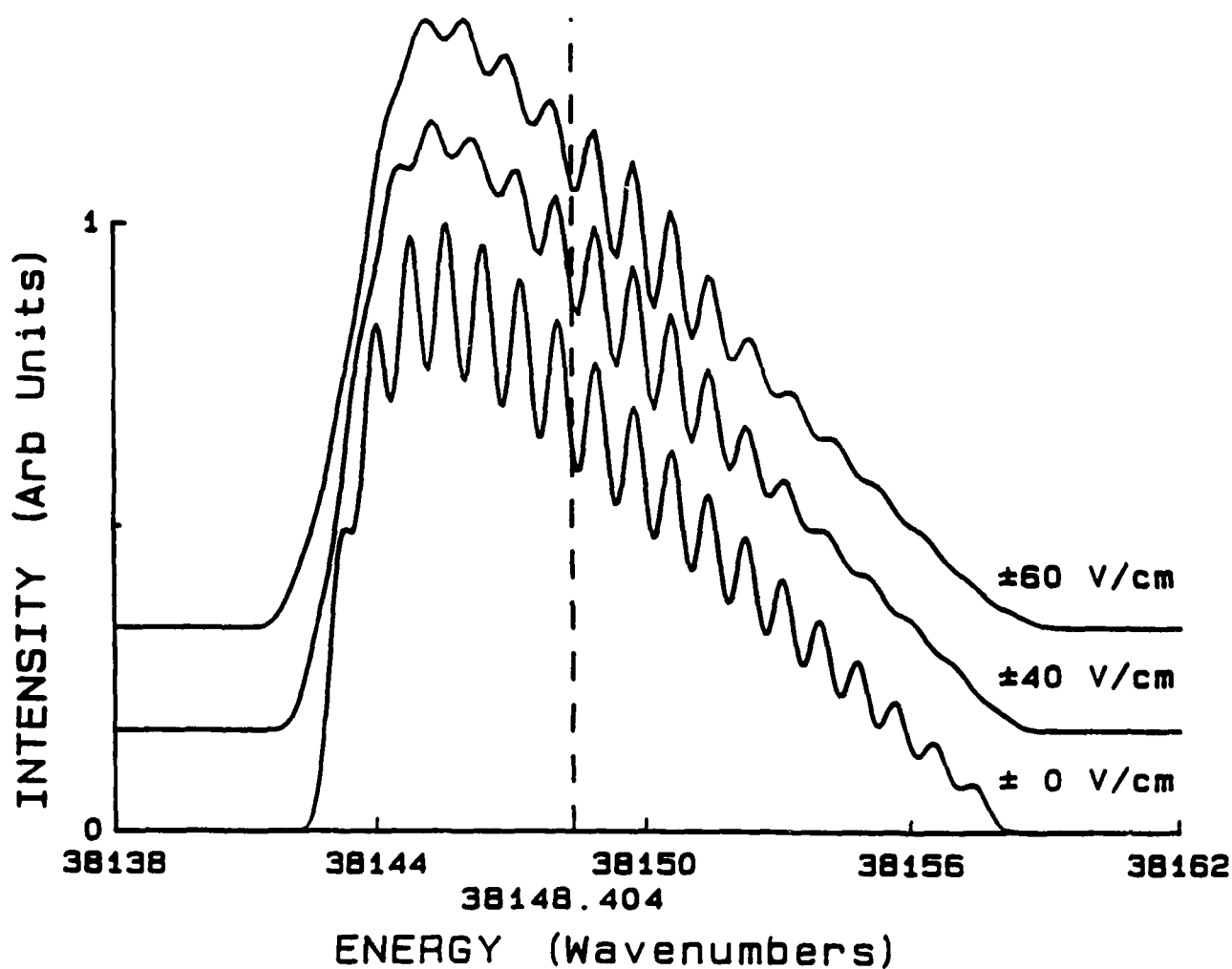


**Figure 18** Calculated Stark spectra for triplet helium  $n=19$  for an average field of 340 V/cm and different field gradients. The dashed line is the zero field position of the  $2^3S$  to  $19^3P$  transition.

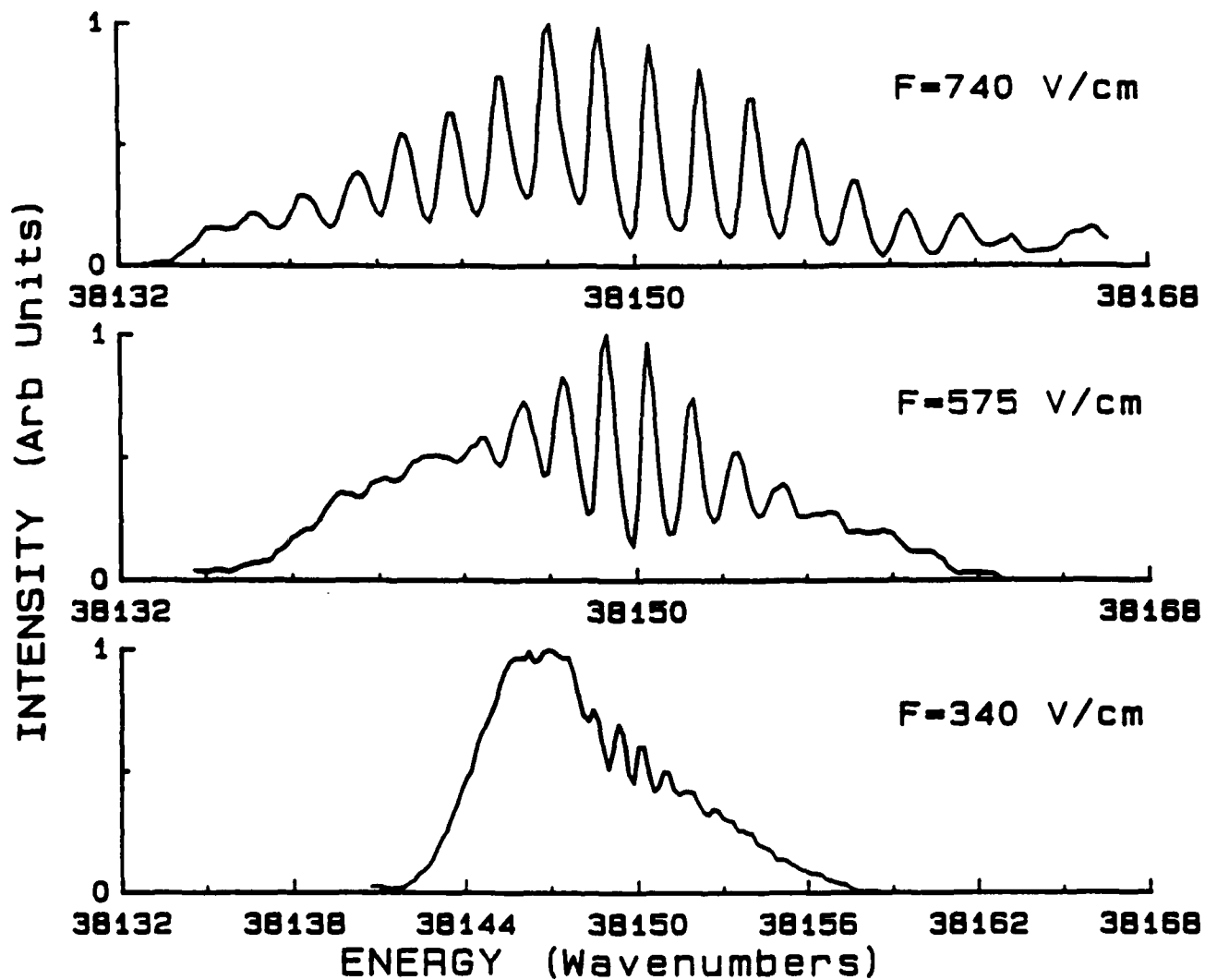


**Figure 19** Measured Stark spectra for triplet helium  $n=19$  in the cathode sheath at positions 0.4, 1.25, and 2.5 mm from the cathode surface. The discharge current was 2.5 mA and the total tube voltage drop was 225 V.

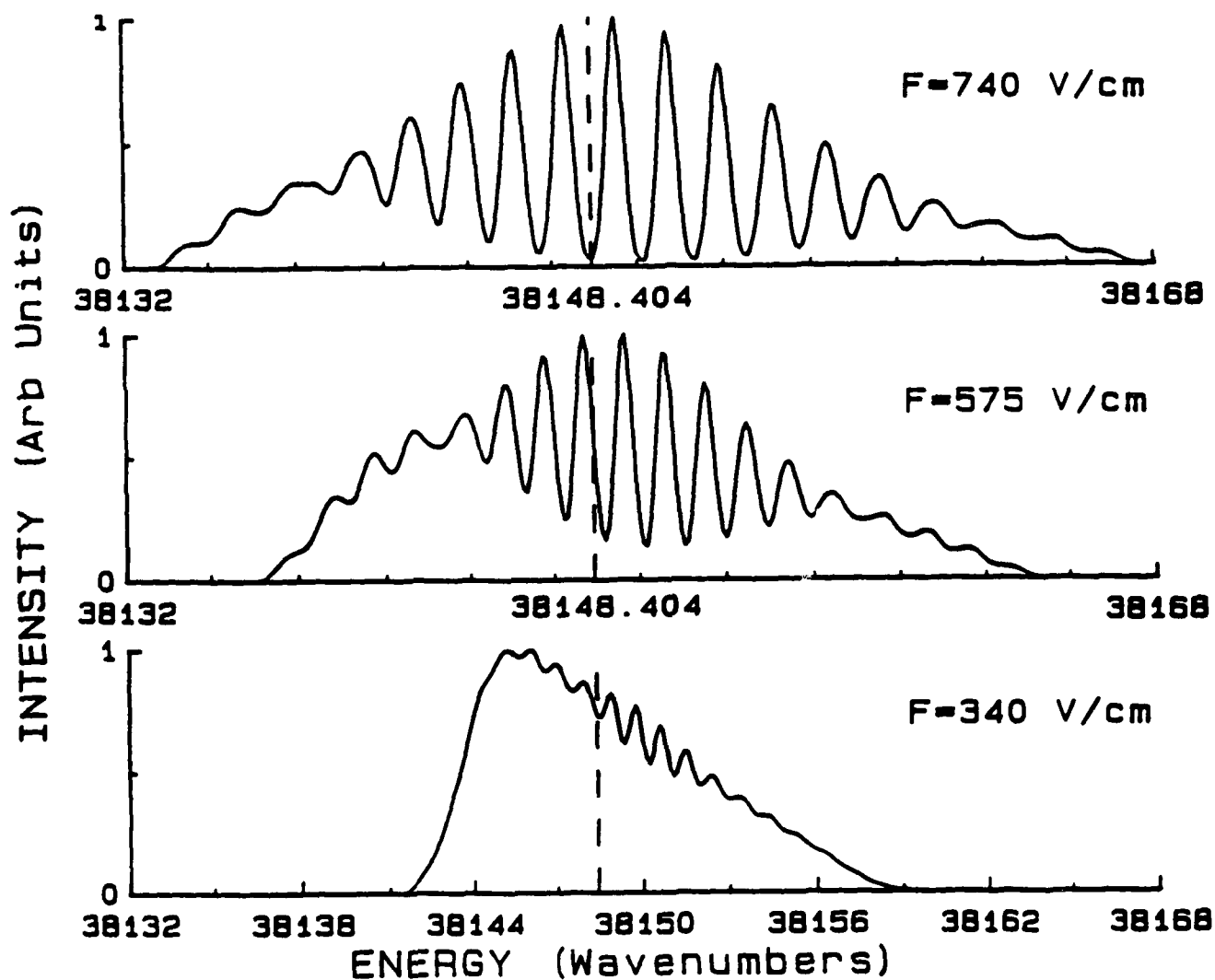


**Figure 20** Calculated intensity profiles for the Stark splitting of the  $n=19$  manifold of triplet helium at electric field values of 745, 575, and 340 V/cm. The dashed line is the zero field position of the  $2^3S$  to  $19^3P$  transition. A field gradient of  $2000$  V/cm<sup>2</sup> gave the best fit between the measured and calculated intensity profiles.

V/cm<sup>2</sup>) are readily measurable.

## B. Low Field Measurements

### 1. Line Broadening Field Measurements

If the l-state separation caused by an external field is below experimental resolution, one observes an apparently broadened single line resulting from the convolution of the unresolved l-state lines. Griem<sup>56</sup> gives a formula for this linewidth as a function of field

$$\Delta(\text{FWHM}) = 3F(n_1^2 - n_f^2) \quad (12)$$

which can be derived from the hydrogen linear Stark formula, with the exception of the minus sign. Griem's line-broadening formula is a standard for electric field measurements in equilibrium plasmas, however, it is not directly applicable over the full range of plasma conditions. Griem's result assumes that the spectral linewidth is caused only by field broadening, which is not always true. In our experiments, the laser linewidth was approximately 0.4 cm<sup>-1</sup> FWHM. The Doppler widths at 300 K are 0.18 and 0.2 cm<sup>-1</sup> respectively for singlet and triplet helium. Initially, it was assumed that the effect of collisions between the Rydberg states and the background ground state helium atoms was negligible and would not contribute to the measured linewidth. However, our attempts to apply the Inglis-Teller relation to the high Rydberg state data indicated that additional line broadening effects were significant. Miller<sup>57</sup> et. al. measured the singlet helium Rydberg series in the positive column of a hollow cathode discharge and noticed

that the linewidths of successive  $n$ -state lines were approximately constant, instead of increasing as  $n^2$  as expected. A thorough analysis of their broadening mechanisms was performed which led them to investigate the pressure dependence. Their measurements indicated that the helium ground state helium Rydberg state collision cross section is  $10^5 \text{ \AA}^2$ . The cross section was found to be roughly constant for  $n > 20$ , and is roughly an order of magnitude less than the geometric cross section for these  $n$  values. Using this cross section for our experimental condition of a neutral pressure of 1 Torr, the collisional linewidth FWHM is approximately  $1.0 \text{ cm}^{-1}$ , as much as 50% of the Rydberg state linewidths. Since each  $l$ -state will have this linewidth and the total manifold linewidth results from the convolution of the  $l$ -state lines, the collisional linewidth is not a simple offset which can be subtracted from the total linewidth. Application of Griem's approach to a situation where one observes field broadening on top of a substantial inherent linewidth will lead to spurious results.

Examining Eq 12 one can see that Griem has used the approximation  $(n_1 - n_2) = n$  which assumes that the half maximum intensity points occur at the extreme  $n_1, n_2$  states. Fig 21 shows the hydrogen  $n_1, n_2$  relative intensity distributions<sup>15</sup> for  $n=30$  in the  $\Delta m = 0$  and  $\Delta m = \pm 1$  polarizations. The shape of these distributions are independent of electric field; the field merely increases the separation between the states. The envelopes plotted are the overall lineshapes generated from the convolution of Voigt profiles for the individual  $l$ -state components. From this figure it is apparent that the approximation  $(n_1 - n_2) = n$  at half max is bad for the  $\Delta m = \pm 1$  polarization. The  $\Delta m = 0$  polarization shows two peaks per  $n$ -manifold and cannot be described by the broadening of a single line,

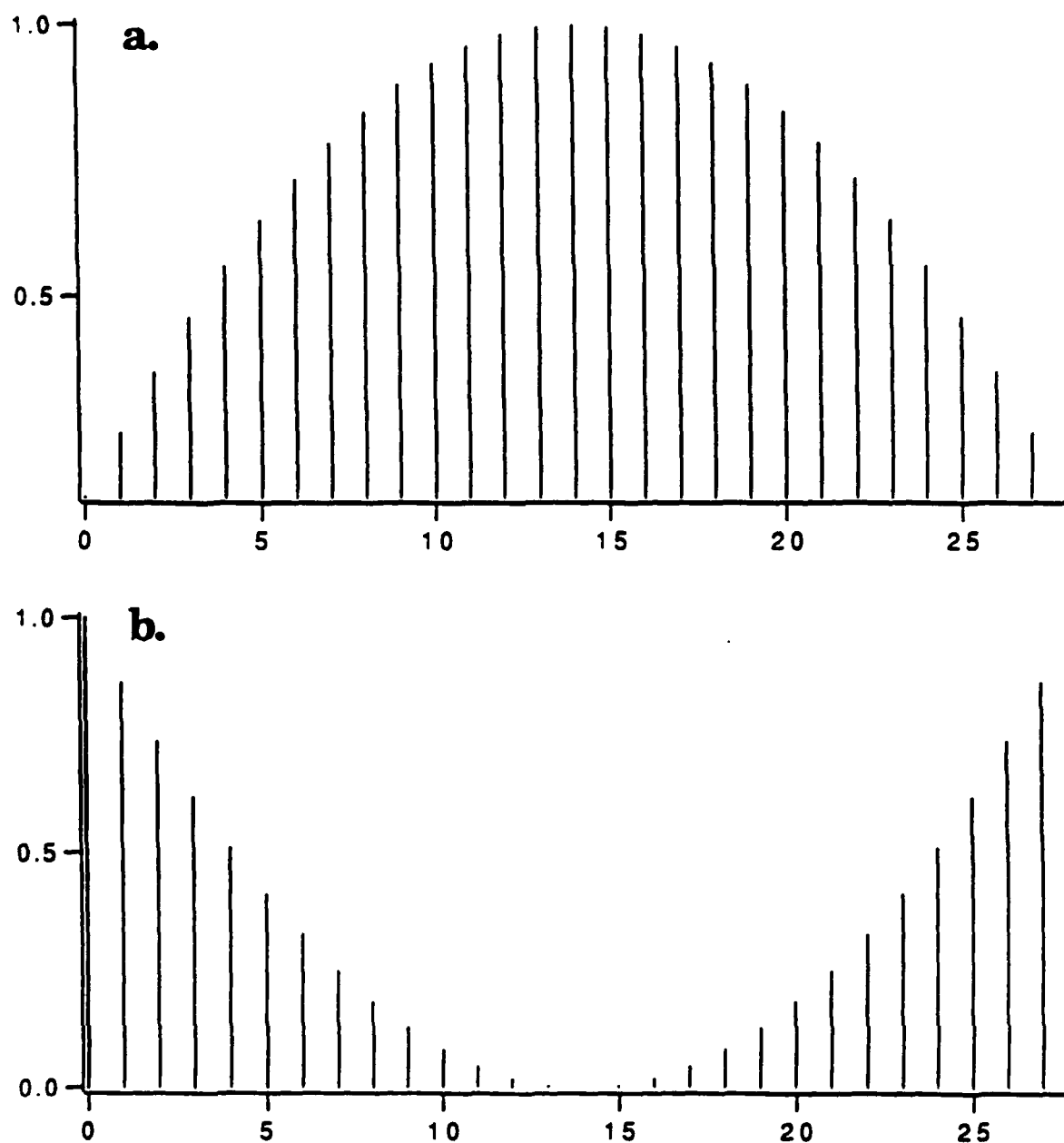


**Figure 21** Calculated  $n = 30$  hydrogen intensity distribution  
 (a.)  $\Delta m = \pm 1$  polarization intensity distribution. (b.)  $\Delta m = 0$  polarization intensity distribution. The x ordinate on each graph corresponds to the  $l$ -states of the  $n = 30$  manifold.



unless the separation of the extrema states is smaller than the total manifold linewidth. However, unless the extrema separation is much smaller than the total linewidth, a distorted line profile will result, displaying apparent saturation at the manifold center. This result is shown in Fig 22a, where the  $\Delta m = 0$  manifold for  $n=30$  is shown. For pure  $\Delta m = \pm 1$  polarization spectra, a better approximation for  $(n_1-n_2)$  half max is  $0.7n$ , which results in a correction of approximately 30% from Griem's result. The  $\Delta m = \pm 1$  manifolds do not distort as the field increases, as is shown in Fig 22b under the same conditions as Fig 22a.

The origin of the negative sign in Eq 12 is explained by Griem as resulting from the approximate selection rules for hydrogen atoms in an electric field: transitions between levels which are shifted in the same direction are much stronger than transitions between levels shifted in opposite directions. However, it is not appropriate to apply this analysis to helium spectra. In the case of helium Rydberg spectra at the fields investigated in our experiments, the broadening of the  $n = 2$  state is negligible and the broadening observed will just be the broadening of the Rydberg states, so the sign in Eq 12 doesn't matter.

Griem's formula for  $n=30$  in hydrogen using the approximation  $(n_1-n_2) = n$  at half max produces the line

$$\Delta = 0.115 \left( \frac{\text{cm}^{-1}}{\frac{V}{\text{cm}}} \right) F \left( \frac{V}{\text{cm}} \right) \quad (13)$$

which predicts zero linewidth at zero field. Using the approximation  $(n_1-n_2)=0.7n$ , the slope changes to  $0.088 \text{ cm}^{-1} / \text{V/cm}$ . One could add in a zero field linewidth

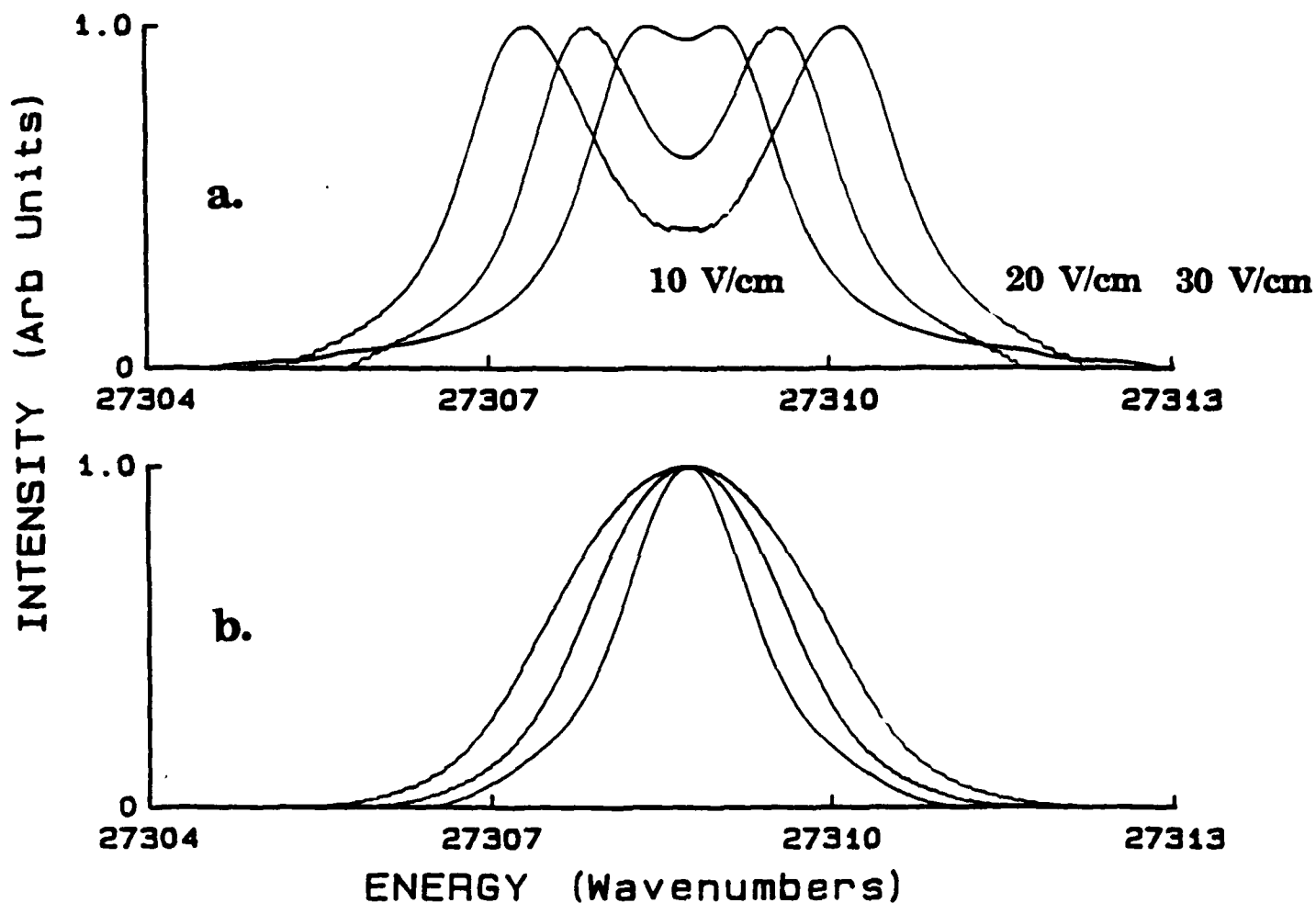


**Figure 22** Calculated  $n = 30$  hydrogen line profiles

(a.)  $\Delta m = 0$  polarization line profiles as a function of electric field.

(b.)  $\Delta m = \pm 1$  polarization line profiles. Notice that only for the  $\Delta m = \pm 1$  polarization does the term "line broadening" accurately describe the field induced line profile modification.

based on experimental resolution and use this slope to measure the field, however, it is better to generate the  $n=30$  manifolds and derive a broadening relation from these results. To simulate the experimental conditions, the l-state components were described by a Voigt profile with a Doppler width FWHM of  $0.2 \text{ cm}^{-1}$  and a Lorentzian width of  $1.0 \text{ cm}^{-1}$ , with the relative intensities given by Eq 5a.

Representative results of the hydrogen simulations are shown in Fig 23 for electric fields of 0, 10, 20, and 30 V/cm. As expected, the  $\Delta m = \pm 1$  line is symmetric and broadens homogeneously. The linewidth saturates at 5 V/cm and below, indicating that the inherent (pressure) linewidth is larger than the Stark width. Neglecting the  $F=0 \text{ V/cm}$  point, a linear fit to this data produces the equation

$$\Delta = 0.726(\text{cm}^{-1}) + 0.064 \left( \frac{\text{cm}^{-1}}{\frac{\text{V}}{\text{cm}}} \right) F \left( \frac{\text{V}}{\text{cm}} \right) \quad (14)$$

This result is valid only above 5 V/cm, which means that the experimental conditions, here the pressure, determine the lower limit of electric field sensitivity.

An interesting result of this procedure is that the slope of the line broadening (broadening coefficient) differs significantly from that predicted by Griem's formula. For a consistency check, the hydrogen simulations were repeated using small linewidths, Doppler  $0.02 \text{ cm}^{-1}$ , Lorentzian  $0.1 \text{ cm}^{-1}$ . For these values, the simulations produce a slope of  $0.88 \text{ cm}^{-1}/\text{V/cm}$ , so in the zero

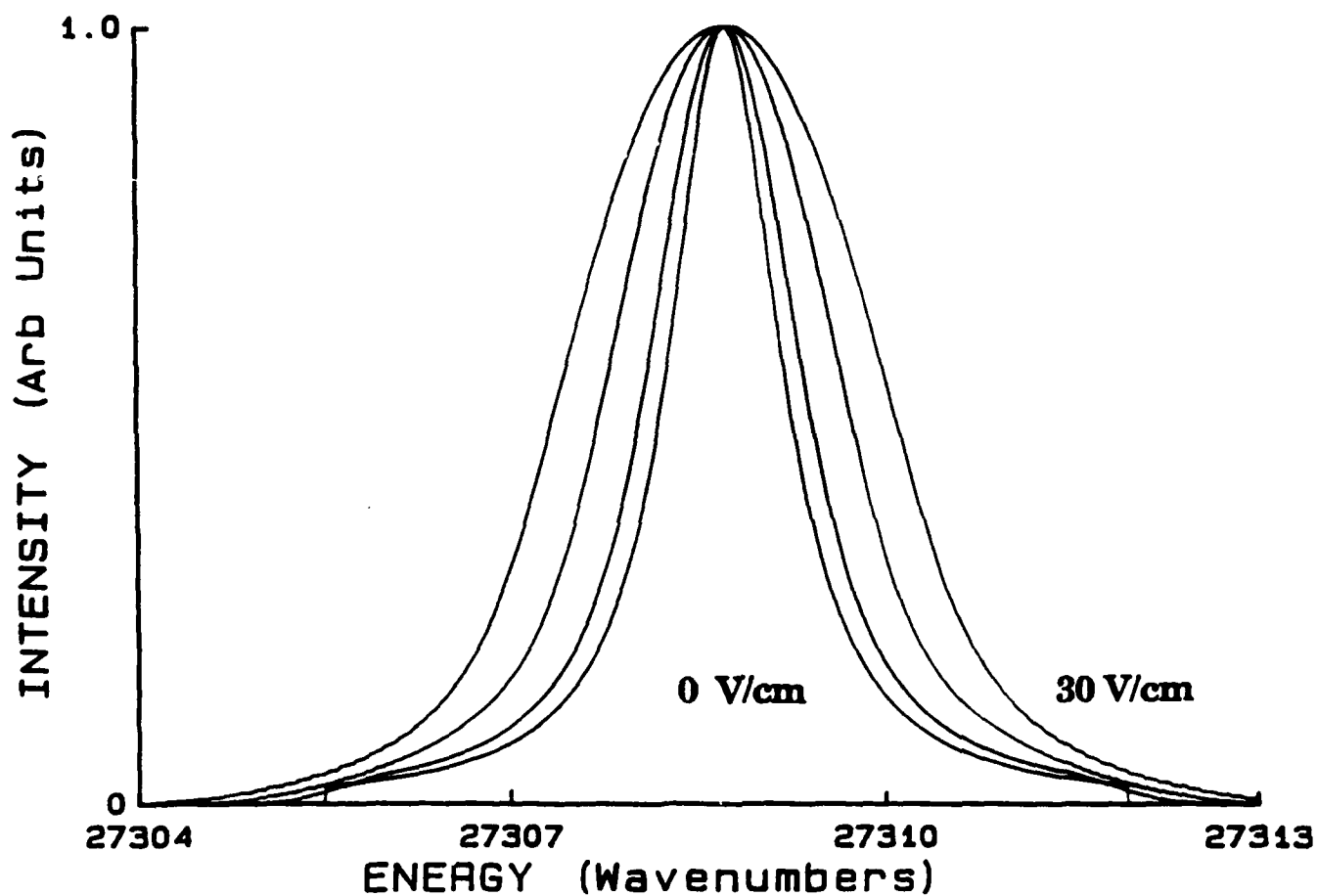


**Figure 23** Calculated hydrogen Stark line profiles,  $n = 30$ ,  $\Delta m = \pm 1$  polarization at 0, 10, 20, and 30 V/cm. A Voigt profile was used in these calculations with a Doppler width (FWHM) of  $0.1 \text{ cm}^{-1}$  and a Lorentzian width of  $1.0 \text{ cm}^{-1}$ .

linewidth limit this procedure does reproduce Griem's broadening formula. Fig 24 shows a comparison of these approaches for  $n = 30$ , emphasizing the importance of linewidth on the broadening relation.

To examine the sensitivity of the simulation to the lineshape used, a set of field-broadened  $n=30$  hydrogen lines were generated using a Gaussian profile with a width FWHM of  $1.0 \text{ cm}^{-1}$ . The slope of a linear fit to these results was nearly equal to the slope from the Voigt profile fit,  $0.0615$  compared to  $0.0638$ . However, the zero field offsets differed significantly,  $0.52 \text{ cm}^{-1}$  compared to  $0.726 \text{ cm}^{-1}$ . Thus, the use of a Gaussian will overestimate the field compared to a Voigt profile fit, in this case by  $3.5 \text{ V/cm}$ . While this is at most a 20% difference for this experiment, from the spectra it is readily apparent that a Gaussian line profile is a poor description of the experimental conditions.

The description of the effect of an electric field on a hydrogen  $\Delta m = \pm 1$  transition is good because the intensity distribution within an  $n$ -manifold ( Eq 5 ) is independent of the field, so hydrogen lines are always symmetric. A FWHM can always be accurately defined for symmetric, homogeneously broadened lines. However, for helium (as shown before) the intensity distribution is very sensitive to the field and produces generally asymmetric lineshapes. In previous analyses of this helium data <sup>55</sup> it was assumed that the hydrogenic line broadening as given by Griem was valid for helium Rydberg state spectra. However, after additional analysis and calculations we now know that this assumption is invalid, and that a generalized formula for line broadening for the conditions considered might not even make sense for helium. To test this hypothesis, synthetic spectra for the helium  $n=30$  singlet and triplet manifolds in the  $\Delta m = \pm 1$  polarization were

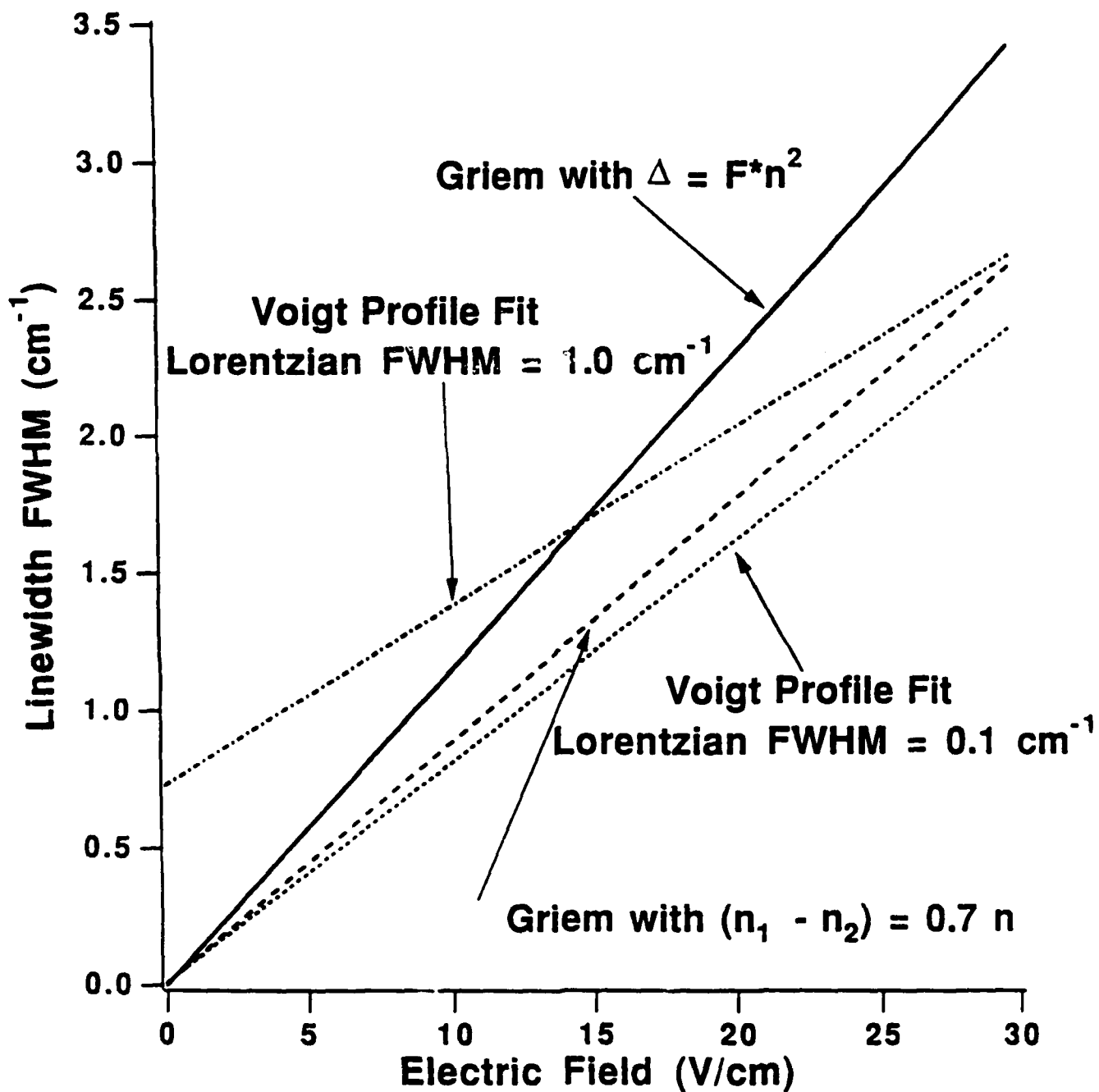


**Figure 24** Comparison of hydrogen line broadening approaches. Notice that in the limit that in the limit that the inherent (zero electric field) linewidth approaches zero, Griem's formula and the convolution of Voigt profiles give the same result.

generated for fields from 0 to 30 V/cm. A Voigt profile with the parameters given before was used for the individual l-state lines, with the relative intensities calculated using Foster's procedure.

Fig 25 a shows the results for triplet helium,  $n=30$ , from 0 to 30 V/cm. As the field increases, the triplet manifolds look like a single, sharp line with a growing asymmetric tail. In measuring the linewidth, one will measure the width of the main peak, which is not representative of the width of the entire manifold. Fig 25 b shows the  $n=30$  singlet helium simulations from 0 to 30 V/cm. Notice that while the singlet helium distorts, it retains a good degree of symmetry, and the linewidth is representative of the entire manifold width. Fig 26 shows a comparison of the broadening of hydrogen, singlet helium, and triplet helium. Hydrogen shows linear broadening. Triplet helium shows distinctly nonlinear broadening, with the linewidths measured from the simulations smaller than the hydrogen results. We believe that earlier field measurements based on triplet broadening are erroneous. Somewhat unexpectedly, the singlet broadening is quite linear and close to the hydrogen results. Thus, field measurements based on singlet helium broadening are valid, though only below fields which will produce a distorted singlet lineshape.

The reason for the marked difference between the singlet and triplet helium Stark lineshapes is that the  $n^3P$  quantum defects are positive, while the  $n^1P$  quantum defects are negative (all other helium quantum defects, singlet and triplet, are positive). The positive quantum defect of an  $n^3P$  means that it is nearest in energy to the  $n^3D$ -state, then the  $n^3F$ , then the  $n^3G$  to  $n^3(l=n-1)$  states. Beyond the  $n^3F$ -state, the remaining l-states are degenerate, having quantum

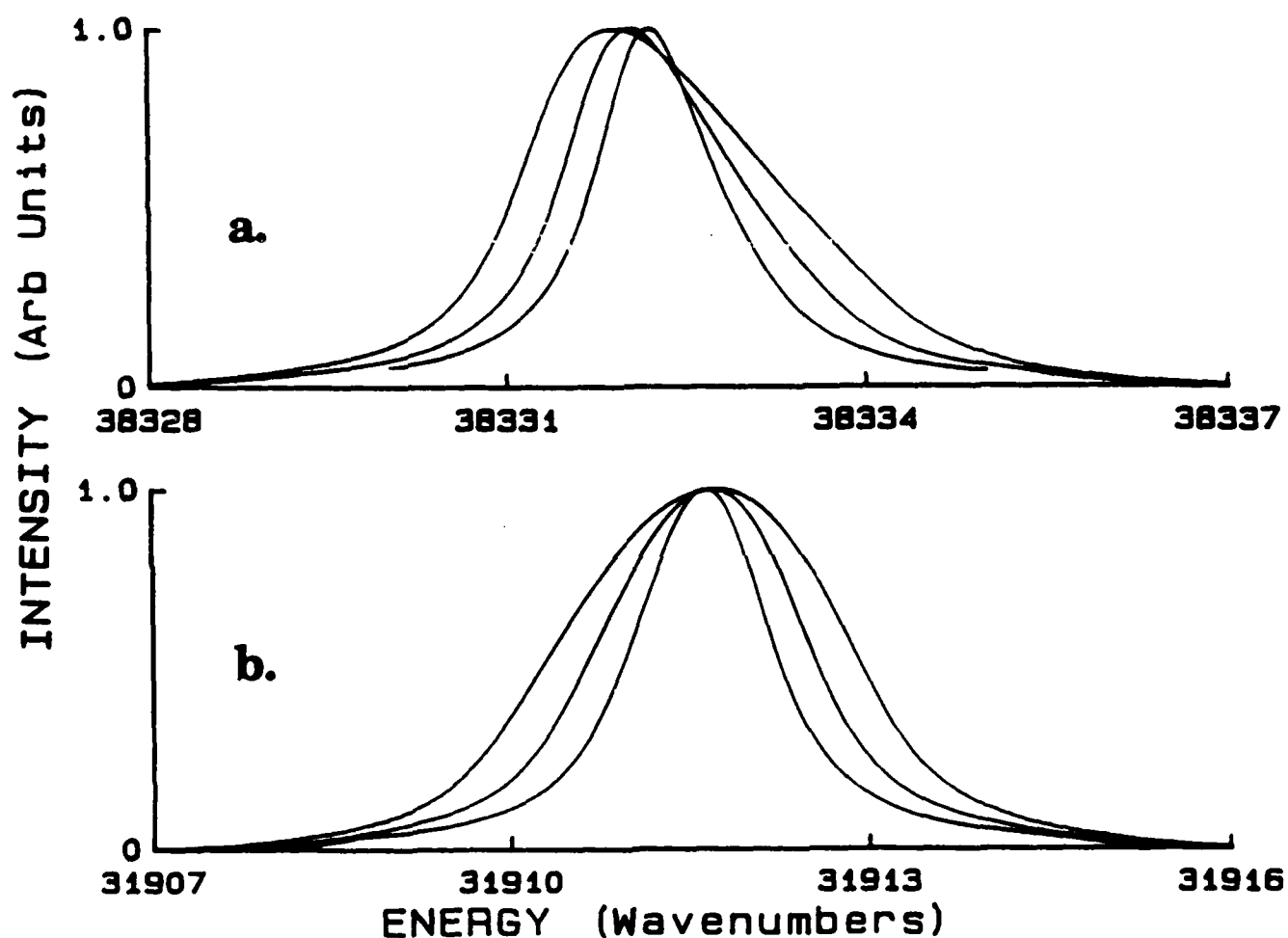


**Figure 25** a. Triplet helium,  $n=30$ ,  $\Delta m = \pm 1$  polarization Stark line profiles. b. Singlet helium,  $n=30$ ,  $\Delta m = \pm 1$  polarization Stark line profiles. Note the asymmetry in the triplet profiles as compared to the singlet.



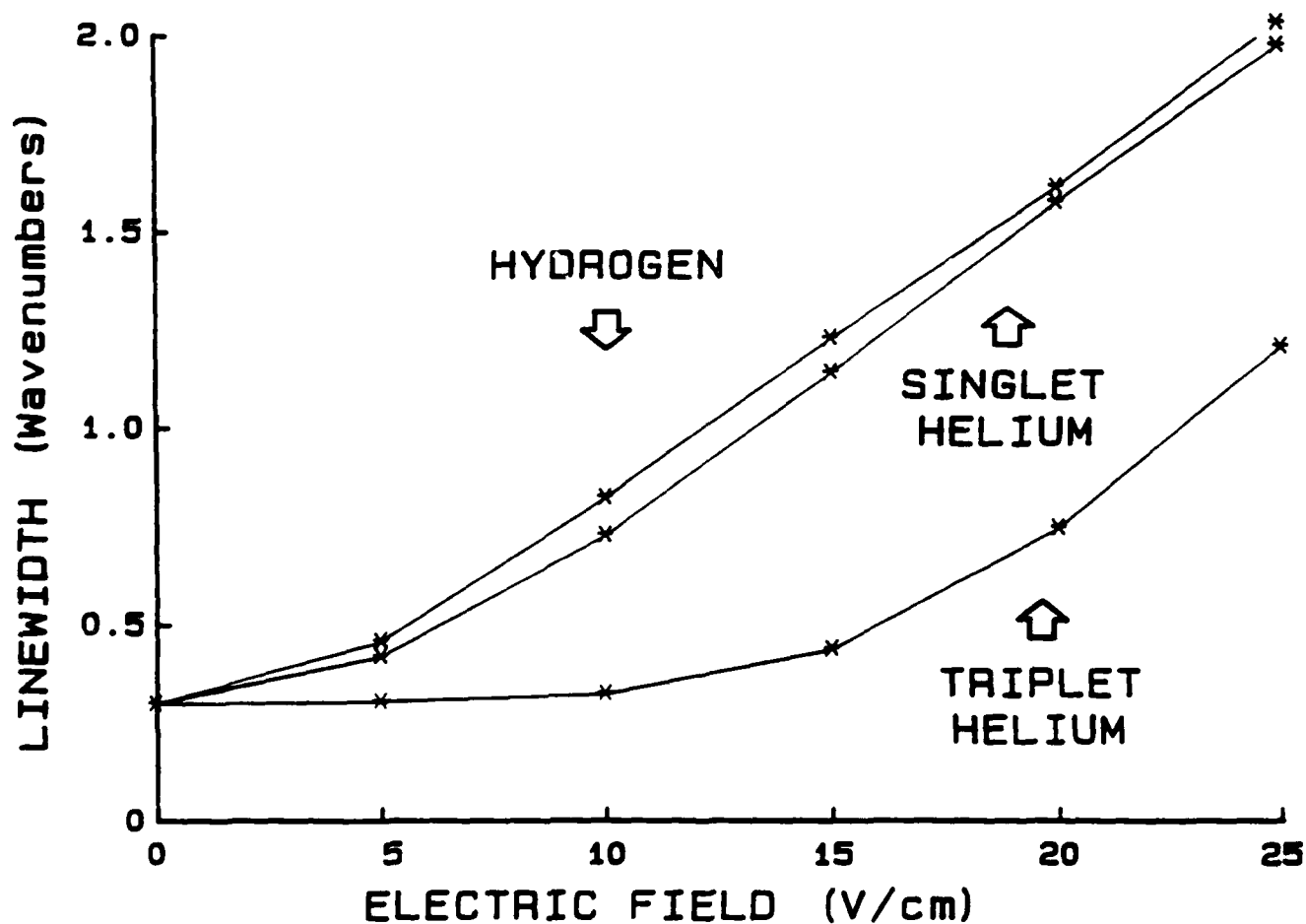


**Figure 26** A comparison of the linewidth (FWHM) variation of hydrogen, singlet helium, and triplet helium as a function of electric field.

defects equal to zero. The electric field induced intensity transfer will occur most rapidly to the l-states nearest in energy to the  $n^3P$ -state (the zero field allowed transition), thus the  $n^3D$ -state intensity will increase most rapidly with increasing field, then the  $n^3F$ -state, and the intensity of the states in the rest of the manifold will grow slowest with increasing field. The result of this intensity transfer behavior is that the triplet helium lineshape is asymmetric, peaked to the low energy side with a growing tail on the high energy side. Thus, the linewidth measured at the intensity half maxima does not represent the width of the entire n-state manifold, and line broadening is an inappropriate way to describe the field-induced lineshape modification.

The negative quantum defect of an  $n^1P$ -state means that it is nearest in energy to the degenerate  $l=G$  to  $n-1$  energy states in the n-manifold. To use the terminology of Ref 33, the  $n^1P$ -state interacts most strongly with the quasi-hydrogenic portion of the helium n-manifold, while the  $n^3P$ -state interacts with the non-hydrogenic portion of the manifold. As the electric field increases, the bulk of the  $n^1P$ -state intensity is transferred nearly equally to the degenerate l-states because their energy separation from the  $n^1P$ -state is nearly equal (the small, increasing electric field changes their energy levels so the intensity transfer to all these states is not identical). The net result is to produce a symmetric lineshape, whose linewidth, FWHM, is linear with the electric field for low electric fields (the exact field value for which this remains true is n-dependent). Theoretically, an  $n^1P$ -state will be driven to lower energies as the field increases; the l-state adjacent to the  $n^1P$ -state will be driven to higher energies as the field increases. Thus the singlet helium Stark manifolds will have an avoided

crossing within the manifold. However, the avoided crossing will be difficult to observe because the singlet manifold will have several peaks with nearly equal intensity, and it is hard to definitely identify the  $n^1P$ -state. Hogervost et al,<sup>5, 37</sup> who have published the highest resolution helium Stark spectra to date, discuss the existence of the avoided crossing but were unable to observe this phenomenon because of the complicated structure of the spectra.

## 2. Series Termination Field Measurements

In the absence of external perturbations, an atom possesses an infinite number of bound  $n$ -state energy levels below its ionization limit. The separation between adjacent energy levels decreases as the ionization limit is approached, so the highest  $n$ -state which can be resolved is limited only by instrumental resolution. The application of an external electric field broadens each line, so the last  $n$ -state which can be resolved will be determined by the ratio of the linewidth to the energy level separation (assuming the instrumental resolution is smaller than the field broadened linewidth). Inglis and Teller<sup>5824</sup> took advantage of this effect to derive a relation between electric field and line overlap. The criterion they used to define "series termination" was that the half linewidth of an  $n$ -state line,  $n=n_m$ , was equal to one half the separation between the line  $n_m$  and  $n_m+1$ . Expressed in terms of the more familiar first-order Stark effect

$$\frac{3}{2}n_m F = \frac{1}{2} \left( \frac{1}{n_m^2} - \frac{1}{(n_m+1)^2} \right) \quad (15)$$

Inglis and Teller made two approximations to simplify this equation. First, the  $RHS \approx n_m^{-3}$ . Second, they set  $(n_1 - n_2) \approx n_m$ . The second approximation is valid only for the extreme  $n_1, n_2$  states of the  $n$ -manifold. Though not explicitly stated, this relation is only valid for the  $\Delta m = \pm 1$  polarization. After these approximations, Eq 15 reduces to

$$F = \frac{1}{3n_m^5} \quad (16)$$

This relation defines the electric field at which the highest  $n_1, n_2$  state of the  $n=n_m$  manifold overlaps with the lowest  $n_1, n_2$  state of the  $n=n_m+1$  manifold, i.e., *the onset of line overlap of adjacent  $n$ 's*.

Series termination, experimentally, is commonly defined as the last principal quantum number state which can be resolved from the background, which is defined as the overlap of two adjacent peaks at their half-maxima (Rayleigh criterion). Thus for the Inglis-Teller criterion to be equivalent to series termination, the intensity of the extreme  $n_1, n_2$  states of the  $n$ -manifold would have to have one-half the intensity of the maximum intensity of any  $n_1, n_2$  state in the  $n$ -manifold. In addition, the Rayleigh criterion assumes a Gaussian line profile, though it can also be applied to the half-maxima overlap of symmetric line profiles, e.g., Voigt or Lorentzian profiles. For hydrogen in the  $\Delta m = 0$  polarization, the intensity half-maxima do occur at the extreme  $n_1, n_2$  states of the manifold, as can be seen from Eq 5. However, unless the field broadening of the line is small, one will observe the distorted lineshape as shown in Fig 22. For the  $\Delta m = \pm 1$  polarization of hydrogen, the intensity half-maxima do not occur at the

extreme  $n_1, n_2$  states. From Eq 5b, the relation  $(n_1 - n_2) \approx 0.7n$  can be derived. The  $\Delta m = \pm 1$  profile in hydrogen is symmetric, so a Rayleigh overlap criteria can be unambiguously defined.

Almost all of the applications of Inglis-Teller series termination have been on high density, fully ionized plasmas.<sup>59</sup> Under these conditions, collisional interactions of the electrons and ions on the atom is the dominant source of electric fields, i.e., the microfield. Because the collisions are isotropic, the spectra produced will have a random (mixed) polarization, possessing equal portions of  $\Delta m = 0$  and  $\Delta m = \pm 1$  polarizations. Series termination occurs at lower lying Rydberg states,  $n \leq 20$ , because the microfield are typically 1000 V/cm or greater, and a quasistatic approximation is used to calculate the effect of the electrons on the radiating atoms. In this experiment, fully resolved Rydberg state spectra were obtained for this range of electric fields and  $n$ 's, while in a high-density fully ionized plasma unresolved spectra are almost guaranteed because the collisional linewidths of the  $l$ -states in these conditions is very large.

The low electric field spectra taken in our experiments differ from most spectra on which series termination is applied in several different ways. First, for helium, the approximation that the half maxima intensities occur at the extreme  $n_1, n_2$  states is not good for either polarization. The electric field is predominantly the applied (axial) electric field which is anisotropic, so pure polarization spectra can be recorded. The intensity profile of the  $\Delta m = 0$  polarization is asymmetric, so only for the  $\Delta m = \pm 1$  polarization can series termination be applied. As discussed in the previous section, the primary source of line broadening in these measurements are the applied field, and collisions, here assumed to be with the

background helium atoms. At the present time, the effect of collisions with charged particles, as well as the validity of the quasistatic approximation for collisions with Rydberg states  $n > 30$ , are neglected.

In order to use series termination to analyze the  $\Delta m = \pm 1$  helium spectra, the approximation

$$(n_1 - n_2)_{\text{Half Max}} \approx 0.7 n_m \quad (17)$$

is used. Using this approximation, Eq 16 changes to

$$F = \frac{1}{2.1 n_m^5} \quad (18)$$

Again, simulated spectra were generated to verify the analysis of the spectra. The same procedure as described earlier was used for each individual  $n$ -manifold. To simulate the Rydberg series, a number of  $n$ -manifold lineshapes were calculated, weighted by a factor of  $n^{-3}$  to represent the decrease in oscillator strength with increasing  $n$ , and the individual line profiles summed. Fig 27 shows simulated singlet helium Rydberg series,  $\Delta m = \pm 1$  polarization, calculated at three electric field values. The field values used in the simulations were selected by solving Eq 18 for integer values of  $n_m$ . To speed up the calculation, a Lorentzian rather than a Voigt profile was used for the individual  $l$ -state lines. Because the collisional width is approximately five times the Doppler width, the use of the Voigt and Lorentzian profiles showed no significant difference for

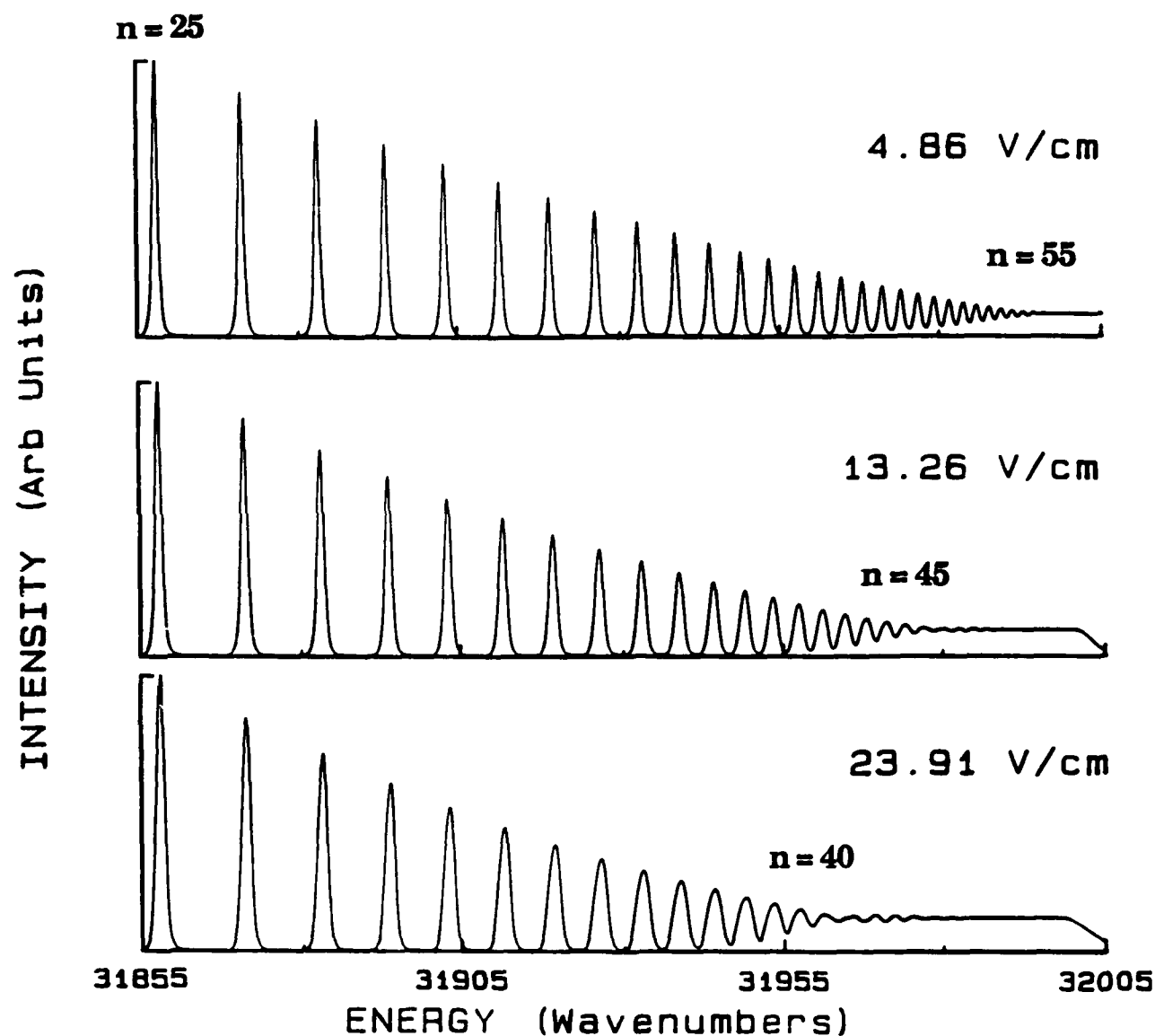


**Figure 27** Calculated singlet helium Rydberg series for  $n = 25$  and above. The electric field values were selected to insure that "series termination" occurred at integer  $n$ -values. The  $n$ -value for series termination at each field value is indicated.

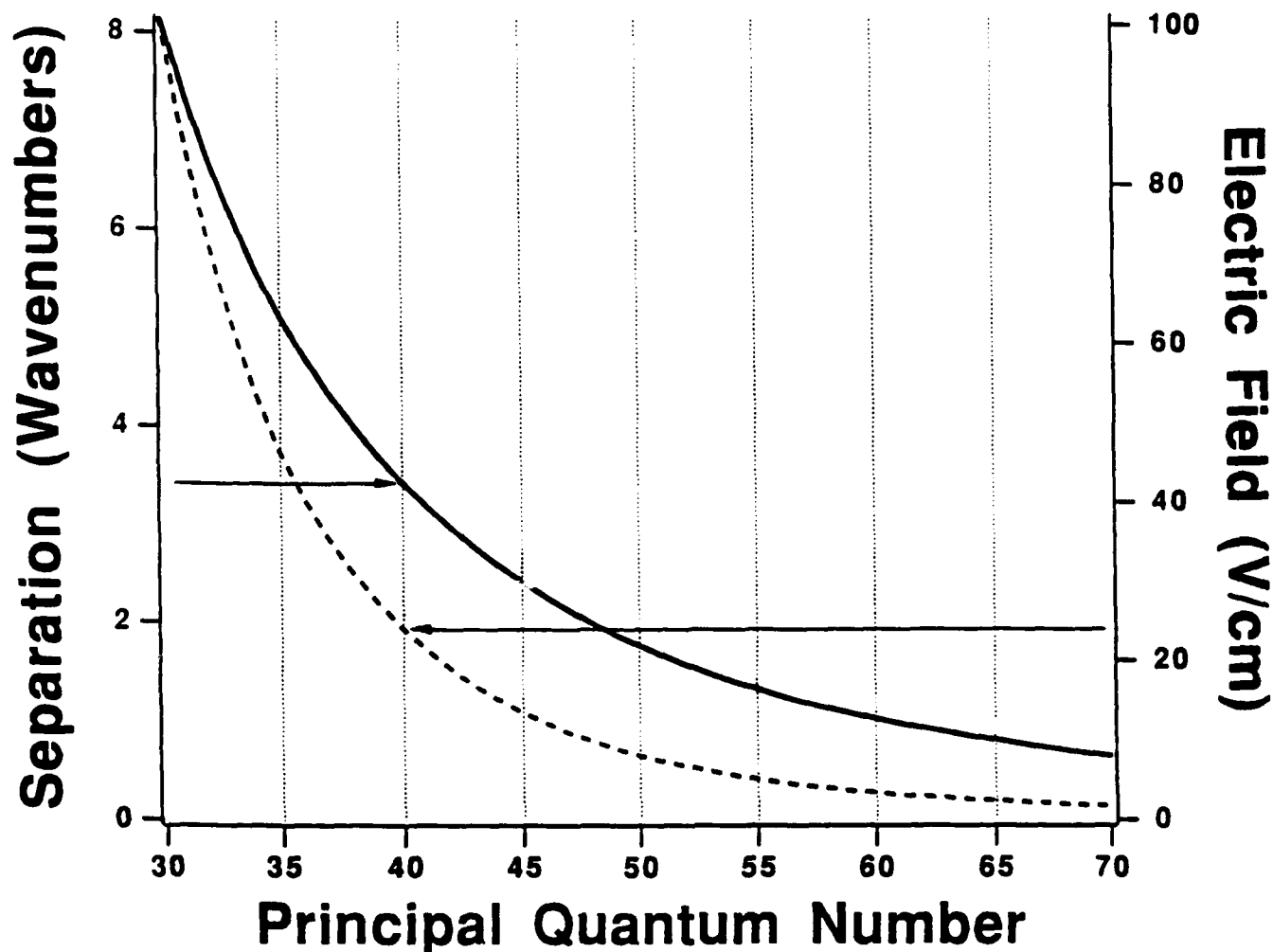


**Figure 28** Experimental resolution limit on electric field sensitivity. For a selected  $n$ -value, the zero electric field  $n$ -state separation is read on the left-hand axis from the solid curve. The electric field which would cause that  $n$ -state to be the last resolved is read on the right-hand axis from the dashed curve. If the experimental resolution is larger than the zero field separation at that  $n$ -value the electric field cannot be determined.



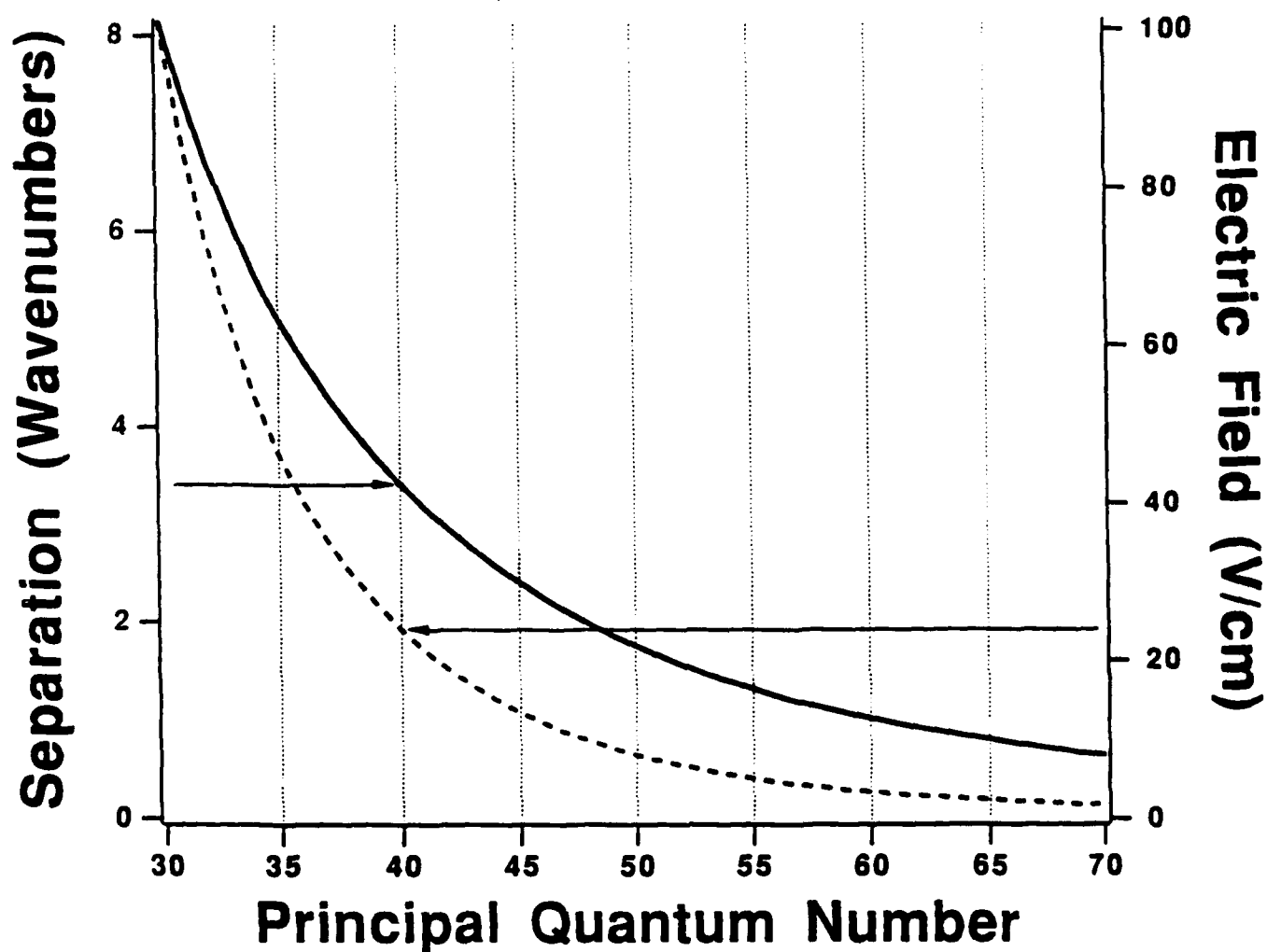


**Figure 28** Experimental resolution limit on electric field sensitivity. For a selected  $n$ -value, the zero electric field  $n$ -state separation is read on the left-hand axis from the solid curve. The electric field which would cause that  $n$ -state to be the last resolved is read on the right-hand axis from the dashed curve. If the experimental resolution is larger than the zero field separation at that  $n$ -value the electric field cannot be determined.

as the last resolved state, which would be caused by an electric field of 3.1 V/cm. This means that at a pressure of 1 Torr, electric fields below 3.1 V/cm cannot be measured by this technique, *independent of instrumental resolution*. This simple treatment agrees well with the hydrogen Rydberg series measurements of Nayfeh<sup>30</sup>, who was able to resolve up to  $n=60$  at a zero electric field, limited by a laser linewidth of 1.0  $\text{cm}^{-1}$ .

### 3. Comparison of Approaches

The consistency of the modified treatments of line broadening and series termination with the spectral simulations are encouraging, however, the real test of the validity of these modifications is a comparison of all the methods on experimental data. This is shown in Table 2 applied to singlet helium spectra recorded in the negative glow and positive column in the hollow cathode tube. This data has been published previously in Ref 54c. The field values obtained from the standard Inglis-Teller relation differ between Ref 54c and Table 2 because in Ref 54c series termination was taken to occur several  $n$ -states beyond the last resolved peak, and in this work the last resolved peak is used. The results of Table 2 are very disconcerting. The electric field values are much too high, by at least a factor of three. The electric field profile in the negative glow shows two maxima, where it would be expected to decrease monotonically. There is no physical reason to justify these results, the operating conditions of the discharge tube were not recorded, and the accuracy of the axial positions is uncertain because the zero location was reset between some of the scans. It is almost certain that other processes, e.g. charged particle collision broadening, which have not

**Table 2** Comparison of the various methods for analyzing helium  
Rydberg spectra

<b>Distance From Cathode (mm)</b>	<b>Inglis-Teller V/cm</b>	<b>Griem Broadening V/cm</b>	<b>Modified Inglis-Teller V/cm</b>	<b>Calculation Broadening V/cm</b>
2.0	$14.1 \pm 2$	$20.8 \pm 2$	$21.1 \pm 4$	$26.2 \pm 2$
3.0	$13.2 \pm 2$	18.2	$18.7 \pm 3$	21.6
4.0	$19.0 \pm 3$	23.4	$27.1 \pm 4$	31.0
5.0	$13.1 \pm 2$	17.4	$18.7 \pm 3$	20.0
6.0	$16.7 \pm 3$	18.2	$23.8 \pm 4$	21.6
8.0	$11.6 \pm 2$	15.6	$16.6 \pm 3$	16.8
20	$16.7 \pm 3$	22.5	$23.8 \pm 4$	29.4
Positive Column	$24.7 \pm 4$	26.0	$35.3 \pm 5$	35.7

been included in the simulations, will have an important effect of the spectra. However, because the operation of the discharge tube was not adequately documented, it is impossible to sort out exactly what is occurring from this data. For these reasons, no conclusions can be made about the discharge tube operation from this data.

## VIII CONCLUSION

The interpretation of fully or partially resolved Stark spectra, even in the presence of an electric field gradient, is unambiguous because the influence of the electric field dominates over all other processes. Thus the cathode sheath data presented in this report is highly reliable. *However, when the Stark spectra is unresolved and the electric field does not dominate over all other processes, e.g. pressure broadening, charged particle collisional broadening, interpretation of the spectra becomes difficult.* Measurement of electric fields from line broadening and series termination (which is a consequence of line broadening), is not reliable unless all other broadening mechanisms can be accurately accounted for. The anomalous peak intensity fall-off of the helium Rydberg series is now easily explained, because the line broadening is not proportional to  $F n^2$ . Fig 29 shows the peak intensities versus principal quantum number for several of the singlet helium Rydberg series simulations discussed in the previous sections. At the lowest field, the peak intensities fall-off as  $n^{-3.2}$ , showing that the field does not significantly alter the  $n^{-3}$  intensity fall-off built into the simulation. At the highest field, the peak intensities decrease as  $n^{-4.8}$ , which is close to the  $n^{-5}$  decrease expected from the combination of decreasing oscillator strength and line broadening. Also shown in Fig 29 is the peak intensity fall-off of an experimental singlet helium Rydberg series recorded at 3mm from the cathode in the hollow cathode tube. These peak intensities decrease as  $n^{-3.4}$ , which clearly shows that the electric field does not have the dominant effect on the linewidth. In contrast to

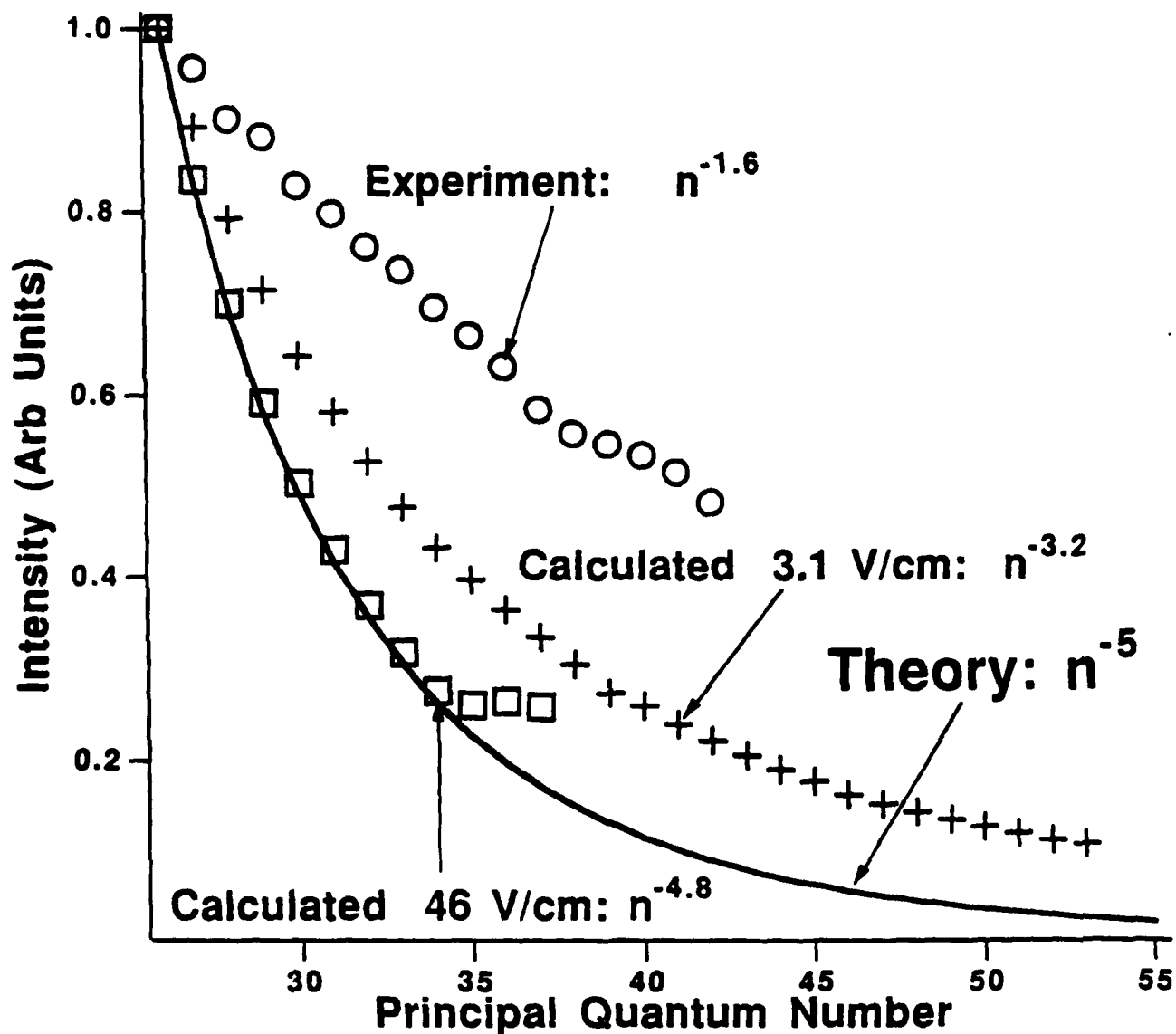


**Figure 29** A comparison of the intensity as a function of  $n$  of representative singlet helium Rydberg series calculations. An inherent linewidth of  $1.0 \text{ cm}^{-1}$  was used for calculations at 3.1 V/cm (crosses) and 46 V/cm (squares). Only at the higher field strength does the  $n$ -state intensity agree with the predicted  $n^{-5}$  relation (solid line). Representative data from a singlet helium spectrum (circles) recorded in the negative glow of a DC discharge shows a significant deviation from what is expected from the zero electric field  $n^{-3}$   $n$ -state intensity dependence.

this data, Vidal <sup>60</sup> shows triplet helium data which has a peak intensity fall-off proportional to  $n^{-4.6}$ , which means that for his conditions ( $n_e \approx 10^{13}$ ) the electric field, here the microfield, is dominant and series termination is valid (though a factor of 1/2.1 instead of 1/3 in Eq 18 is recommended). At present, only the effect of background neutral atom collisions is included in the spectral simulations. Charged particle collisions almost certainly have a significant effect, however, the quality of our present data is not good enough to enable the magnitude of this effect to be determined. Additional experiments are in progress using a thermionic cathode discharge tube whose operation will be stable over a large enough range of pressures and currents to enable neutral and charged particle effects to be observed independently.

Rydberg state Stark spectroscopy of helium is well enough understood to provide a reliable, non-intrusive electric field diagnostic for plasmas. Fully or partially resolved Stark spectra can be interpreted unambiguously. In high-density plasmas where the electric field present results primarily from the space charge, line broadening and series termination provide reliable electric field values for hydrogen and singlet helium; results for triplet helium are not as reliable. In intermediate conditions, where the electric field does not dominate over other processes, linewidth alone does not uniquely define the electric field, so line broadening and series termination will not provide reliable field values unless all other sources of broadening are well known. In order to accurately measure electric fields from such data, the entire line profile must be fitted. This profile fitting may be very difficult if the quasistatic approximation for electron collisions with Rydberg atoms is not valid. The lower limit of the electric field

values which can be measured will depend heavily on pressure, so that at one Torr, electric field below 5 V/cm cannot be resolved by any of the methods discussed in this report. Because the collisional linewidth scales linearly with pressure, a reduction in pressure to 100 mTorr will reduce the collisional linewidth by an order of magnitude to approximately  $0.1 \text{ cm}^{-1}$ . This is roughly equal to the Doppler width for helium at 300 K. Sensitivity to electric fields lower than 5 V/cm is possible, though only at pressures below 1 Torr.



## IX. REFERENCES

1. J. Stark, Sitzberger Akad. Wiss., Berlin, **47**, 932 (1913), referenced in *Atoms and Molecules in Electric Fields*, N. Ryde, (Almquist and Wiksell International, Stockholm, Sweden, 1976).
2. A. LoSurdo, Atti. R. Akad. Naz. Lincei **22**, part 2, 664 (1913), referenced in *Atoms and Molecules in Electric Fields*, N. Ryde, (Almquist and Wiksell International, Stockholm, Sweden, 1976).
3. N. Ryde, *Atoms and Molecules in Electric Fields* (Almquist and Wiksell International, Stockholm, Sweden, 1976).
4. J. Neukammer, H. Rinneberg, K. Vietzke, H. Hieronymous, M. Kohl, and H. J. Grabka, Phys. Rev. Lett. **59**, 2947 (1987).
5. C. T. W. LaHaye and W. Hogervost, Phys. Rev. A, **39**, 5658 (1989).
6. W. Voigt, Ann. der Phys. **69**, 297 (1899); **4**, 197 (1901), referenced in *The Theory of Atomic Spectra*, E. U. Condon and G. H. Shortley, (Cambridge University Press, Cambridge, England, 1970).
7. N. Bohr, Phil Mag **26**, 1; 476; 857 (1913).
8. P. S. Epstein, Ann. der Phys **50**, 489 (1916).
9. K. Schwarzschild, Sitzber Berliner Akad., 548 (1916).
10. H. A. Kramers, Danske Vidensk Selsk. Skrifter (8), III, 3, 287 and Zeits. fur Phys. **3**, 169 (1920).

11. E. Schrodinger, *Ann. der Phys.*, **80**, 457 (1926).
12. P. S. Epstein, *Phys. Rev.* **28**, 695 (1926).
13. J. S. Foster and L. Chalk, *Proc. Roy. Soc.* **123**, 108 (1929).
14. E. U. Condon and G. H. Shortley, *The Theory of Atomic Spectra*, (Cambridge University Press, Cambridge, England, 1970).
15. H. Bethe and E. Salpeter, *Quantum Mechanics of One and Two Electron Atoms*, (Plenum Publishing Corp, New York ,1977).
16. S. P. Alliluyev and M. I. Malkin, *Zh. Eksp. Teor. Fiz.* **66**, 1283 (1974);[*Sov. Phys. J.E.T.P.* **66**, 128 (1974)]; H. Silverstone, *Phys. Rev. A* **18**, 1853 (1978).
17. H. Rausch v. Traubenberg, *Z. Physik* **54**, 307; **56**, 254 (1929); **62**, 289 (1930); **71**, 291(1931). ; *Naturwiss.*, **18**, 417 (1930).
18. J. Mehra and H. Rechenberg, *Historical Development of Quantum Theory*, vol. 4, (Springer-Verlag, New York, 1975).
19. J. Dewey, *Phys. Rev.* (2), **28**, 1108 (1926); **30**, 770 (1927).
20. J. S. Foster, *Proc. Roy. Soc. A* **114**, 47 (1927).
21. J. Cooper and E. B. Salomon, *Phys. Rev. A* **26**, 1452 (1982).
22. M. L. Zimmerman, M. G. Littman, M. M. Kash, and D. Kleppner, *Phys. Rev. A* **20**, 2251 (1979).
23. C. Lanczos, *Z. Phys.* **68**, 204 (1931).

24. A. von Engel, *Ionized Gases*, (Oxford University Press, Oxford, Great Britain, 1965).
25. J. S. Foster, *Can. J. of Phys.* **37**, 1202 (1959).
26. B. N. Ganguly, Gaseous Electronics Conference, 17-20 Oct 1989, Palo Alto CA.
27. P. M. Koch in *Rydberg States of Atoms and Molecules*, edited by R. F. Stebbings and F. B. Dunning (Cambridge University Press 1983); P. M. Koch and D. R. Mariani, *J. Phys. B* **13**, L645 (1980).
28. L. A. Pinnaduwa, *Experimental Studies of Highly Excited Hydrogen Atoms in Strong External Static and Microwave Electromagnetic Fields*, Ph.D. Dissertation, U. of Pittsburgh (1986).
29. M. Nayfeh and K. N. G. D. Yao in *Atomic Excitation and Recombination in External Fields*, edited by M. Nayfeh and C. W. Clark (Gordon and Breach Scientific Publishers, New York, 1985).
30. C. Delsart, L. Caberet, C. Blondel, and R.-J. Champeau, *J. Phys. B* **20**, 4699 (1987).
31. G. J. Hatton, *Phys. Rev. A* **16**, 1347 (1977).
32. C. Chardonnet, D. Delande, and J. C. Gay, *Phys. Rev. A* **39**, 1066 (1988).
33. J.-Y. Liu, P. M. McNicholl, D. A. Harmin, J. Ivri, T. Bergeman, and H. J. Metcalf, *Phys. Rev. Lett.* **55**, 189 (1985).
34. P. M. McNicholl, T. Bergeman, and H. J. Metcalf, *Phys. Rev. A* **37**, 3302 (1988).
35. D. H. Yang, D. Lieberman, P. van der Straten, T. Bergeman, and H. Metcalf,

Phys. Rev. A **40**, 5026 (1989).

36. W. Vassen and H. Hogervost, Phys. Rev. A **39**, 4615 (1989).

37. D. R. Mariani, W. van der Water, and P. M. Koch, Phys. Rev. A **39**, 1066 (1988).

38. R. D. Knight and L.-G. Wang, Phys. Rev. A **32**, 896 (1985).

39. D. K. Doughty and J. E. Lawler, Phys. Rev. A **28**, 773 (1983); Appl. Phys. Lett. **45**, 611 (1984). for example

40. G. L. Duke, *Investigation of Sheath Phenomena in Electronegative Glow Discharges*, AFWAL-TR-84-2099, and references therein.

41. J. R. Shoemaker, B. N. Ganguly, A. Garscadden, Appl. Phys. Lett. **52**, 2019 (1988).

42. D. E. Doughty, S. Salih, and J. E. Lawler, Phys. Lett. **103A**, 41 (1984).

43. I. A. Sellin, Phys. Rev. **136**, 1245 (1964).

44. R.A. Gottscho, Phys. Rev. A **36**, 2233 (1987); C. A. Morre, G. P. Davis, and R. A. Gottscho, Phys. Rev. Lett. **52**, 538 (1984).

45. J. Derouard, H. Debontride, and N. Sadeghi, J. Phys. (Paris) **48**, C7-725 (1987); J. Derouard and N. Sadeghi, IEEE Tran. Plasma Sci. **PS14**, 515 (1986); J. Derourard, H. Debontride, T. D. Nguyen, and N. Sadeghi, J. Chem. Phys. **90**, 5936 (1989).

46. H. Debontride, J. Derouard, and N. Sadeghi, Gaseous Electronics Conference, 18-21 Oct. 1988, Minneapolis MN.

47. J. E. Bayfield, Phys. Rep. **51**, 317 (1979).
48. A. Giutsi-Suzor and P. Zoller, Phys. Rev. A **36**, 5178 (1987).
49. G. Alber and P. Zoller, Phys. Rev. A **37**, 377 (1988).
50. J. Parker and C. R. Stroud, Jr., Phys. Rev. Lett. **56**, 716 (1986).
51. M. D. Perry, O. L. Landen, A. Szöke, and E. M. Campbell, Phys. Rev. A **37**, 747, (1988).
52. J. J. Thompson, Phil. Mag. **18**, 441 (1909).
53. F. W. Aston, Proc. Roy. Soc. A **80** 526 (1910).
54. B. N. Ganguly and A. Garscadden, Phys Rev A **32**, 2544 (1985); B. N. Ganguly, A. Garscadden, J. Appl. Phys. **57**, 4856 (1985); B. N. Ganguly, J. Appl. Phys. **60**, 571 (1986); A. Garscadden in *Radiative Processes in Discharge Plasmas*, edited by J. M. Proud and L. H. Leussen (Plenum Publishing Corp, New York, 1986).
55. H. R. Griem, *Plasma Spectroscopy*, (McGraw-Hill Book Company, New York, 1964).
56. A finite laser beam misalignment relative to the surface of the cathode of  $\theta$  degrees (typically  $2^\circ$ ) explains why a flat-top intensity profile in the model calculation best fitted the data. If the cathode diameter is  $D$ , then the beam samples over a length in the field direction of  $D \sin \theta$ . When the probe beam diameter is small, then the result is a sampling by an apparent flat-top beam intensity profile, over a length larger than the beam diameter.
57. D. H. Katayama, J. M. Cook, V. E. Bondybey, and T. A. Miller, Chem. Phys. Lett. **62**, 542 (1979).

58. D. R. Inglis and E. Teller, J. of Astrophys. **90** 439 (1939).
59. B. I. Henry, Laser and Particle Beams **V. 1** , Pt 1 11 (1983); Y. Matsuura and K. Fukuda, Jap. J. of Appl. Phys. **17** 977 (1987).
60. C. R. Vidal, J. Quant. Spectrosc. Radiat. Transfer, **6**, 461 (1966).